5368O4

DISPOSAL ROOM CALCULATIONS WITH ALTERNATIVE TRU WASTE MODELS

Topical Report RSI-1783

prepared for

Sandia National Laboratories
P.O. Box 5800
Albuquerque, New Mexico 87185-5800

September 2004

RESPEC
CONSULTING & SERVICES

DISPOSAL ROOM CALCULATIONS WITH ALTERNATIVE TRU WASTE MODELS

Topical Report RSI-1783

by

Gary D. Callahan
Gary D. Callahan 9/27/04
RESPEC
P.O. Box 725
Rapid City, South Dakota 57709-0725

prepared for

Sandia National Laboratories
P.O. Box 5800
Albuquerque, New Mexico 87185-5800

September 2004

TABLE OF CONTENTS

LIST OF TABLES

LIST OF FIGURES

LIST OF FIGURES
(Continued)

LIST OF FIGURES
(Continued)

LIST OF FIGURES
(Continued)

LIST OF FIGURES
(Continued)

EXECUTIVE SUMMARY

Performance assessment calculations at the Waste Isolation Pilot Plant (WIPP) require estimates of the porosity in a waste-filled disposal room, which varies with time and the magnitude of gas generated by degradation of the waste. To accommodate this need, Stone [1997] constructed a porosity surface through a series of nonlinear finite element analyses using the program **SANTOS** [Stone, 1990]. Questions have arisen regarding aspects of these analyses, including the development of out-of-plane tensile stresses in the two-dimensional, plane-strain calculations and the adequacy of the soils and crushable foams (crushable foam) model used to represent the mechanical behavior of the transuranic (TRU) waste.

This report documents a study of WIPP disposal rooms analyzed using alternative TRU waste models. The purpose of the study is to investigate the influence of the TRU waste material model on the WIPP disposal room results with a special focus on the average room porosity. The study includes scoping investigations and corroborative analyses to support existing calculations and is not intended for use directly in performance assessment of the WIPP.

This study reexamines the constitutive model for TRU waste, which was integral to porosity surface calculations used in the initial WIPP compliance determination. The main objectives of the study are to examine the influence of the TRU waste constitutive model and to gain an understanding of the generation of out-of-plane tensile stresses including their impact on room porosity. Therefore, TRU waste models with different elastic and inelastic attributes are included in the investigation. Specifically, three different TRU waste constitutive models are examined, including elastic-plastic crushable foam (CF), nonlinear elastic (NE), and fluid (FL) constitutive models. These three models provide distinct differences in their representation of the TRU waste. The volumetric behavior of the initially highly porous TRU waste is of primary interest, but its deviatoric response also affects the resulting deformation and stresses. The three models used in the analyses conducted in this study provide a wide range in material behavior for comparison. However, the volumetric behavior for all three models used in this study is the same; i.e., the mean stress-volumetric strain description is identical for every model. Therefore, differences in results obtained in the analyses are created exclusively by the model's prescribed deviatoric response along with any associated changes in mean stress.

Thirteen different analyses (six crushable foam, six nonlinear elastic, and one fluid) were performed to examine the influence of model parameters on the results using the finite element program **SPECTROM-32** [Callahan et al., 1989]. Parameters evaluated include Poisson's ratio and the deviatoric yield envelope for the crushable foam model. In addition, gas generation resulting from the degradation of TRU waste was considered in four of the analyses. The range in results obtained from the analyses shows that the most important factor causing differences between the models is the resulting out-of-plane stress and its effect on mean stress when no

gas generation is included in the analyses. The two items that impact the out-of-plane stress most in these analyses are Poisson's ratio and the crushable foam deviatoric yield envelope. When gas generation is present, the uncertainty in the constitutive model for the waste is minor and inconsequential because the presence of the waste is overshadowed by the support provided by the generated gas pressures.

Figures E-1 and E-2 provide a brief overview of the results. Figure E-1 includes the final computed room periphery configurations from all 13 analyses. The figure displays a significant amount of information, illustrating that despite the substantial differences in the TRU waste constitutive models, the resulting room deformations are not appreciably different with or without gas generation for comparable cases.

Figure E-2 compares average room porosities obtained in this study to those obtained by Stone [1997] using **SANTOS** for the Compliance Certification Application (CCA) calculations. In Figure E-2, curve labeling CF/0.2, f = 1.0 means the crushable foam model was used with a Poisson's ratio of 0.2 and a gas generation rate of 1.0. Figure E-2 compares results for gas generation rates (f) of 0, 0.4, and 1. For the case with no gas generation, the **SPECTROM-32** porosity results are slightly higher than the **SANTOS** results earlier in time and slightly lower than the **SANTOS** results later in time. For the gas generation cases (f = 0.4 and f = 1.0), the **SPECTROM-32** results were computed using a nonlinear elastic model for the TRU waste with a Poisson's ratio of zero; whereas, the **SANTOS** results were generated using the crushable foam model for the TRU waste with a Poisson's ratio of 0.2. Despite these TRU waste model differences, the **SPECTROM-32** and **SANTOS** room porosity results are quite similar with the **SPECTROM-32** results being consistently higher than the **SANTOS** results with gas generation. Table E-1 provides a numerical comparison of the results presented in Figure E-2 at 10,000 years.

An expectation is that the porous TRU waste in an underground drift will not exhibit tensile stresses along the length of the drift as the underground structure deforms and imparts load to the waste. Based on this expectation and the results of this study, the nonlinear elastic model is probably more representative than the crushable foam model, as it is currently used to describe the mechanical behavior of TRU waste. Therefore, the average disposal room porosity values may be somewhat lower than the minimum porosity values computed earlier by Stone [1997]. However, this conclusion only applies to those cases where the gas generation rate is zero. When gas generation is included in the analyses, the resulting pressures generated in the room serve to reduce room closure, result in increased room porosity values, and reduce the differences between results obtained with the alternative TRU waste models examined in this study.

RSI-1487-04-075

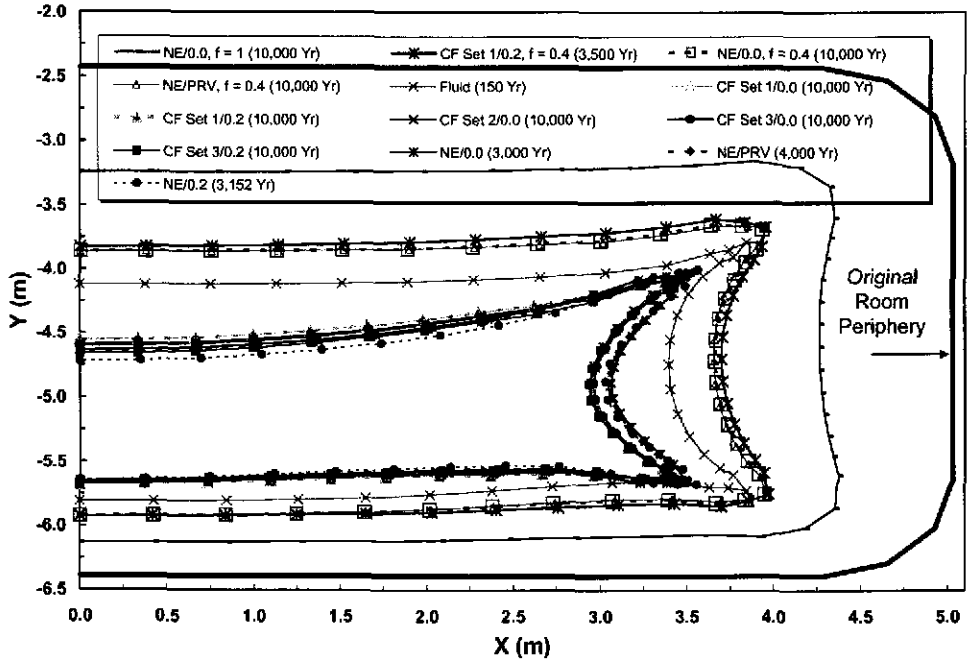

Figure E-1. Comparison of Final Calculated Room Peripheries for Each Analysis.

RSI-1487-04-076

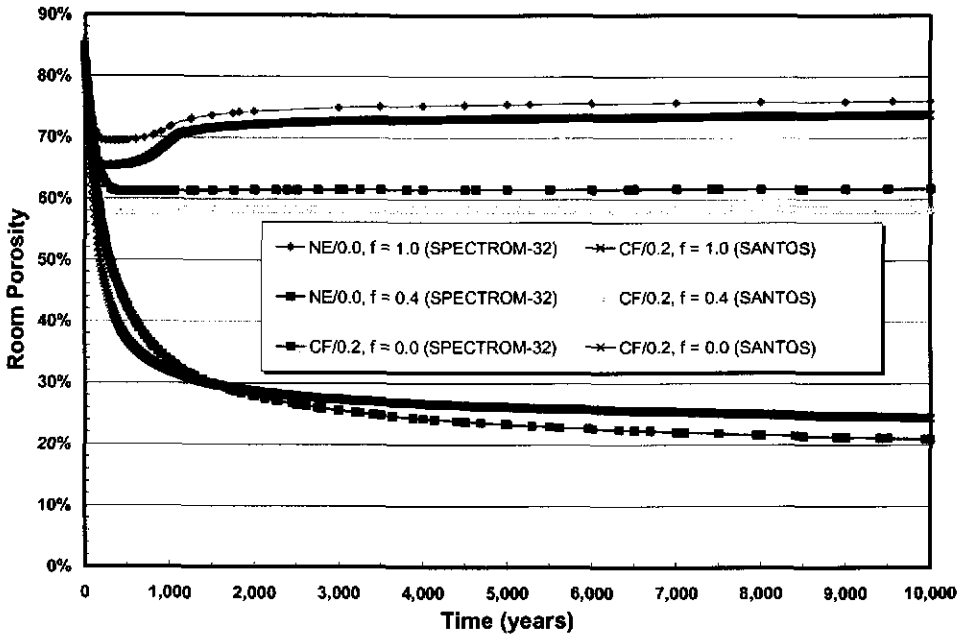

Figure E-2. Comparison of **SANTOS** and **SPECTROM-32** Results for Three Different Gas Generation Rates.

Table E-1. Results Comparison at 10,000 Years

Figure E-2 Gas Generation Rate (f)	Room Porosity (%)		Percent Room Porosity Difference	Results Difference (%)
	SANTOS	SPECTROM-32		
0.0	24.3	20.9	3.4	14.0
0.4	58.3	61.7	3.4	5.8
1.0	73.8	76.0	2.2	3.0

Improvement to the TRU waste model can be obtained by using the nonlinear elastic model, which eliminates the out-of-plane tensile stresses or by changing parameter values in the deviatoric portion of the crushable foam model, which can also eliminate the out-of-plane tensile stresses. A reduced deviatoric envelope in the crushable foam model (e.g., Parameter Set 3 in this study) may be used describe the TRU waste. The reduced deviatoric envelope serves to reduce the out-of-plane tensile stresses, producing more realistic stress results along the length of the disposal room. Neither of these TRU waste model modifications changes the fundamental waste behavior; however, the global response of the pillar and drift would change, resulting in moderately lower room porosities. The uncertainty in the constitutive model for the waste is minor and inconsequential in cases involving moderate gas generation because the mechanical presence of the waste is less important when the drift and pillar are supported by the gas pressure.

The results of this study show that the stresses can be modeled perhaps slightly more realistically than previously calculated by **SANTOS**, but the trends and magnitudes produced by **SANTOS** compare favorably with those produced in this study using an independent finite element program, **SPECTROM-32**.

1.0 INTRODUCTION

The Waste Isolation Pilot Plant (WIPP) is a United States Department of Energy (DOE) facility designed for the safe management, storage, and long-term disposal of contact-handled and remote-handled transuranic (TRU) wastes generated by defense activities in the United States. Performance assessment calculations help establish regulatory compliance for the long-term performance of WIPP. The performance assessment calculations require estimates of the porosity in a waste-filled disposal room, which varies with time and the magnitude of gas generated by degradation of the waste. To accommodate this need, Stone [1997] constructed a porosity surface through a series of nonlinear finite element analyses using the program **SANTOS** [Stone, 1990]. Recently, questions have arisen regarding aspects of these analyses, including the development of out-of-plane tensile stresses in the two-dimensional, plane-strain calculations and the adequacy of the soils and crushable foams (crushable foam) model used to represent the mechanical behavior of the TRU waste.

The purpose of the study discussed in this report is to investigate the influence of the TRU waste material model on the WIPP disposal room results. The study includes scoping investigations and corroborative analyses to support existing calculations and is not used directly in performance assessment of the WIPP. The calculational results presented here are not qualified and cannot be implemented in performance assessment calculations because **SPECTROM-32** has not been qualified for use on the WIPP program. The main objective is to gain an understanding of the generation of the out-of-plane tensile stresses including their effect on room porosity. The out-of-plane calculational results are driven by the plane-strain assumption used in the numerical modeling. The plane-strain assumption requires that the total out-of-plane (z-direction in these analyses) strain rate be zero. Stated mathematically, the plane-strain requirement is

$$\dot{\varepsilon}_z = \dot{\varepsilon}_z^e + \dot{\varepsilon}_z^i = 0 \tag{1-1}$$

where the superscripts e and i indicate the elastic and inelastic portions of the total strain rate. Thus the out-of-plane results of the calculations depend on the elastic and inelastic characteristics of the constitutive model used to represent the TRU waste. Therefore, TRU waste models with different elastic and inelastic attributes were selected for investigation. Specifically, three different TRU waste material models were investigated, viz;

1. Elastic-plastic crushable foam material (CF)
2. Nonlinear elastic material (NE)
3. Fluid material (FL).

These three material models provide distinct differences in their representation of the TRU waste. The crushable foam elastic-plastic constitutive model produces an out-of-plane inelastic

strain rate by virtue of the mean stress-driven volumetric plastic cap portion of the model. The inelastic plastic cap out-of-plane strain rate must be balanced by an equal and opposite out-of-plane elastic strain rate, which can produce out-of-plane tensile stress. For the nonlinear elastic analyses, the out-of-plane stress is equal to Poisson's ratio times the sum of the in-plane stresses. The TRU waste fluid material representation removes all out-of-plane stress and strain interactions as well as any deviatoric behavior of the waste. The fluid material waste characterization simulates bulk waste behavior through tractions applied to the room periphery. The magnitude of the tractions is determined from a given pressure-volume relationship. Each of these TRU waste material models is described in more detail in separate chapters of this report.

To isolate the characteristics of the individual TRU waste models, each of the models used the same basic mean stress-volumetric strain relationship. The geometric model (two-dimensional plane-strain), initial and boundary conditions, and material properties were all selected to be identical and as close as possible to those used by Stone [1997]. The calculations were performed using **SPECTROM-32** [Callahan, 2002; Callahan et al., 1989]. In addition, the gas generation rate included as a study parameter by Stone [1997] was assumed to be zero for most of the analyses. Gas generation rates ($f = 1$ and $f = 0.4$) were considered in four of the analyses to investigate its influence on the results. The parameter f is a multiplier used to scale the gas generation rate. A value of $f = 1$ corresponds to the reference gas generation potential; whereas, a value of $f = 0$ corresponds to no gas generation. For both the nonlinear elastic model analysis and the elastic portion of the crushable foam model analysis, Poisson's ratio was assumed to be zero. For comparison, additional analyses were performed with Poisson's ratio equal to 0.20 and a variable Poisson's ratio that evolves from zero to 0.35 as the waste compacts. In addition, three different parameter value sets were used for the deviatoric portion of the crushable foam model. The plane-strain assumption, combined with the attributes of the specific TRU waste model, causes significant differences in the stress fields within the TRU waste. The specific calculations performed and the differences in the analyses are discussed in detail in Chapter 8.0.

Before the constitutive model details and analyses results are presented, disposal room geometry and relationships between volume, porosity, and density are considered in the next chapter. Chapters 3.0, 4.0, and 5.0 present theoretical considerations for the crushable foam, nonlinear elastic, and fluid waste models, respectively. Chapter 6.0 presents the results of simple, constant stress, plane-strain, and axisymmetric problems to compare differences in the results of the crushable foam and nonlinear elastic models. Chapter 7.0 describes the disposal room geomechanical model. The disposal room analyses results are discussed in Chapter 8.0, which is followed by a summary given in Chapter 9.0. The report concludes with a list of cited references and an appendix with graphical displays of selected calculated results.

2.0 VOLUME, POROSITY, DENSITY, AND STRAIN RELATIONSHIPS

This section presents various relationships between volume, porosity, density, and strain for ease in understanding the presentation of the results. The disposal room geometry is then examined with a discussion of the void volume-room porosity relationship. In this discussion, volume expansion is assumed to be positive.

Total volume (V) is expressed as the sum of the volume of the voids (V_v) and the volume of the solids (V_s)

$$V = V_v + V_s \tag{2-1}$$

Density (ρ) represents mass (m) per unit volume

$$\rho = \frac{m}{V} \tag{2-2}$$

Porosity (ϕ) is defined as the ratio of the volume of the voids to the total volume

$$\phi = \frac{V_v}{V} = \frac{V - V_s}{V} = 1 - \frac{\rho}{\rho_s} \tag{2-3}$$

where ρ_s is the final or ultimate density of the solid material when the porosity is zero. The initial porosity (ϕ_0) is given by

$$\phi_0 = \frac{V_v^0}{V_0} = \frac{V_0 - V_s}{V_0} = 1 - \frac{\rho_0}{\rho_s} \tag{2-4}$$

where V_v^0 is the initial void volume and V_0 is the initial total volume. Thus,

$$\begin{aligned} V_v^0 &= \phi_0 V_0 \\ V_v &= \phi V \end{aligned} \tag{2-5}$$

The ratio of the volume and void volume to the initial volume may be expressed as

$$\begin{aligned} \frac{V}{V_0} &= \frac{\phi_0 - 1}{\phi - 1} \\ \frac{V_v}{V_0} &= \frac{\phi(\phi_0 - 1)}{\phi - 1} \end{aligned} \tag{2-6}$$

The ratio of the void volume to the initial void volume may be written as

$$\frac{V_v}{V_v^0} = \frac{\phi(\phi_0 - 1)}{\phi_0(\phi - 1)} \tag{2-7}$$

Engineering volumetric strain (e_v) is defined as the change in volume per unit original volume, or

$$e_v = \frac{\Delta V}{V_0} \tag{2-8}$$

From Equations 2-2 and 2-8, the density can be expressed in terms of the volumetric strain as

$$\rho = \frac{m}{V} = \frac{m}{V_0 + \Delta V} = \frac{m/V_0}{1 + \Delta V/V_0} = \frac{\rho_0}{1 + e_v} \tag{2-9}$$

Thus the engineering volumetric strain is given in terms of density as

$$e_v = \frac{\rho_0}{\rho} - 1 \tag{2-10}$$

True strain is defined in terms of the engineering strain as

$$\varepsilon_v = \ln(1 + e_v) \tag{2-11}$$

Thus in terms of the true or natural strain, the density is

$$\rho = \frac{\rho_0}{\exp(\varepsilon_v)} \tag{2-12}$$

Thus true strain may be expressed in terms of the density as

$$\varepsilon_v = \ln\left(\frac{\rho_0}{\rho}\right) \tag{2-13}$$

If volume reduction is assumed to be positive, the ratio within the natural log is inverted.

The room geometry and waste characteristics of the disposal room model used in the analyses presented in this report are given in Table 2-1. To the extent possible, the room geometry and waste characteristics are the same as those given by Stone [1997]. The finite element mesh used in the analyses presented here includes a 0.75-meter fillet; whereas, Stone [1997] used a square-cornered room in his analyses. The analyses conducted in this study did not include the contact surfaces that Stone [1997] used in his analyses. Thus a concession had to be made in representing the TRU waste as an equivalent material occupying the entire

disposal room. Introduction of the fillets in the corners of the disposal room enabled the analyses to extend farther in time until the mesh distortion became so severe that the elements were invalid.

Table 2-1. Model Room Geometry and Waste Characteristics

Item	Value	Units	Half-Room Planar Model[a]	Half-Room Planar Model Corrected[b]
Initial Room Height	3.96	m	3.96	3.96
Initial Room Width	10.06	m	5.03	5.03
Room Length	91.44	m	1	1
Initial Room Area	39.838	m^2	19.919	19.677
Initial Room Volume	3,642.75	m^3	19.919	19.677
Initial Waste Volume	1,728	m^3	9.449	9.334
Initial Waste Density	559.5	kg/m^3	559.5	559.5
Waste Mass	966,816	kg	5,286.614	5,222.534
Waste Mass/Meter of Drift	10,573.228	kg/m of drift	5,286.614	5,222.534
Waste Volume/Meter of Drift	18.898	m^3/m of drift	9.449	9.334
Ultimate Waste Density	1,757	kg/m^3	1,757	1,757
Ultimate Waste Volume	550.265	m^3	3.010	2.972
Initial Waste Porosity	68.156	%	68.156	68.156
Initial Room Porosity	84.894	%	84.894	84.894
Effective Density for Full Room	265.408	kg/m^3	265.408	265.408

(a) The unit depth of the finite element model dramatically changes the associated volume calculations.

(b) Correction is for the 0.75-meter fillets in the room corners.

Using the basic room information given in Table 2-1 and Equation 2-7, the void volume and porosity of the disposal room are compared in Figure 2-1. The figure provides a clear depiction of the magnitude of the changing void volume and illustrates that smaller changes in void volume occur for the same change in porosity as the room porosity decreases. This fact must be kept in mind when viewing room porosity values (i.e., V_v/V) because both the void volume and total volume are decreasing, which produces seemingly high porosities even though the actual void volume is quite small.

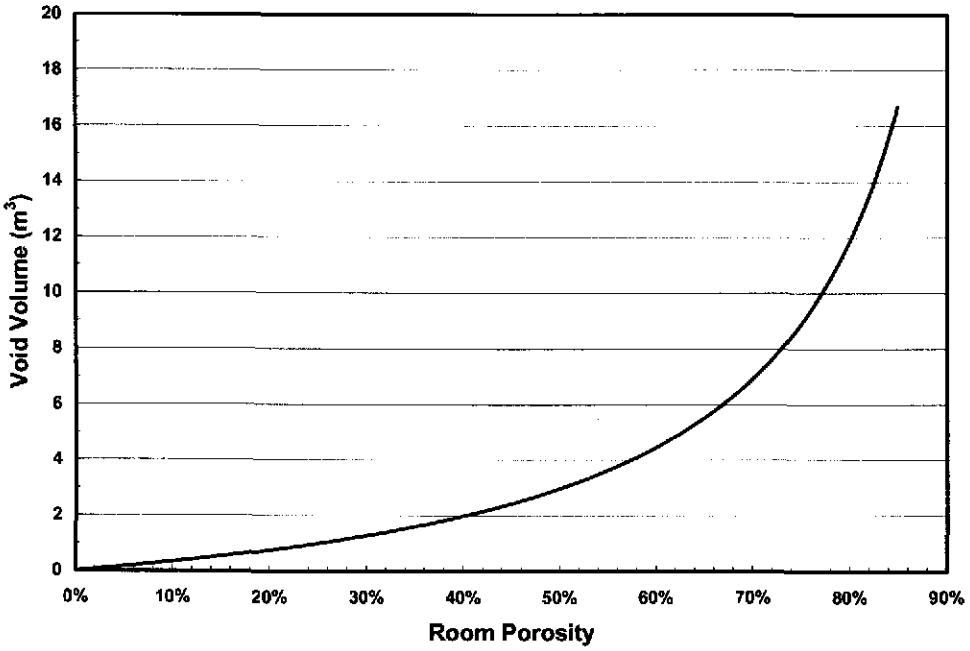

Figure 2-1. Relationship Between Room Void Volume and Room Porosity.

3.0 THEORETICAL CONSIDERATIONS FOR CRUSHABLE FOAM

The basic equations describing the crushable foam and soils TRU waste constitutive model (crushable foam model) are given by Stone et al. [1985] and are presented in this section. The crushable foam model is an elastic-plastic model with a flat volumetric cap coincident with the deviatoric plane in principal stress space. The deviatoric part of the model is elastic-perfectly plastic such that the surface of revolution in principal stress is stationary (i.e., neither kinematic nor isotropic hardening is allowed). The cap portion of the model hardens with volumetric straining such that the cap moves outward along the hydrostatic axis during volumetric yielding. The deviatoric and volumetric hardening parts of the models are uncoupled. The deviatoric yield function is given by

$$F_d = J_2 - \left(a_0 - a_1\sigma_m + a_2\sigma_m^2\right) \tag{3-1}$$

where:

$$\begin{aligned} J_2 &= \frac{1}{2}s_{ij}\,s_{ij} \\ s_{ij} &= \sigma_{ij} - \sigma_m\delta_{ij}, \text{ deviatoric stress} \\ \sigma_m &= \frac{\sigma_{kk}}{3}, \text{ mean stress} \\ a_0, a_1, a_2 &= \text{material constants.} \end{aligned} \tag{3-2}$$

At yield, $F_d = 0$ and we may write Equation 3-1 as

$$\sqrt{J_2} = \sqrt{a_0 - a_1\sigma_m + a_2\sigma_m^2} \tag{3-3}$$

which can more readily be compared to usual yield functions of degree one in stress. Note that Equation 3-1 differs from Stone's equation in that the a_1 term is opposite in sign. This sign change occurs because Stone assumed compression positive; whereas, in **SPECTROM-32**, tension is taken to be positive.

The deviatoric portion of the crushable foam model is implemented into **SANTOS** [Stone, 1990] in a slightly different manner than is given in Equation 3-3. For **SANTOS**, the equation is written at yield as

$$\sqrt{3J_2} = b_0 - b_1\,\sigma_m + b_2\,\sigma_m^2 \tag{3-4}$$

assuming tension is positive. Stone [1997] gives constants for the crushable foam model disposal room analyses as

$$b_0 = 1 \qquad [\text{MPa}]$$
$$b_1 = 3 \qquad [\ -\ ] \tag{3-5}$$
$$b_2 = 0 \qquad [\text{MPa}^{-1}]$$

Thus Equation 3-4 may be rewritten as

$$\sqrt{3J_2} = b_0 - b_1 \sigma_m \tag{3-6}$$

With manipulation and selection of appropriate constant values, Equation 3-3 can be made equivalent to Equation 3-6. First, to complete the square on the right-hand side of Equation 3-3, the value of a_1 is restricted to the following value:

$$a_1 = 2\sqrt{a_0}\sqrt{a_2} \tag{3-7}$$

Substituting Equation 3-7 into Equation 3-3 yields:

$$\sqrt{J_2} = \sqrt{a_0} - \sqrt{a_2}\,\sigma_m \tag{3-8}$$

Equations 3-8 and 3-6 will be equivalent if the following constant values are prescribed for Equation 3-3:

$$a_0 = \frac{b_0^2}{3} \qquad [\text{MPa}^2]$$
$$a_1 = \frac{2\,b_0\,b_1}{3} \qquad [\text{MPa}] \tag{3-9}$$
$$a_2 = \frac{b_1^2}{3} \qquad [\ -\ ]$$

The volumetric yield function is simply

$$F_v = \sigma_m - f(\varepsilon_v) \tag{3-10}$$

where $\varepsilon_v = \varepsilon_{kk}$ is the volumetric strain and $f(\varepsilon_v)$ describes the volumetric hardening by a set of pressure-volumetric strain relations (i.e., data pairs entered in tabular form). As an alternative, **SPECTROM-32** also includes a mean stress-porosity functional form, which is identical to the nonlinear elastic mean stress-porosity function described in the next section (see Equation 4-1).

In addition to the deviatoric and volumetric parts of the plastic constitutive model, a tensile limit is also imposed. Tensile fracture does not occur as long as a particular tensile pressure is not large enough to produce a zero or imaginary deviatoric yield stress. Mathematically, fracture has not occurred if:

$$\sigma_m < h \tag{3-11}$$

where h is the minimum root of the polynomial $a_0 - a_1 \sigma_m + a_2 \sigma_m^2 = 0$. If Equation 3-11 is not satisfied, the mean stress is set equal to h.

The plastic strain increment vector $d\varepsilon_{ij}^p$ is given by the flow rule

$$d\varepsilon_{ij}^p = d\lambda \frac{\partial Q}{\partial \sigma_{ij}} \tag{3-12}$$

where Q is the plastic potential function. If the yield function (F_d) is equal to the plastic potential function, F_d replaces Q in Equation 3-12, and it is termed an associative flow rule; otherwise, the term nonassociative flow is used. For associative flow, the normality rule is satisfied which ensures a unique solution for boundary-value problems. For the deviatoric portion of the model, the crushable foam model uses a nonassociative flow rule so that deviatoric strains produce no volume change. This requires that the plastic potential function for the deviatoric model be

$$Q = \sqrt{J_2} \tag{3-13}$$

and Equation 3-12 becomes

$$d\varepsilon_{ij}^p = d\lambda \frac{S_{ij}}{2\sqrt{J_2}} \tag{3-14}$$

For the volumetric portion of the model, Drucker's stability postulate for work-hardening materials (linearity requirement) is considered (e.g., see Chen and Han [1988]), which requires that

$$d\varepsilon_{ij}^p = \frac{1}{h} \partial F_v \frac{\partial F_v}{\partial \sigma_{ij}} = \frac{1}{h} \frac{\partial F_v}{\partial \sigma_{ij}} \frac{\partial F_v}{\partial \sigma_{mn}} d\sigma_{mn} \tag{3-15}$$

where h is a scalar-hardening function which may depend upon stress, strain, and loading history. Using Equation 3-10, $\partial F_v / \partial \sigma_{ij} = \delta_{ij}/3$, and $\partial F_v = d\sigma_m$, Equation 3-15 takes the form

$$d\varepsilon_{ij}^p = \frac{1}{h} \frac{\delta_{ij}}{3} d\sigma_m \tag{3-16}$$

Rewriting Equation 3-16 for the plastic volumetric strain gives

$$d\varepsilon_{kk}^p = \frac{1}{h} d\sigma_m \tag{3-17}$$

which may be rearranged to produce

$$h = \frac{d\sigma_m}{d\varepsilon_{kk}^p} \tag{3-18}$$

Therefore, the hardening modulus describes the relationship between increments in mean stress (pressure) and increments in volumetric strain. Rather than prescribe a specific hardening function, Stone [1997] uses a tabular pressure-volumetric strain relationship to describe the volumetric-hardening behavior $f(\varepsilon_v)$, which is shown by Stone [1997] plotted schematically as pressure (i.e., σ_m) versus $\ln(\rho/\rho_0)$ in Figure 6 with the tabular data given in Stone's Table 4.

To simulate the TRU waste as a crushable foam material in the disposal room, the gap element feature in **SPECTROM-32** was used. The material filling the disposal room had to deform very easily until the room volume reduced to the actual original volume of the TRU waste. The gap element feature provides the ability to change the type of material behavior on an element-by-element basis after a prescribed change in volume has occurred. Thus the initial average porosity of the room is 84.9 percent (see Table 2-1) with an initial density of 265.4 kg/m^3. After the volume of an element decreased to the point that its porosity was the same as the initial waste porosity (68.2 percent, see Table 2-1) with a density of 559.5 kg/m^3, the element was changed to deform according to the TRU waste properties given in Table 3-1 [Stone, 1997]. The volumetric compaction strain corresponding to this deformation is 0.746 (Equation 2-13). The ratio of the volume to initial volume when the conversion to TRU waste properties occurs is given by Equation 2-6. Substituting the porosity values gives $V/V_0 = 0.474$. The only negative aspect of simulating the TRU waste in this manner is that the conversion of the room contents to TRU waste properties occurs on an element-by-element basis.

Table 3-1. Pressure-Volumetric Strain Data Used for the Plasticity Model in Representing the Room Averaged TRU Waste Drums

Pressure (MPa)	Volumetric Strain, ln (ρ/ρ_0) (Compaction)
1.53	0.510
2.03	0.631
2.53	0.719
3.03	0.786
3.53	0.838
4.03	0.881
4.93	0.942
12.00	1.140

Elastic material properties and constants for the deviatoric portion of the crushable foam model are taken from Stone [1997]. Although Stone [1997] reports the values for shear and bulk modulus given in Table 3-2, a review of the sample input file given in Appendix A of his report indicates he actually used a value for shear modulus equal to one-half the value given in Table 3-2. The shear and bulk modulus values given in Table 3-2 are equivalent to a Poisson's ratio of zero; whereas, assuming one-half the shear modulus value is equivalent to a Poisson's ratio of 0.2. Analysis results are presented for both of these Poisson's ratio values.

Table 3-2. Elastic and Deviatoric Plastic Material Constants for Crushable Foam

Parameter	Set 1	Set 2	Set 3
Shear Modulus, G	333 MPa	333 MPa	333 MPa
Bulk Modulus, K	222 MPa	222 MPa	222 MPa
a_0	1/3 MPa^2	1/3 MPa^2	1.0 MPa^2
a_1	2.0 MPa	2.0 MPa	3.0 MPa
a_2	3.0	$\sqrt{3}$	0.0

Equivalent deviatoric material parameters are computed using the relationships derived in Equation 3-9. The elastic and deviatoric crushable foam model parameter sets are given in Table 3-2. Material Property Set 1 produces a deviatoric model identical to the one used by Stone, and two other material property sets were used in additional analyses for comparison. The three deviatoric yield envelopes used in the analyses are compared with the **SANTOS** yield envelope (Equation 3-6) in Figure 3-1.

A Poisson's ratio value of zero is prescribed for the crushable foam material in all three parameter sets given in Table 3-2 from the relationship for Poisson's ratio (ν) with the elastic constants:

$$\nu = \frac{3K - 2G}{2(3K + G)} \tag{3-19}$$

Two cases are investigated for Parameter Sets 1 and 3 with Poisson's ratio equal to 0.0 and 0.2, the latter of which requires G to be one-half the value given in Table 3-2.

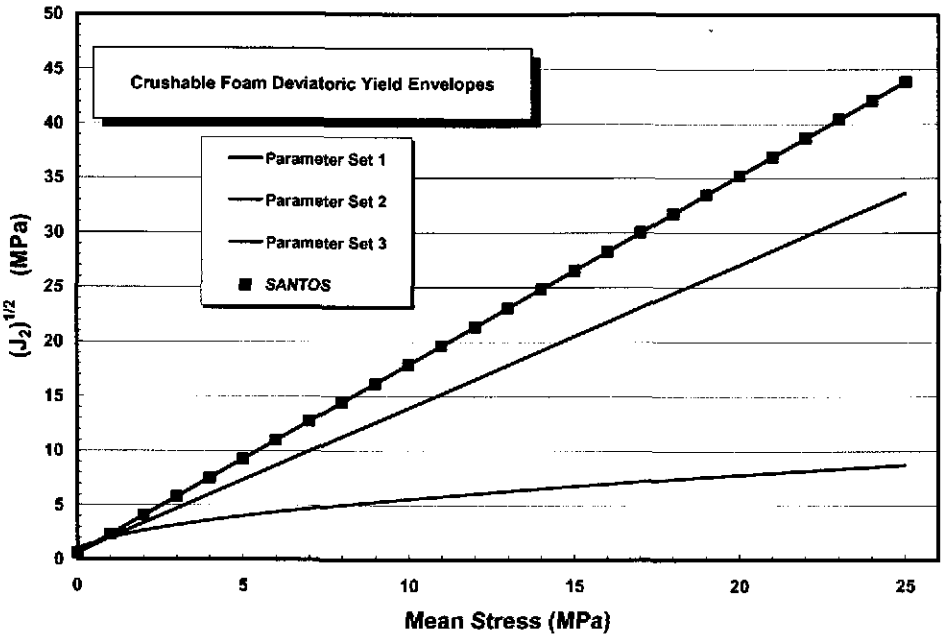

Figure 3-1. Comparison of Three Crushable Foam Deviatoric Yield Envelope Parameter Sets With the Envelope Used by Stone [1997].

4.0 THEORETICAL CONSIDERATIONS FOR NONLINEAR ELASTICITY

As an alternative to the TRU waste tabulated data, Callahan and DeVries [1991] adopted a mean stress-porosity functional relationship by which the volumetric hardening can be evaluated. This function is written as

$$\sigma_m = \frac{1}{3\kappa} \ln\left(\frac{\phi}{\phi_0}\right) \tag{4-1}$$

where κ is a material parameter. Figure 4-1 shows Equation 4-1 fitted to the pressure-volumetric strain data provided in Table 3-1. Two fits to the data were performed that included and excluded the last data point, providing two different values for parameter κ. The fit excluding the last data point fits a majority of the data in the lower stress regime much better, which was felt to be more important in these simulations. Thus Equation 4-1 with $\kappa = 0.0889$ was taken to be representative of the TRU waste mean stress-volumetric strain relationship.

RSI-1487-04-002

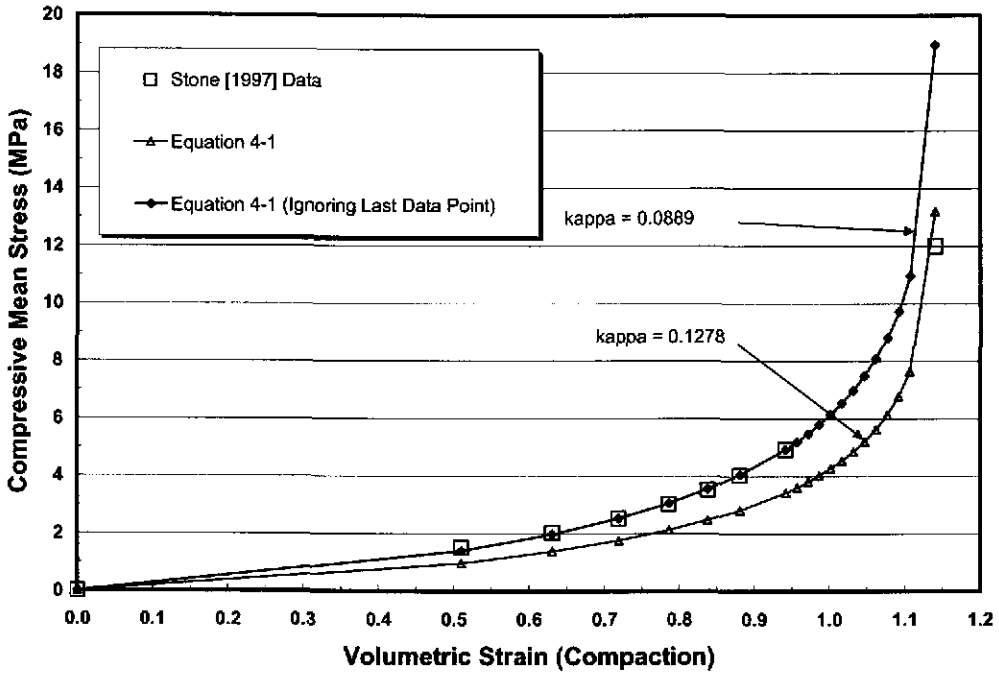

Figure 4-1. Mean Stress (Pressure) Volumetric Strain Data and Function Fit.

The functional form in Equation 4-1 is used in the nonlinear elastic model to determine the continually changing bulk modulus (i.e., $K = d\sigma_m/d\varepsilon_v$). The tangent bulk modulus used to model the TRU waste as a nonlinear elastic material is given by

$$K_t = \frac{d\sigma_m}{d\varepsilon_v} \tag{4-2}$$

where the mean stress-volumetric strain is written in terms of the porosity ϕ as given in Equation 4-1. Using the chain rule of differentiation, the tangent bulk modulus may be determined in terms of the material density as

$$K_t = \frac{d\sigma_m}{d\varepsilon_v} = \frac{d\sigma_m}{d\phi}\frac{d\phi}{d\rho}\frac{d\rho}{d\varepsilon_v} \tag{4-3}$$

Using Equations 2-3, 2-12, 4-1, and 4-3, the tangent bulk modulus may be expressed as

$$K_t = \frac{\rho}{3\kappa(\rho_s - \rho)} \tag{4-4}$$

In terms of engineering strain increments, the tangent bulk modulus is

$$K_t = \frac{d\sigma_m}{de_v} = \frac{\rho^2}{3\kappa\rho_0(\rho_s - \rho)} \tag{4-5}$$

In the finite strain analyses performed in this study, Equation 4-4 was used. For the shear modulus, a function identical to the bulk modulus is used with a new material constant (λ), which is written as

$$G_t = \frac{\rho}{3\lambda(\rho_s - \rho)} = \frac{\kappa}{\lambda}K_t \tag{4-6}$$

This assumed shear representation is required because no experimental data exists to help describe the shear behavior of TRU waste. Typically, the value of λ is determined from an assumed constant value for Poisson's ratio. Poisson's ratio (ν) is defined in terms of the bulk and shear modulus as

$$\nu = \frac{3K_t - 2G_t}{2(3K_t + G_t)} \tag{4-7}$$

Solving for G_t gives

$$G_t = \frac{3(1-2\nu)}{2(1+\nu)}K_t \tag{4-8}$$

Thus if Poisson's ratio is zero, then

$$G_t = \frac{3}{2}K_t \qquad (\text{for } \nu = 0) \tag{4-9}$$

and $\lambda = 2/3\ \kappa$. If Poisson's ratio is 0.2, then $\lambda = 4/3\ \kappa$.

For the TRU waste, a value of zero for Poisson's ratio is probably a reasonable assumed value when the waste is initially in a highly porous state. However, Hansen and Mellegard [1998] performed tests on a degraded waste surrogate and recommended a value of 0.35 for Poisson's ratio for the material. Thus a Poisson's ratio that evolves from zero to 0.35 similar to the bulk modulus shown in Figure 4-1 may be a more realistic assumption. To evaluate the influence of a variable Poisson's ratio, a functional form for λ given in Equation 4-6 was developed as

$$\lambda(\rho) = \lambda_0 + \lambda_1 \frac{\rho}{\rho_s - \rho} \tag{4-10}$$

Thus for the variable Poisson's ratio, Equation 4-6 is written as

$$G_r = \frac{\rho}{3\left(\lambda_0 + \lambda_1 \dfrac{\rho}{\rho_s - \rho}\right)(\rho_s - \rho)} \tag{4-11}$$

The relationship for the variable Poisson's ratio is determined by substituting Equations 4-4 and 4-11 into Equation 4-7, which gives

$$\nu(\rho) = \frac{3\left(\lambda_0(\rho_s - \rho) + \lambda_1 \rho\right) - 2\kappa(\rho_s - \rho)}{6\left(\lambda_0(\rho_s - \rho) + \lambda_1 \rho\right) + 2\kappa(\rho_s - \rho)} \tag{4-12}$$

Equation 4-12 is subject to the conditions that $\nu = 0$ when $\rho = \rho_0$ and $\nu = 0.35$ when the porosity in the waste is 1 percent $(\phi = 1 \text{ percent})$ or $\rho = 0.99\rho_s$. Thus the values for λ_0 and λ_1 are determined to be 0.0583 and $2.105 \cdot 10^{-3}$, respectively. The resulting variable value of Poisson's ratio is shown in Figure 4-2.

From Equation 4-1 and Figure 4-1, a basic equivalency exists between the nonlinear elastic tangent bulk modulus and the flat, volumetric, plastic-cap hardening modulus. Thus the volumetric strain behavior produced by the nonlinear elastic and crushable foam plastic models should yield equivalent results as long as the same pressure-volumetric strain relationships are used to define the tangent bulk modulus and the plastic hardening modulus. This is also a conclusion of Sandler et al. [1976] who state that the behavior of a cap model with a vertical cap and a bulk modulus, K (which may be a constant or a function of pressure), which is the same for loading and unloading (i.e., $K_L = K_U$), is identical to the uncapped model with $K_L < K_U$. This is readily seen because with an associative flow rule applied to the vertical cap, only plastic volume changes occur. The crushable foam model uses the initial bulk modulus K_0 for loading and unloading. The **SPECTROM-32** nonlinear elastic model uses the tangent bulk modulus for loading and unloading (loads and unloads along the same path). Therefore, if we neglect unloading, the crushable foam plastic and nonlinear elastic models should produce equivalent volumetric behavior. This conclusion is basically true but is violated in plane-strain types of problems because of the nature of the out-of-plane behavior in elastic and plastic types of problems. In elastic problems, the out-of-plane stress created by loading is equal to Poisson's

ratio times the sum of the in-plane components. In elastic-plastic problems, the out-of-plane stress created by loading is altered by the out-of-plane plastic flow. Thus the mean stresses obtained for the two problems will be different. These facts are illustrated in the example problem section for simple one-element comparison problems.

RSI-1487-04-044

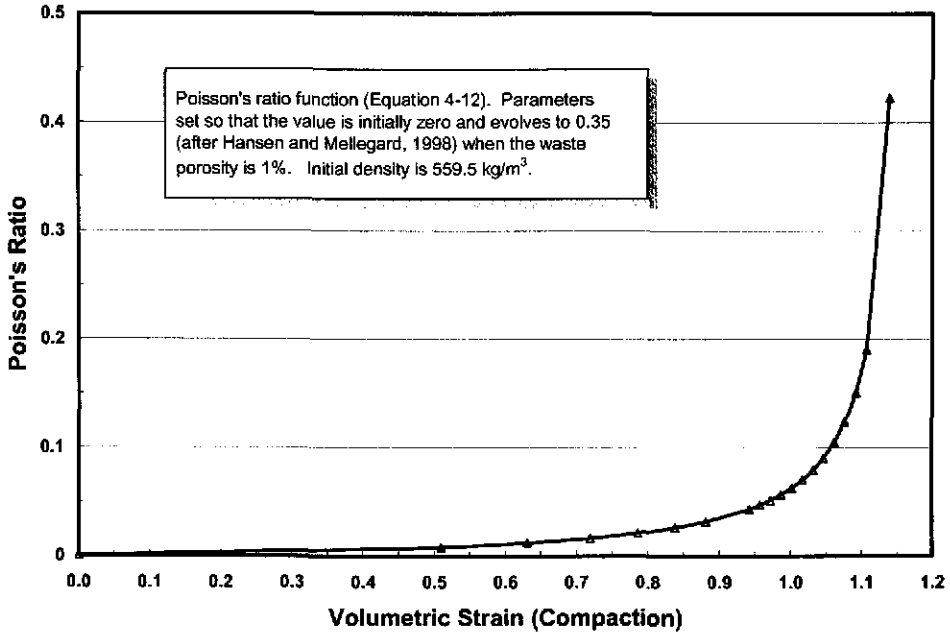

Figure 4-2. Variable Poisson's Ratio Values as a Function of Volumetric Strain.

To simulate the TRU waste in the disposal room, the waste was assumed to be averaged over the entire room volume. The material filling the disposal room had to deform very easily until the room volume reduced to the actual original volume of the TRU waste. To accomplish the representation of the waste, the pressure-volumetric strain relationship was modified (translated in volumetric strain) so that the waste characteristics would be representative after the room had deformed the appropriate amount. Thus the initial porosity of the TRU waste was assumed to be the same as the initial room porosity (84.9 percent, see Table 2-1) with an initial density of 265.4 kg/m^3. After the room volume decreased to the point that the average room porosity was the same as the initial waste porosity (68.2 percent, see Table 2-1) with a density of 559.5 kg/m^3, the material in the room deformed according to the TRU waste properties. The volumetric compaction strain corresponding to this deformation (i.e., from a density of 265.4 kg/m^3 to a density of 559.5 kg/m^3) is 0.746 (Equation 2-13). The translated pressure-volumetric strain data for the room-averaged TRU waste is given in Table 4-1. Thus Equation 4-1 was fitted to the translated volumetric strain given in Table 4-1 with the results (κ = 0.1117) shown in Figure 4-3. Figure 4-3 also shows the fluid material representation discussed in the next section.

Table 4-1. Pressure-Volumetric Strain Data Used for the Nonlinear Elastic Model in Representing the Room-Averaged TRU Waste Drums

Pressure (MPa)	Volumetric Strain, ln (ρ/ρ_0) (Compaction)
0.00	0.746
1.53	1.256
2.03	1.377
2.53	1.465
3.03	1.532
3.53	1.584
4.03	1.627
4.93	1.688
12.00	1.886

RSI-1487-04-003

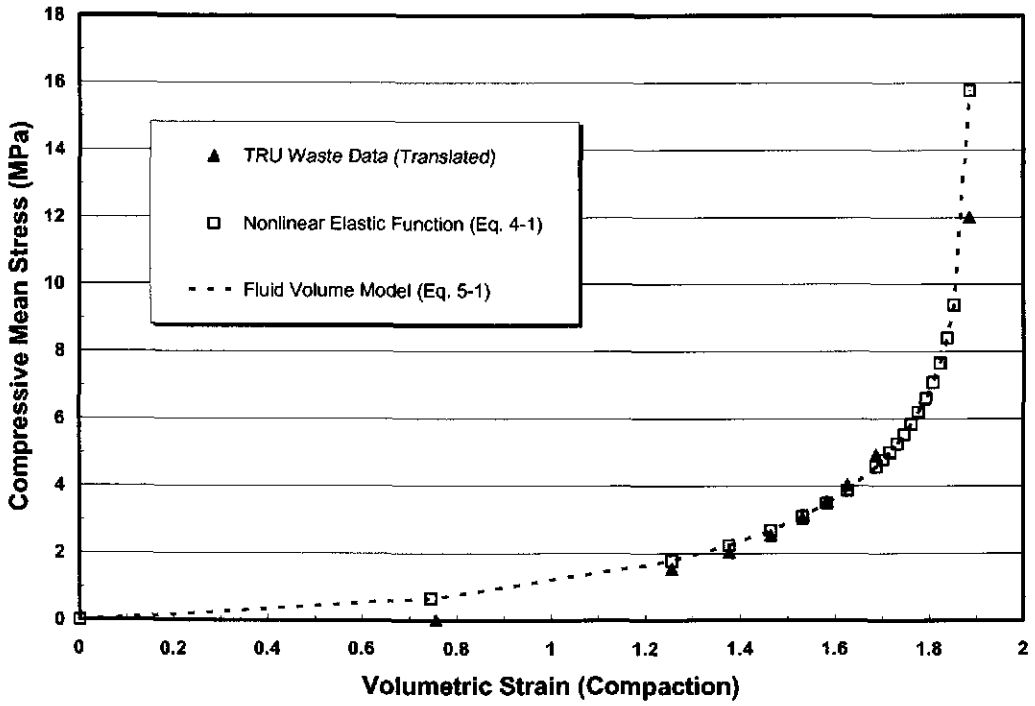

Figure 4-3. Mean Stress (Pressure) Volumetric Strain Data and Function Fits for the Translated Volumetric Strain Data.

Similarly, the parameter values for the variable Poisson's ratio function given in Equation 4-12 need to be determined for the translated (high porosity) waste function. In this case, the same conditions apply (i.e., $\nu = 0$ when $\rho = \rho_0$ and $\nu = 0.35$ when the porosity in the waste is 1 percent $(\phi = 1 \text{ percent})$ or $\rho = 0.99\,\rho_0$) except ρ_0 is now 265.4 kg/m^3. Under these conditions, the values for λ_0 and λ_1 are determined to be 0.074 and $2.637 \cdot 10^{-3}$, respectively. The resulting variable value of Poisson's ratio is shown in Figure 4-4.

RSI-1487-04-045

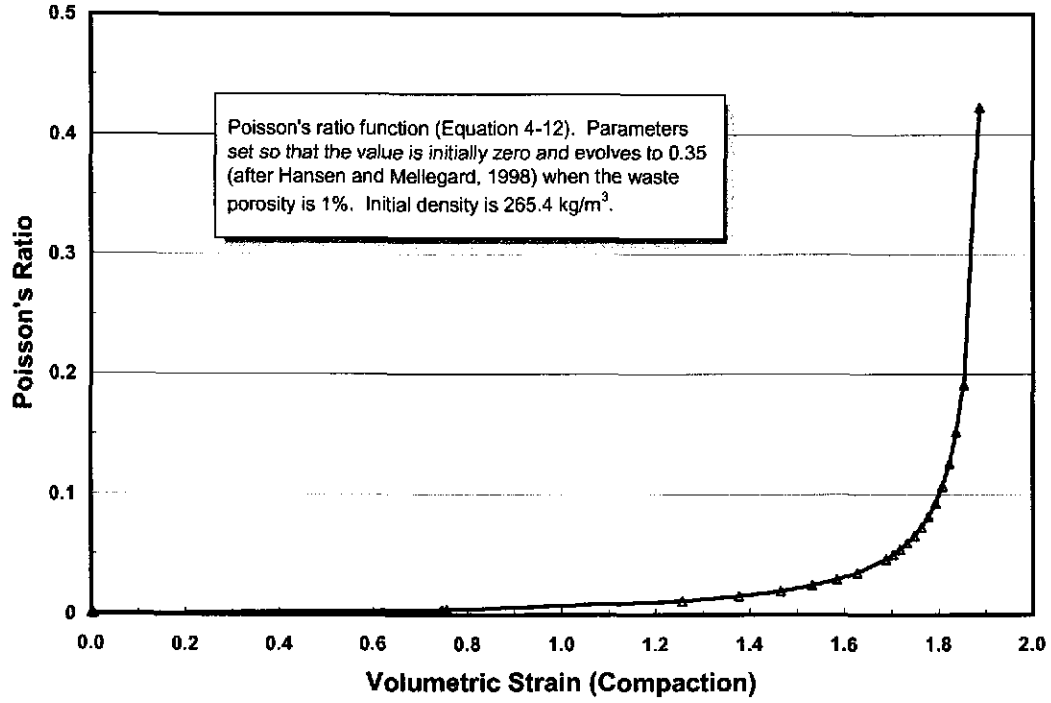

Figure 4-4. Variable Poisson's Ratio Values as a Function of Volumetric Strain for the Translated TRU Waste Properties.

5.0 CONSIDERATION OF A TRU WASTE FLUID REPRESENTATION

Representation of the TRU waste as a fluid (*material with no shear strength*) provides a useful comparison by eliminating all deviatoric or shear response of the material. In the finite element simulations, this is accomplished using a pressure-volume relationship. The room pressure (i.e., bulk resistance of the TRU waste) is simulated as a traction on the periphery of the room. **SPECTROM-32** includes routines that monitor the volume of a region, computes the pressure in the region from a given equation-of-state, and applies the pressure to a boundary through surface tractions. Equation 4-1 was used as the equation-of-state for the pressure-volume relationship in the room, but the equation was implemented in a different form because the software computes the pressure based on the void volume. Thus for the fluid material characterization, Equation 4-1 is rewritten as:

$$P = H \ln\left(\frac{\phi_0 V_v + V_v^0(1-\phi_0)}{V_v}\right) \tag{5-1}$$

where $H = 1/(3\kappa)$. Equation 5-1 is plotted in Figure 4-3 and is identical to the nonlinear elastic function, as it should be.

6.0 SIMPLE EXAMPLE PROBLEMS FOR MODEL COMPARISON

Example problems analyzed consist of a single finite element at a constant temperature of 297 K that is incrementally loaded up to 5.0 MPa and then incrementally unloaded. Two geometric situations are investigated: axisymmetric and plane strain. For the cylindrical specimen, the loading is hydrostatic, and for the planar specimen, the loading is equal in the plane. The mean stress, volumetric strain, and out-of-plane stresses produced by the two material characterizations are of interest. Thus one eight-noded element (radius/width = 1 meter and height = 1 meter) is used with 0.5 MPa increments in the vertical and lateral surface tractions. The problem is one of constant stress; thus, the dimensions are immaterial because the strain is also constant throughout the element. The material properties for the crushable foam material are given in Tables 3-1 and 3-2 (Set 3). For the nonlinear elastic material, Equation 4-1 is used with $\kappa = 0.0889$. To be consistent with the zero value for Poisson's ratio in the crushable foam model, $\lambda = 2/3\ \kappa$ defines the value for the shear modulus. Any other properties required for the analyses are given in Table 2-1. In essence, the properties used for these simple example problems are identical to some of those cases used for the disposal room analyses discussed later.

Results for these analyses are given in Figures 6-1 and 6-2. Figure 6-1 shows the out-of-plane-stress for both material characterizations, assuming axisymmetric and plane-strain geometrical configurations. Figure 6-2 shows the mean stress versus volumetric strain behavior for both material characterizations, assuming axisymmetric and plane-strain geometrical configurations. Out-of-plane stress is a misnomer for the axisymmetric analysis where all three principal stresses are equal (hydrostatic loading). For the axisymmetric configuration, the nonlinear elastic and crushable foam material characterizations produce equivalent results. However, the plane-strain analyses are different for a variety of reasons. The plane-strain assumption requires that the total out-of-plane (z-direction in these analyses) strain rate be zero (see Equation 1-1). The plane-strain assumption causes significant differences in the stress fields. For the elastic analyses, the out-of-plane stress is equal to Poisson's ratio (zero in this case) times the sum of the in-plane stresses. Figure 6-1 shows that the nonlinear elastic analysis maintains an out-of-plane stress of zero. However, the crushable foam elastic-plastic constitutive model produces an out-of-plane inelastic strain rate by virtue of the mean stress-driven volumetric plastic cap portion of the model. The inelastic plastic cap out-of-plane strain rate must be balanced by an equal and opposite out-of-plane elastic strain rate, which produces an out-of-plane tensile stress, as shown in Figure 6-1. The out-of-plane stress differences produce different mean stresses, which creates the different mean stress versus volumetric strain behavior shown in Figure 6-2. The crushable foam out-of-plane plastic flow drives the stress component into tension, which reduces the mean stress to a level lower than the comparable nonlinear elastic analysis where the out-of-plane stress remains zero. The stair-step nature of the curves in Figures 6-1 and 6-2 occurs from the inclusion of the interim elastic loading result, which is only an interim step in finding the solution. In other words, each incremental load is applied followed by iterations until the final solution is obtained.

RSI-1487-04-004

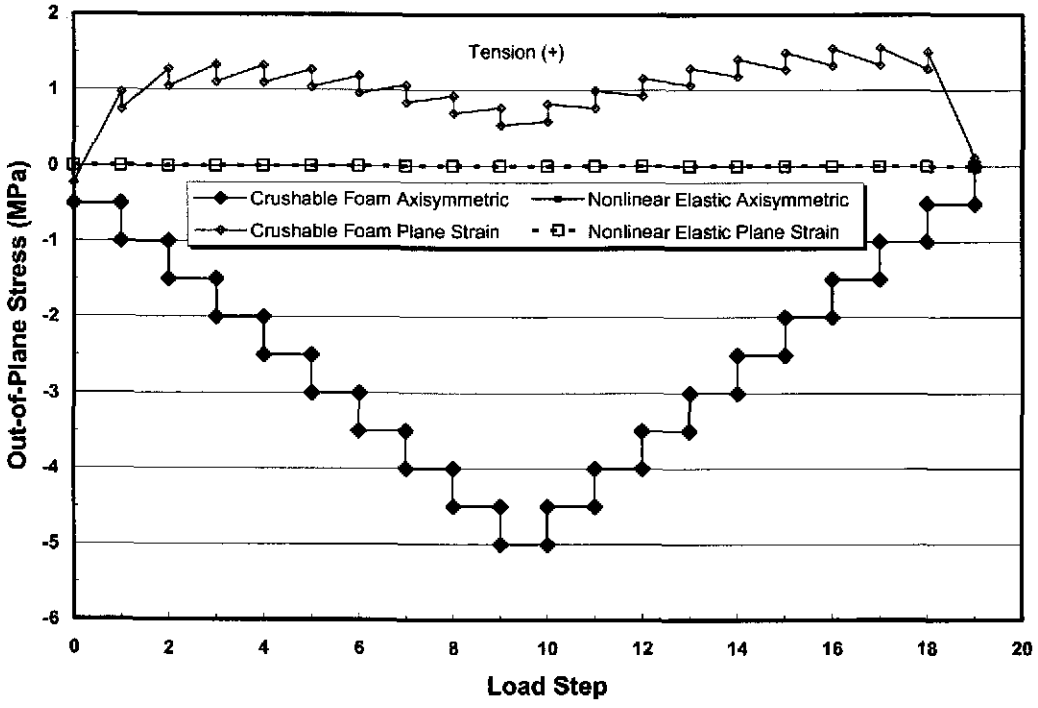

Figure 6-1. Out-of-Plane Stress for the Example Problems.

RSI-1487-04-005

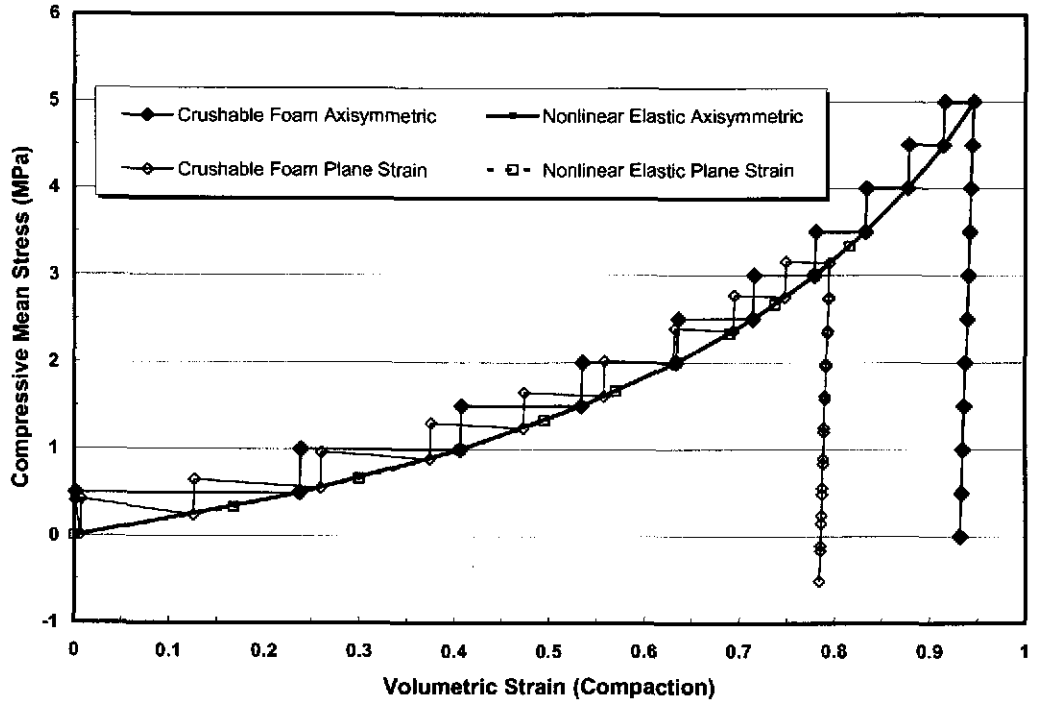

Figure 6-2. Mean Stress Versus Volumetric Strain for the Example Problems.

7.0 WASTE DISPOSAL ROOM GEOMECHANICAL MODEL

The geometry, initial conditions, and stratigraphy for this problem are identical to those used by Stone [1997]. The finite element representation is shown in Figure 7-1. Figure 7-1 shows that in addition to the TRU waste models described previously, constitutive models are required for clean and argillaceous halite and anhydrite. The constitutive models used for these materials are described next.

7.1 CLEAN AND ARGILLACEOUS HALITE CONSTITUTIVE MODEL

The model used for the halite is an elastic-viscoplastic model. The elastic portion of the model is Hooke's law. The viscoplastic portion of the model is described by the Munson-Dawson (MD) constitutive model [Munson and Dawson, 1982; Munson et al., 1989] that provides a continuum description of the creep response for rock salt. Dislocation motion is assumed to contribute directly to the macroscopic inelastic strain rate. The generalized form of the MD model is given by

$$\dot{\varepsilon}_{ij}^{c} = \dot{\varepsilon}_{eq}^{c} \frac{\partial \sigma_{eq}}{\partial \sigma_{ij}} \tag{7-1}$$

where $\dot{\varepsilon}_{ij}^{c}$ is the inelastic strain rate and σ_{eq} and $\dot{\varepsilon}_{eq}^{c}$ are power-conjugate equivalent stress measures and equivalent inelastic strain rates for the dislocation creep. Note that tension is taken to be positive in this development. The kinetic equation for the dislocation mechanisms is

$$\dot{\varepsilon}_{eq}^{c} = F\dot{\varepsilon}_{s} \tag{7-2}$$

where F is the transient function representing transient creep behavior and $\dot{\varepsilon}_{s}$ is the steady-state strain rate. The steady-state creep of salt is the sum of three dominant mechanisms: (1) a high-temperature, low-stress regime controlled by dislocation climb; (2) a low-temperature, low-stress regime controlled by an undefined mechanism; and (3) a high-stress regime controlled by various possible dislocation slip mechanisms. The steady-state creep rates of the three relevant mechanisms, respectively, are given by

$$\dot{\varepsilon}_{s_1} = A_1 e^{-Q_1/RT}\left(\frac{\sigma_{eq}^{c}}{\mu}\right)^{n_1} \tag{7-3}$$

$$\dot{\varepsilon}_{s_2} = A_2 e^{-Q_2/RT}\left(\frac{\sigma_{eq}^{c}}{\mu}\right)^{n_2} \tag{7-4}$$

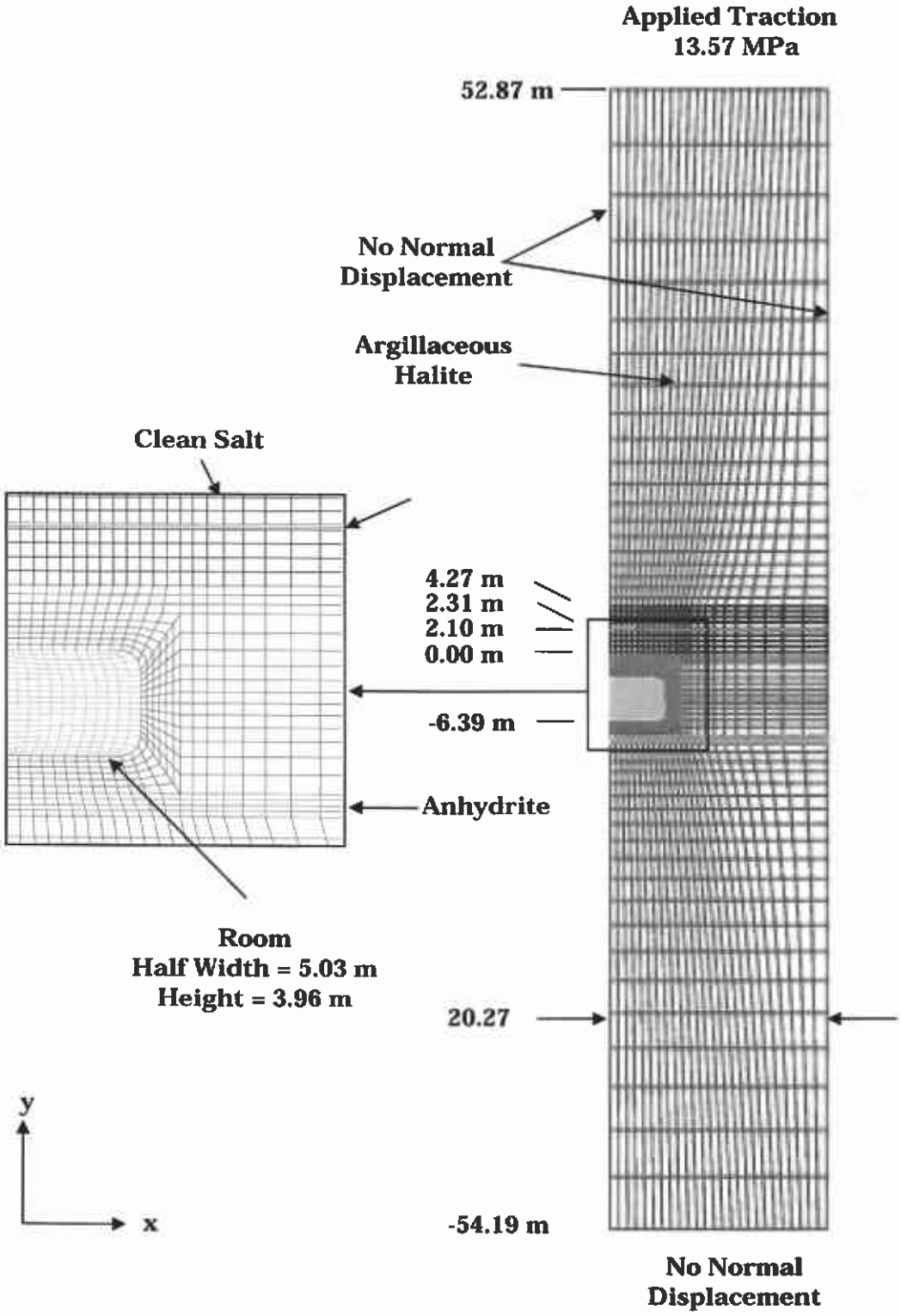

Figure 7-1. Finite Element Discretization and Boundary Conditions Used for the Disposal Room Analyses.

$$\dot{\varepsilon}_{s_3} = \left(B_1 e^{-Q_1/RT} + B_2 e^{-Q_2/RT}\right)\sinh\left[\frac{q\left(\sigma_{eq}^c - \sigma_0\right)}{\mu}\right] H\left(\sigma_{eq}^c - \sigma_0\right) \tag{7-5}$$

where the A's and B's are constants, Qs are activation energies, T is the absolute temperature, R is the universal gas constant, μ is the shear modulus, n's are the stress exponents, q is the stress constant, σ_0 is the stress limit of the dislocation slip mechanism, and H is a Heaviside step function. The transient creep function F is given by

$$F = \begin{cases} \exp\left[\Delta\left(1 - \dfrac{\varsigma}{\varepsilon_t^*}\right)^2\right] & \text{for } \varsigma < \varepsilon_t^* \\ 1 & \text{for } \varsigma = \varepsilon_t^* \\ \exp\left[-\delta\left(1 - \dfrac{\varsigma}{\varepsilon_t^*}\right)^2\right] & \text{for } \varsigma > \varepsilon_t^* \end{cases} \tag{7-6}$$

F is composed of a work-hardening branch, an equilibrium branch, and a recovery branch, respectively. In Equation 7-6, Δ and δ represent the work-hardening and recovery parameters, respectively, and ε_t^* is the transient strain limit. The transient strain limit is a function of temperature and stress and is represented by

$$\varepsilon_t^* = K_0 e^{cT}\left(\frac{\sigma_{eq}^c}{\mu}\right)^m \tag{7-7}$$

where K_0, c, and m are constants. The work-hardening and recovery parameters are functions of stress given by

$$\Delta = \alpha_w + \beta_w \log\left(\frac{\sigma_{eq}^c}{\mu}\right) \tag{7-8}$$

$$\delta = \alpha_r + \beta_r \log\left(\frac{\sigma_{eq}^c}{\mu}\right) \tag{7-9}$$

where the α's and β's are constants with the subscripts denoting either work-hardening (w) or recovery (r). The evolutionary rate, $\dot{\varsigma}$, of the internal variable, ς, given in Equation 7-6 is governed by

$$\dot{\varsigma} = \text{sign}\left(\varepsilon_t^* - \varsigma\right)\left(F - 1\right)\dot{\varepsilon}_s \tag{7-10}$$

which diminishes to zero when the steady-state condition is achieved.

The maximum shear stress or Tresca criterion is used for dislocation-induced flow. The power-conjugate equivalent stress measure, σ^c_{eq}, for the dislocation mechanisms, assuming the Tresca criterion, is given by

$$\sigma^c_{eq} = 2\cos\psi\sqrt{J_2} = \sigma_1 - \sigma_3 \tag{7-11}$$

where ψ is the Lode angle; J_2 is the second invariant of the deviatoric stress tensor; and σ_1 and σ_3 are the maximum and minimum principal stresses, respectively. The shear-induced dislocation flow of rock salt is assumed to be associative. The flow potential is an important factor in extending data obtained from constant stress laboratory creep tests to generalized three-dimensional states of stress. Differentiation of the power-conjugate stress given by Equation 7-11 with respect to stress leads to

$$\frac{\partial\sigma^c_{eq}}{\partial\sigma_{ij}} = \left[\frac{\cos 2\psi}{\cos 3\psi}\right]\frac{s_{ij}}{\sqrt{J_2}} + \left[\frac{\sqrt{3}\sin\psi}{J_2\cos 3\psi}\right]t_{ij} \tag{7-12}$$

where s_{ij} is the deviatoric stress tensor and $-\frac{2}{3}J_2\delta_{ij}$. Equation 7-12 is indeterminate when $\pm\pi/6$. To eliminate this problem computationally, the flow potential is taken as the average of the flow potentials on either side of the indeterminacy and evaluated in the limit as $\psi \to \pm\pi/6$ whenever the Lode angle is within 0.25 degree of the indeterminacy. For both conditions $(\pm\pi/6)$, the result is

$$\frac{\partial\sigma^c_{eq}}{\partial\sigma_{ij}} = \frac{s_{ij}}{\sqrt{3J_2}} \pm \frac{t_{ij}}{2J_2} \tag{7-13}$$

Thus at the corners of the Tresca potential, the indeterminacies are removed by assuming a von Mises flow which makes the direction of straining unique.

The material constants for the MD constitutive model corresponding to the clean and argillaceous halite are taken from Stone [1997] and are listed in Table 7-1.

7.2 ANHYDRITE CONSTITUTIVE MODEL

The deformation of the anhydrite layers above and below the disposal room is governed by an elastic-plastic constitutive model. The total strain rate for the elastic-plastic model is assumed to have elastic and plastic components in the form:

$$\dot{\varepsilon}_{ij} = \dot{\varepsilon}^e_{ij} + \dot{\varepsilon}^p_{ij} \tag{7-14}$$

The elastic portion of the total strain rate, denoted by the superscript *e*, is described by Hooke's law. The plastic strain rates, denoted by the superscript *p*, are described here.

Table 7-1. Munson-Dawson Parameter Values for Halite

Parameter	Units	Clean	Argillaceous
Elastic Parameter Values			
E	MPa	31,000	31,000
ν	—	0.25	0.25
Munson-Dawson Creep Parameter Values			
A_1	yr^{-1} s^{-1}	2.645E+30 8.386E+22	4.440E+30 1.407E+23
A_2	yr^{-1} s^{-1}	3.050E+20 9.672E+12	4.147E+20 1.314E+13
Q_1/R Q_1	K cal/mol	12,581 25,000	12,581 25,000
Q_2/R Q_2	K cal/mol	5,032 10,000	5,032 10,000
n_1	—	5.5	5.5
n_2	—	5.0	5.0
B_1	yr^{-1} s^{-1}	1.919E+14 6.0856E+06	2.840E+14 8.998E+06
B_2	yr^{-1} s^{-1}	9.568E+05 3.034E–02	1.354E+04 4.289E–02
q	—	5.335E+03	5.335E+03
σ_0	MPa	20.57	20.57
μ	MPa	12,400	12,400
m	—	3	3
K_0	—	6.275E+5	2.470E+6
c	K^{-1}	9.198E–3	9.198E–3
α	—	–17.37	–14.96
β	—	–7.738	–7.738
α_r	—	0.58	0.58
β_r	—	0	0

When perfectly plastic materials (i.e., no hardening) are considered, the flow rule is written:

$$\dot{\varepsilon}_{ij}^{p} = \lambda \frac{\partial Q}{\partial \sigma_{ij}} \tag{7-15}$$

where λ is a positive, unspecified scalar. In classical plasticity theory, associative behavior is invoked with $Q \equiv F$. In soil and rock mechanics, this restriction is often ignored because pressure-sensitive, associative-plastic behavior generally predicts dilation in excess of experimental observations. When $Q \neq F$, the term nonassociative plasticity is used. In these analyses, the associative flow rule was used. The yield function used to describe the anhydrite behavior is the Drucker-Prager criterion. The yield function for the Drucker-Prager criterion is as follows:

$$F = 3\alpha\sigma_m + \sqrt{J_2} - K = 0 \tag{7-16}$$

where α and K are material constants. The plastic potential function is also given by Equation 7-16 for the assumed associative flow. Thus performing the differentiation indicated in Equation 7-15, the flow rule for the Drucker-Prager criterion is

$$\frac{\partial Q}{\partial \sigma_{ij}} = \alpha\delta_{ij} + \frac{s_{ij}}{2\sqrt{J_2}} \tag{7-17}$$

An important consequence of the mean-stress dependence in the Drucker-Prager criterion is observed by considering the volumetric plastic strain. Equations 7-15 and 7-17 give:

$$\dot{\varepsilon}_{kk}^{p} = 3\alpha\lambda \tag{7-18}$$

Therefore, plastic deformation is accompanied by dilation of the material. The material constants for the anhydrite are taken from Stone [1997] and given in Table 7-2.

Table 7-2. Elastic and Drucker-Prager Material Constants

Material	Young's Modulus (MPa)	Poisson's Ratio	*K* (MPa)	α
Anhydrite	75,100	0.35	1.35	0.45

8.0 DISPOSAL ROOM ANALYSIS RESULTS

In this section, results are presented for a disposal room containing TRU waste. All of the analyses performed used the same mesh, initial conditions, and boundary conditions. Differences in the analyses included the constitutive model used to describe the TRU waste and whether or not the disposal room included gas generation. The specific analyses conducted are listed in Table 8-1.

Table 8-1. Characteristics of Analyses Performed

TRU Waste Constitutive Model	ID No.	Final Results Time (Yrs)	Poisson's Ratio	Gas Generation Parameter *f*	Deviatoric Parameter Set No.
Crushable Foam	1	10,000	0.0	0	1
	2	10,000	0.0	0	2
	3	10,000	0.0	0	3
	4	10,000	0.2	0	1
	5	10,000	0.2	0	3
	6	3,500	0.2	0.4	1
Nonlinear Elastic	7	3,000	0.0	0	NA
	8	4,443	0.2	0	NA
	9	4,000	Eq. 4-12	0	NA
	10	10,000	0.0	1	NA
	11	10,000	0.0	0.4	NA
	12	10,000	Eq. 4-12	0.4	NA
Fluid	13	150	NA	0	NA

NA = Not Applicable.

Comparison of Analyses 1 through 3 illustrates the influence of the deviatoric portion of the crushable foam model. Comparison of Analyses 1 through 3 with Analysis 7 provides basic differences between the nonlinear elastic and crushable foam elastic-plastic TRU waste models. Comparison of Analyses 1 and 4, 3 and 5, and 7 through 9 provides differences obtained by changing the out-of-plane stress through different values of Poisson's ratio. Comparison of

Analyses 4 and 8 and Analyses 6 and 11 provides basic differences between the nonlinear elastic and crushable foam elastic-plastic TRU waste models with and without gas generation. Analyses 11 and 12 show the influence of a variable Poisson's ratio when gas generation is present. Analysis 13 gives an indication of the importance of the deviatoric response of the TRU waste by providing only a bulk fluid type of resistance to the room deformation. Labels for the curves included in the graphical presentations are:

1. CF Set *n*/*p* – Elastic-plastic crushable foam material using deviatoric parameter set *n* (where $n = 1$, 2, or 3) with Poisson's ratio *p* (where $p = 0.0$ or 0.2)
2. NE/*n* – Nonlinear elastic material with Poisson's ratio equal to *n* (where $n = 0.0$, 0.2, or PRV with PRV meaning the variable Poisson's ratio given in Equation 4-12).
3. FL – Fluid material.
4. f = *n* – Gas generation included at rate *n* (where $n = 0.0$, 0.4, or 1).

When values for Poisson's ratio or the gas generation are not listed, their value is zero.

Each of the analyses was simulated using **SPECTROM-32** for variable periods of times with a goal of 10,000 years. However, some of the analyses did not reach 10,000 years. The analyses conducted in this study did not include contact surfaces that Stone [1997] used in his analyses. Contact surfaces enable the room to deform freely until it contacts the waste package and begins to transfer load. Thus a variety of modeling techniques was used to represent the TRU waste. Specifically, methods to effectively capture room deformation through the volume of air until the waste was contacted had to be implemented. This involved the inclusion of elements in the entire room volume and modification of the elements' properties to simulate the TRU waste after significant deformation through the air space. The specific methodologies for modeling the air-gap deformation were slightly different for the nonlinear elastic and crushable foam models. For the nonlinear elastic model analyses, the elements filling the room were given properties described in Table 4-1, Figure 4-3, and Equation 4-8. Thus the room-filling elements offered negligible resistance to deformation until the air gap effectively disappeared. For the crushable foam model analyses, the elements filling the room were initially given a very low Young's modulus (0.1 MPa). After an element filling the room deformed an amount equivalent to the air-gap removal, the element was assigned material properties described in Tables 3-1 and 3-2. Again, the room-filling elements offered negligible resistance to deformation until the air gap effectively disappeared. The resulting high initial room porosities with little stiffness included in the room elements cause severe mesh distortion in these finite strain analyses. In some cases, the mesh distortion was so severe that the analyses halted before the desired simulation time was reached. Introduction of fillets in the corners of the disposal room (Figure 7-1) enabled the analyses to extend farther in time until the mesh distortion became so severe that the elements were invalid. The simulation times achieved for each of the analyses are provided in Table 8-1. The elements in the room for the fluid type characterization of the TRU waste did not obtain any increase in stiffness as the deformation

increased. Thus with the extremely low stiffnesses of these elements, mesh distortion occurred much more rapidly than in the other analyses.

Room closure, room porosity, and room volume results through time for Analyses 1, 2, 3, 7, 8, and 13 are illustrated in Figures 8-1 through 8-6. For each plotted variable, two figures are presented – one with a time scale through 10,000 years and one with a time scale through 1,000 years. The shorter time scale provides a better comparison of the earlier time data from the analyses. The vertical and horizontal room closures are compared in Figures 8-1 and 8-2, average room porosities are compared in Figures 8-3 and 8-4, and total room volumes and room void volumes are compared in Figures 8-5 and 8-6. In all of these figures, the hierarchy of results for the different analyses remains fairly constant (i.e., crushable foam set 1, crushable foam set 2, crushable foam set 3, nonlinear elastic with Poisson's ratio equal to 0.0, nonlinear elastic with Poisson's ratio equal to 0.2, and fluid). Essentially, this hierarchy correlates with the resulting magnitudes of the out-of-plane stress, which changes the magnitude of the mean stress. The out-of-plane stresses for the crushable foam TRU waste representation are tensile for a period of time in all three deviatoric parameter sets used. However, crushable foam model Parameter Sets 1 and 2 out-of-plane stresses remain tensile while the Parameter Set 3 results eventually become compressive. The nonlinear elastic out-of-plane stresses remain zero for Poisson's ratio equal to zero. The out-of-plane stresses are equal to Poisson's ratio times the sum of the in-plane stresses for a Poisson's ratio value of 0.2. For the fluid representation of the TRU waste, the room contents are immaterial because the resistance of the waste to room deformation is represented by tractions acting on the room periphery; thus, the fluid model provides the most flexible or least stiff representation of the TRU waste. In spite of all these model differences, the results are not significantly different. If one examines Figure 8-5 where the total room volumes are plotted, the volumes differ by less than 0.65 m^3 at 3,000 years, and the differences decrease as time progresses. Using the crushable foam set 1 result as the base, this difference amounts to 15.7 percent, which is equivalent to 3.2 percent of the original room volume. Changes from that point forward are small because the void volume is quite small and the TRU waste is fairly stiff. Room porosity plots amplify these differences even though the void volume is quite small (see Figure 2-1).

The influence of Poisson's ratio on the solutions for the crushable foam and nonlinear elastic models are shown using room closure, room porosity, and room volume results through time for Analyses 1, 3, 4, 5, 7, 8, and 9 in Figures 8-7 through 8-12. As with the first series of figures, for each plotted variable, two figures are presented – one with a time scale through 10,000 years and one with a time scale through 1,000 years. For the variables shown in the figures, Poisson's ratio has minimal influence on the crushable foam model results. For a Poisson's ratio value of 0.2, the out-of-plane stresses are still tensile but lower than those produced for a Poisson's ratio of 0.0. This results in moderately higher mean stresses, which are reflected in the slightly lower porosities during the first 1,500 years. The differences in results for the nonlinear elastic model are substantial when comparing Poisson's ratio values of 0.0 and 0.2.

RSI-1487-04-007

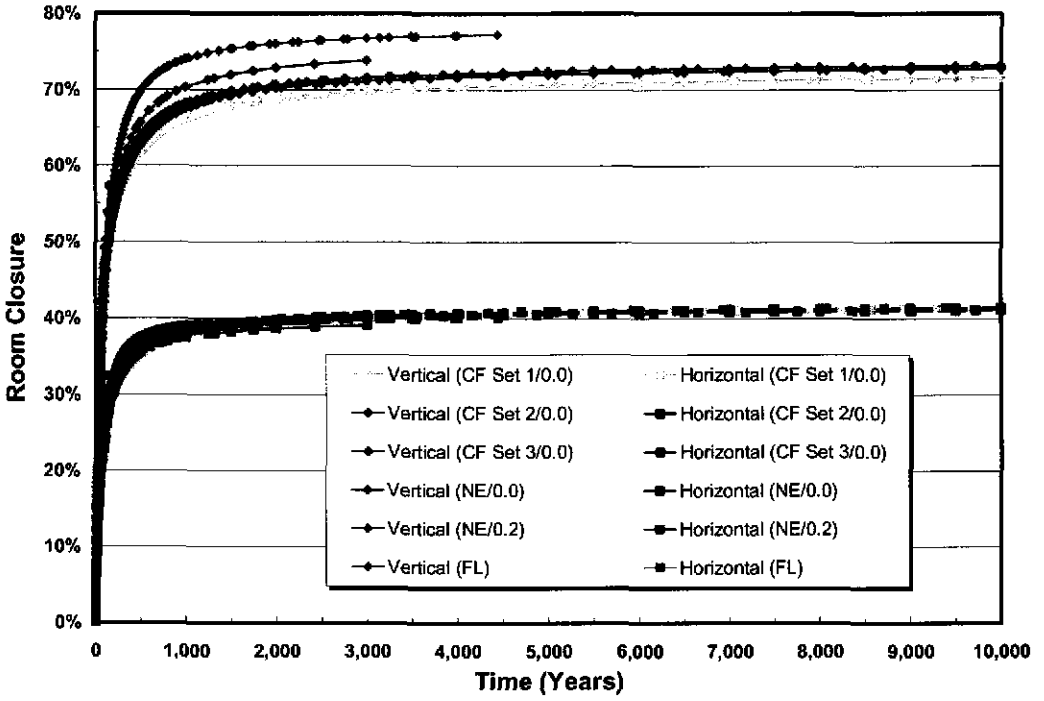

Figure 8-1. Comparison of Vertical and Horizontal Room Closures Through 10,000 Years.

RSI-1487-04-008

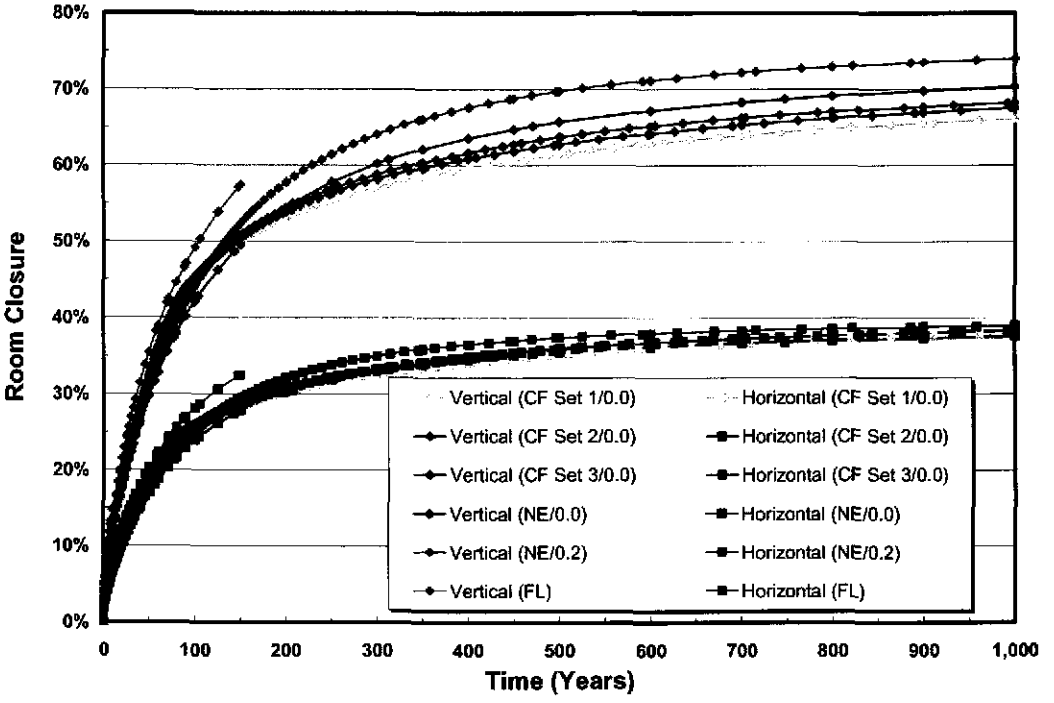

Figure 8-2. Comparison of Vertical and Horizontal Room Closures Through 1,000 Years.

RSI-1487-04-009

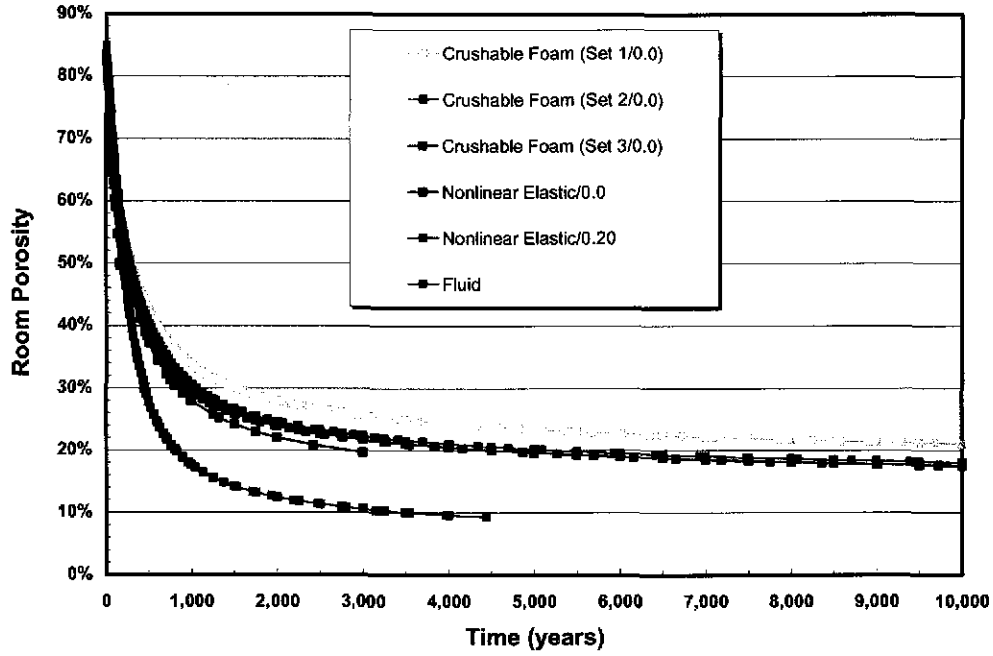

Figure 8-3. Comparison of Average Room Porosities Through 10,000 Years.

RSI-1487-04-010

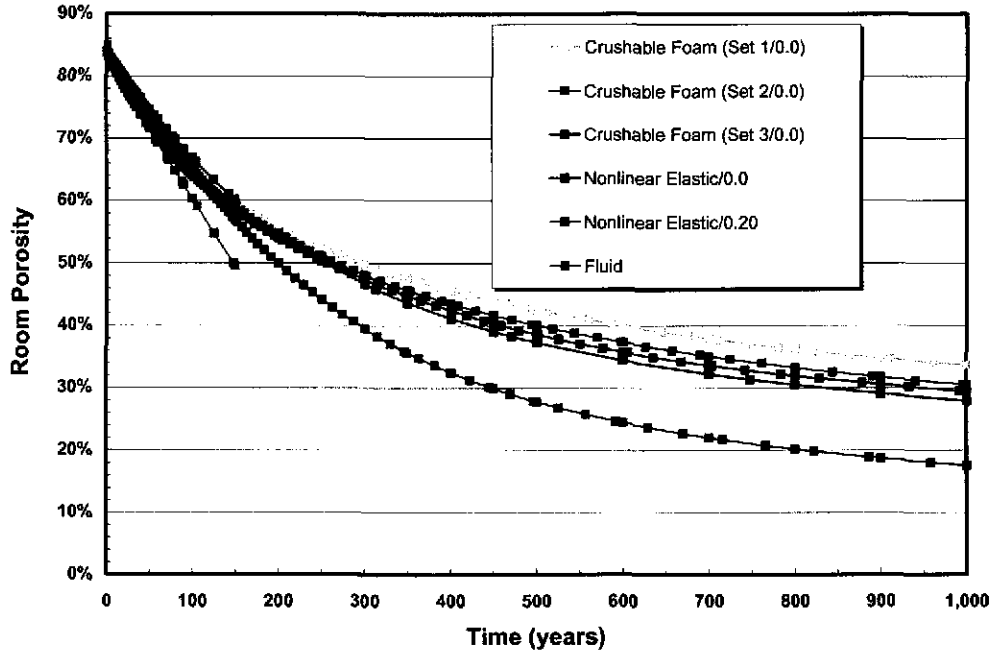

Figure 8-4. Comparison of Average Room Porosities Through 1,000 Years.

RSI-1487-04-011

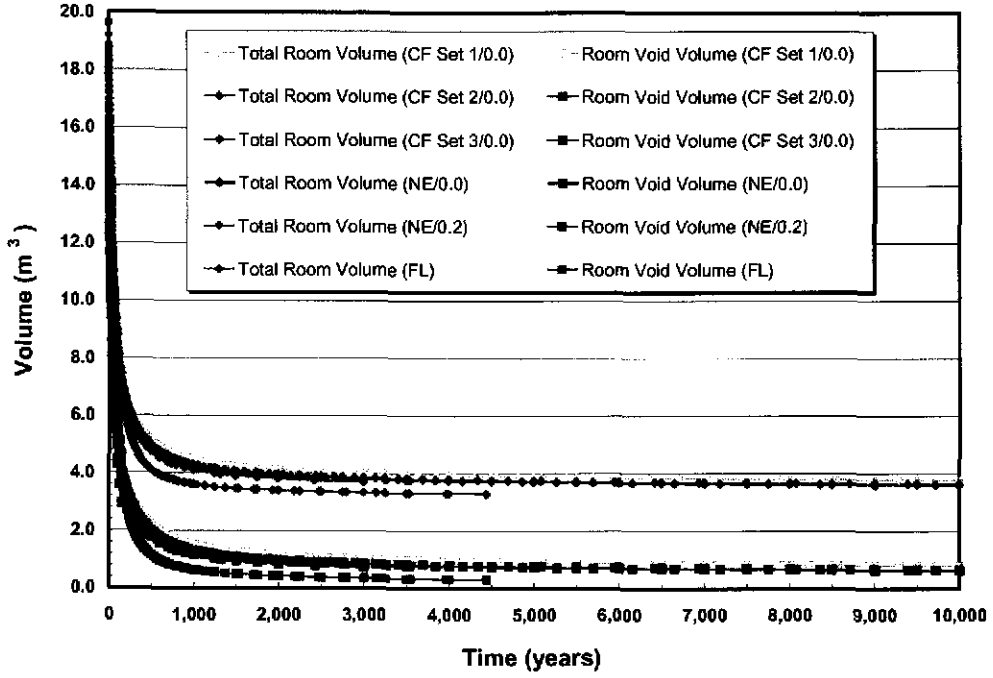

Figure 8-5. Comparison of Room Total and Void Volumes per Unit Depth Through 10,000 Years.

RSI-1487-04-012

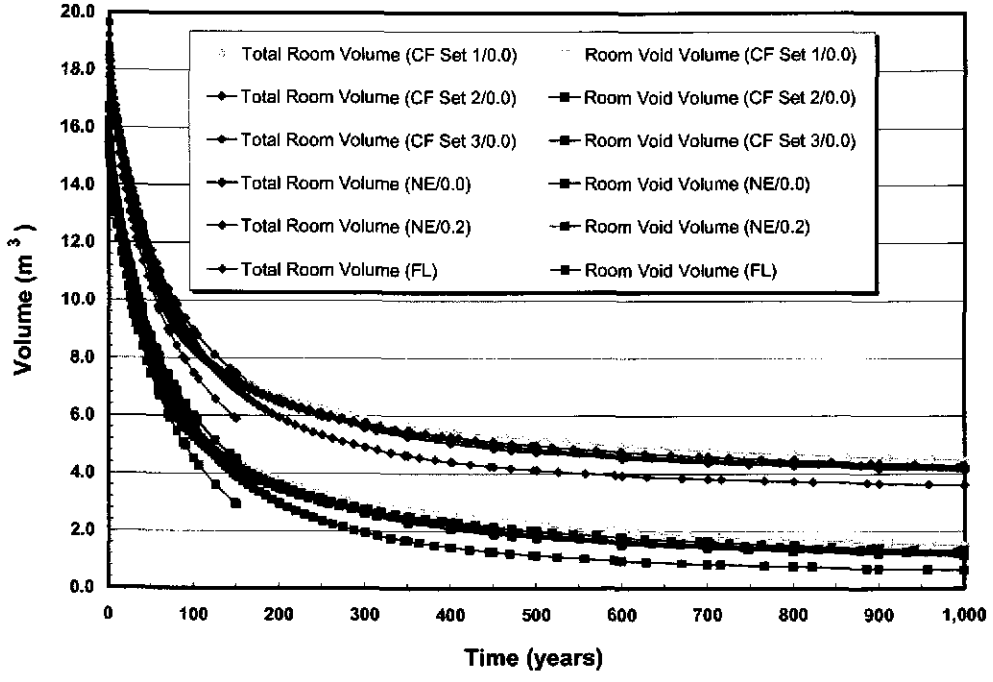

Figure 8-6. Comparison of Room Total and Void Volumes per Unit Depth Through 1,000 Years.

RSI-1487-04-046

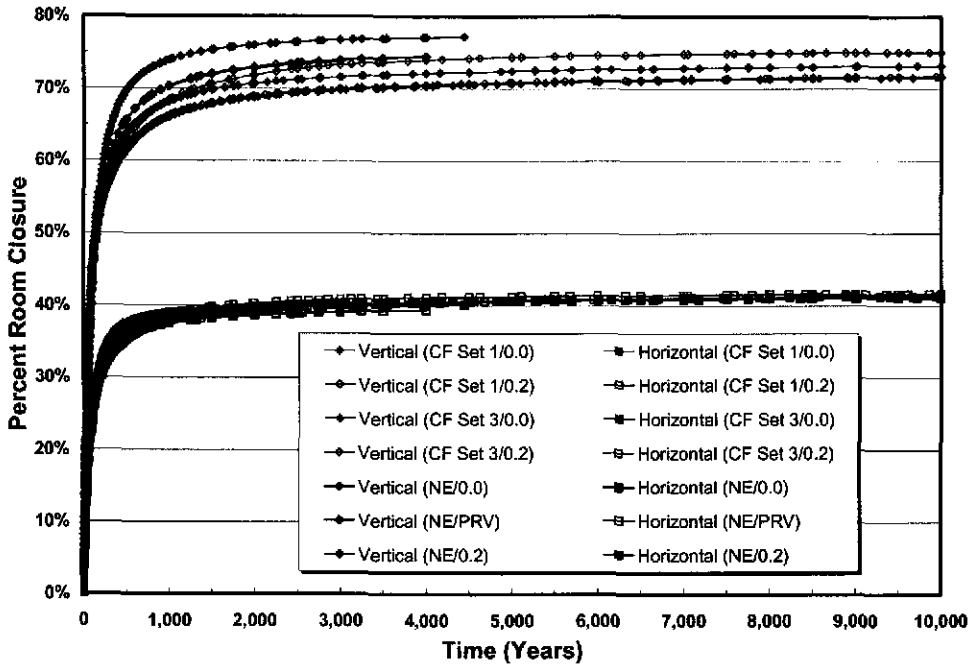

Figure 8-7. Comparison of Vertical and Horizontal Room Closures With Different Poisson's Ratios Through 10,000 Years.

RSI-1487-04-047

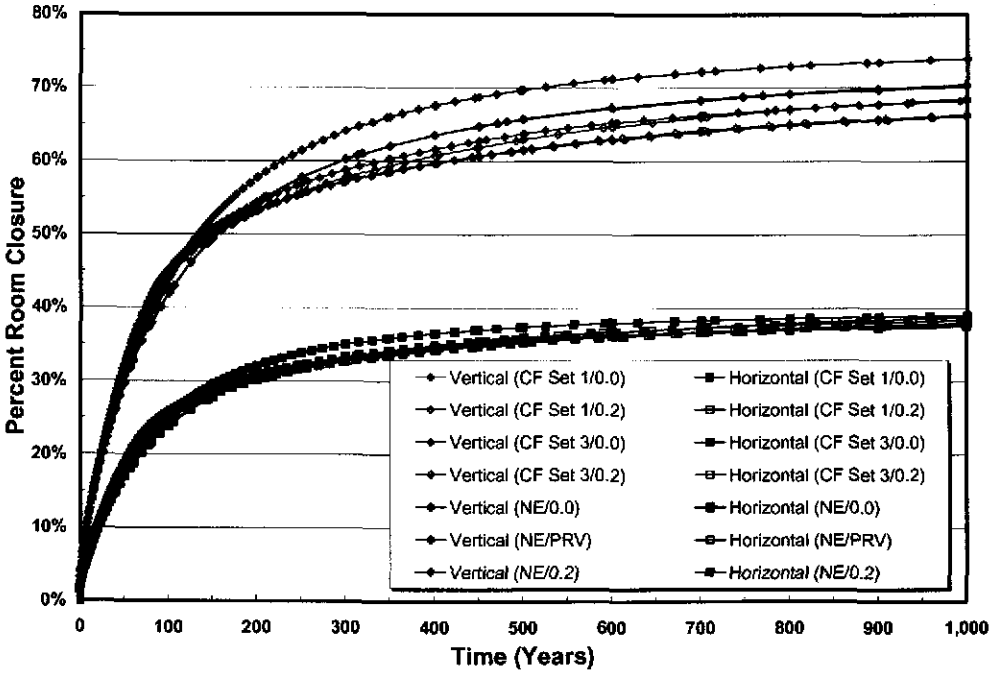

Figure 8-8. Comparison of Vertical and Horizontal Room Closures With Different Poisson's Ratios Through 1,000 Years.

RSI-1487-04-048

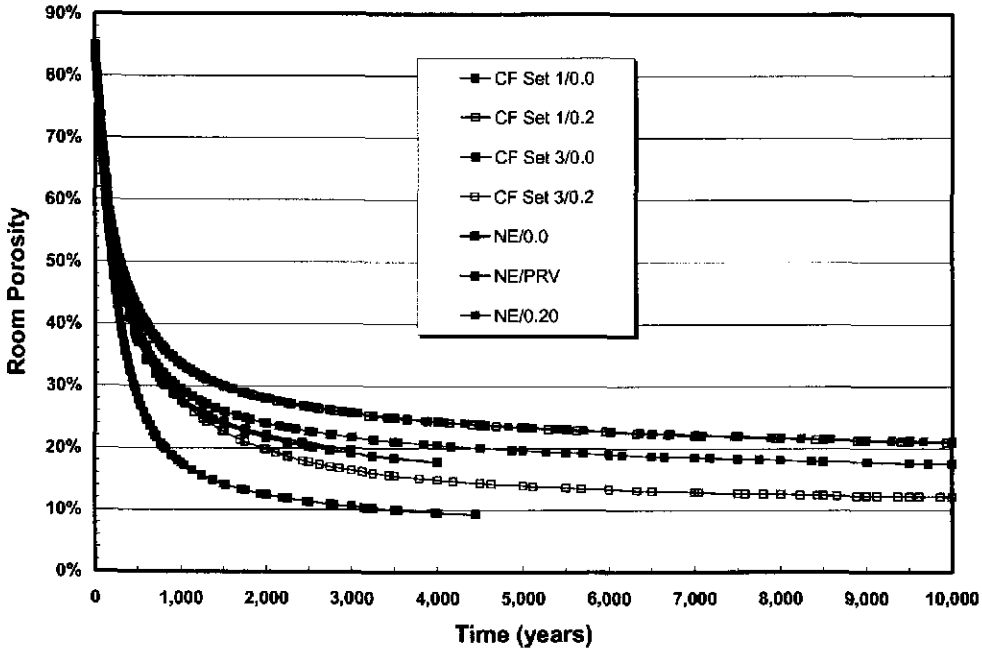

Figure 8-9. Comparison of Average Room Porosities With Different Poisson's Ratios Through 10,000 Years.

RSI-1487-04-049

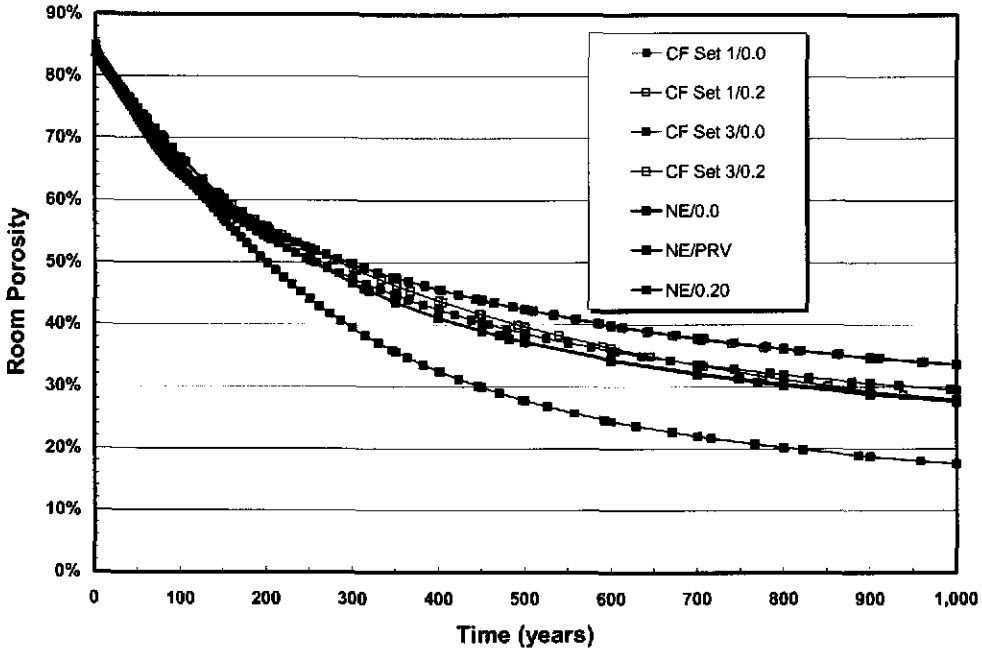

Figure 8-10. Comparison of Average Room Porosities With Different Poisson's Ratios Through 1,000 Years.

RSI-1487-04-050

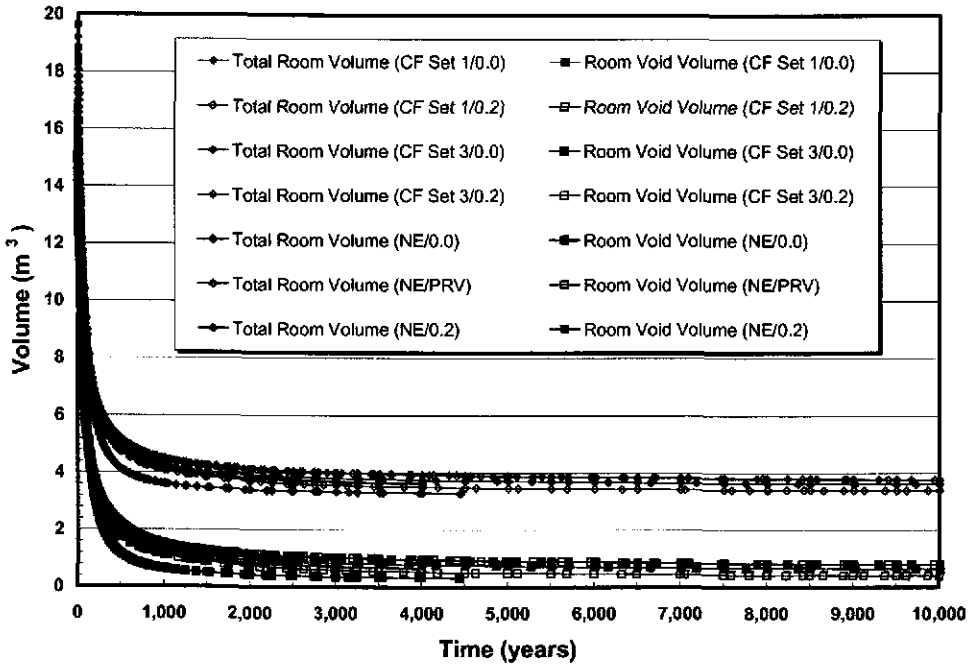

Figure 8-11. Comparison of Room Total and Void Volumes per Unit Depth With Different Poisson's Ratios Through 10,000 Years.

RSI-1487-04-051

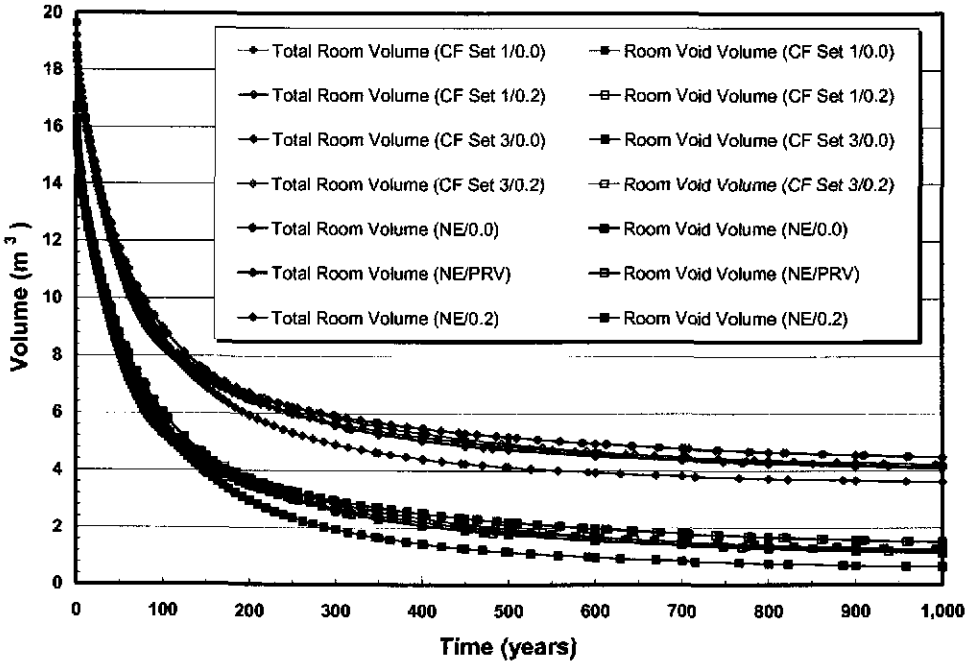

Figure 8-12. Comparison of Room Total and Void Volumes per Unit Depth With Different Poisson's Ratios Through 1,000 Years.

However, the differences between the variable Poisson's ratio (Equation 4-12) and Poisson's ratio equal to zero are almost imperceptible. These results are very similar because the variable Poisson's ratio is nearly zero while much of the deformation and loading occurs in the waste (see Figure 4-4). These conclusions are valid even though the analyses did not reach 10,000 years. If the assumption is made that the variable Poisson's ratio analysis room porosity (Figure 8-9) decreased another 5 percent between 4,000 years and 10,000 years (i.e., from 17.73 percent to 12.73 percent), the value for the average room Poisson's ratio at 10,000 years would be about 0.07; whereas, the value for the average room Poisson's ratio at 4,000 years is about 0.05. This moderate value for and change in Poisson's ratio from 4,000 to 10,000 years would not be expected to cause significant differences in the zero and variable Poisson's ratio analysis results. For Poisson's ratio equal to zero, the nonlinear elastic out-of-plane stress results remain zero, but for the variable Poisson's ratio, the out-of-plane stresses increase moderately in compression to values less than 1 MPa. A variable Poisson's ratio that evolves with the reduction in porosity in the waste is probably the most realistic representation of the waste; however, Poisson's ratio equal to zero can be used to obtain virtually identical porosity results.

The impact of gas generation on room closure, room porosity, room volume, and room pressure for the crushable foam and nonlinear elastic models are shown using results through time for Analyses 6, 10, 11, and 12 in Figures 8-13 through 8-20. Again, for each plotted variable, two figures are presented – one with a time scale through 10,000 years and one with a time scale through 1,000 years. Regardless of the TRU waste constitutive model used, the results are quite close. With gas generation, room deformation is reduced, and the amount of load transferred to the waste is reduced. Therefore, the properties of the waste become inconsequential. Very little difference is seen between the results of the nonlinear elastic analyses with gas generation ($f = 0.4$) for Poisson's ratio of zero and the variable Poisson's ratio (Equation 4-12). The room porosity and room pressure results are shown for the **SANTOS**[1] calculation [Stone, 1997] in Figures 8-15, 8-16, 8-19, and 8-20. The **SANTOS** room porosity results are within a few percent of those obtained using the nonlinear elastic model. The **SANTOS** room pressures are higher than the pressures obtained using the nonlinear elastic model, which is consistent with the lower room porosities. These differences are most likely attributable to the different geometric modeling methods used for the waste in the room.

Appendix A includes additional results for each of the analyses. Note that the plotted variables are not included for all of the analyses. Five different element locations within the room are compared in some of the figures: (1) room center near the roof (roof center), (2) room center (room center), (3) room center near the floor (floor center), (4) near the upper right-hand corner of the room (upper corner), and (5) at the pillar midheight near the rib (rib).

[1] Calculations performed using **SANTOS** for the Compliance Certification Application (CCA) as reported by Stone [1997].

RSI-1487-04-052

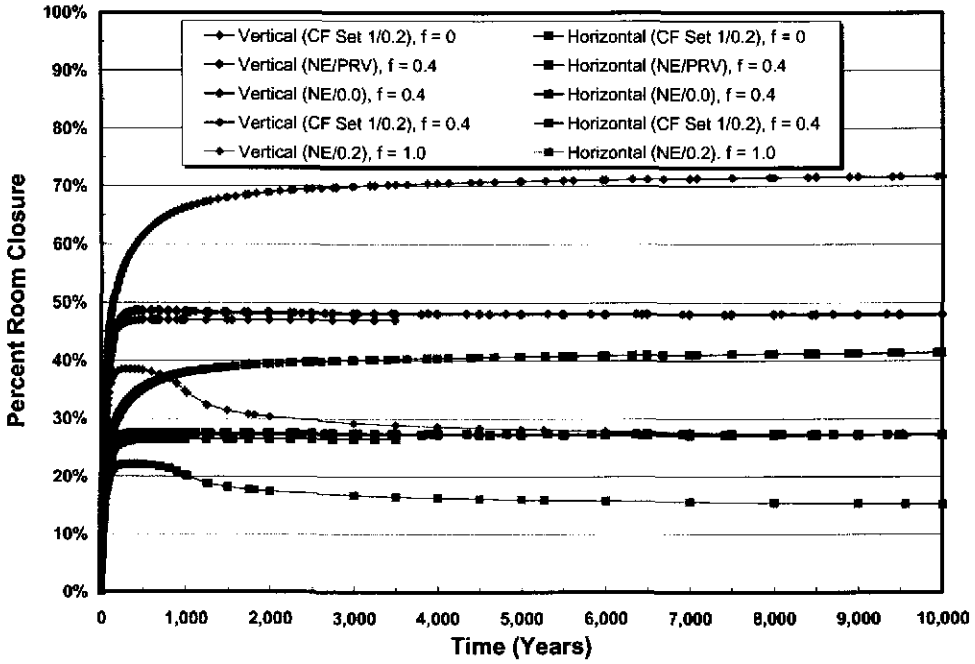

Figure 8-13. Comparison of Vertical and Horizontal Room Closures With Gas Generation Through 10,000 Years.

RSI-1487-04-053

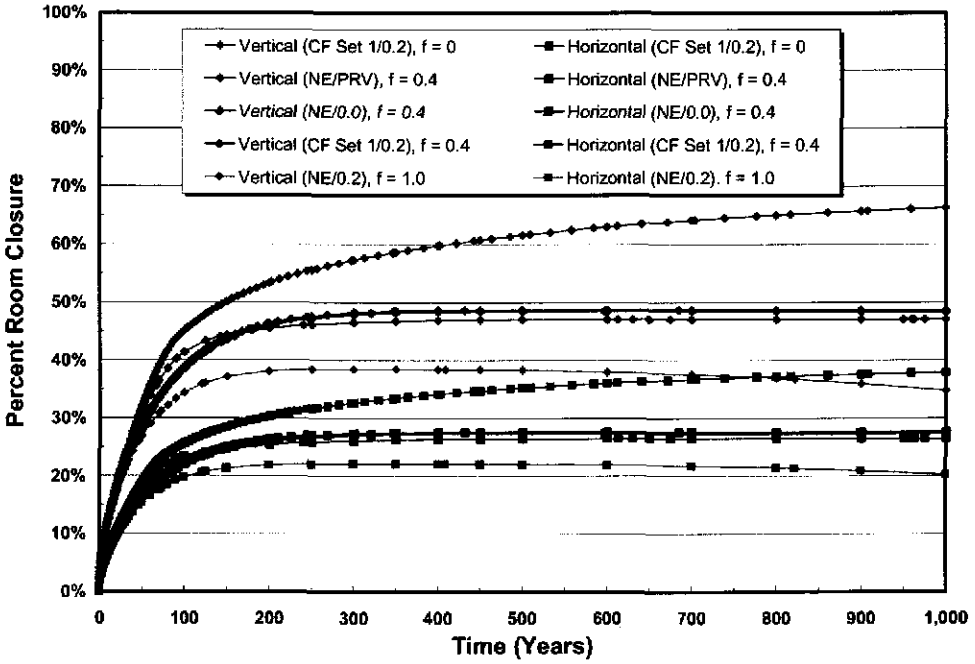

Figure 8-14. Comparison of Vertical and Horizontal Room Closures With Gas Generation Through 1,000 Years.

RSI-1487-04-054

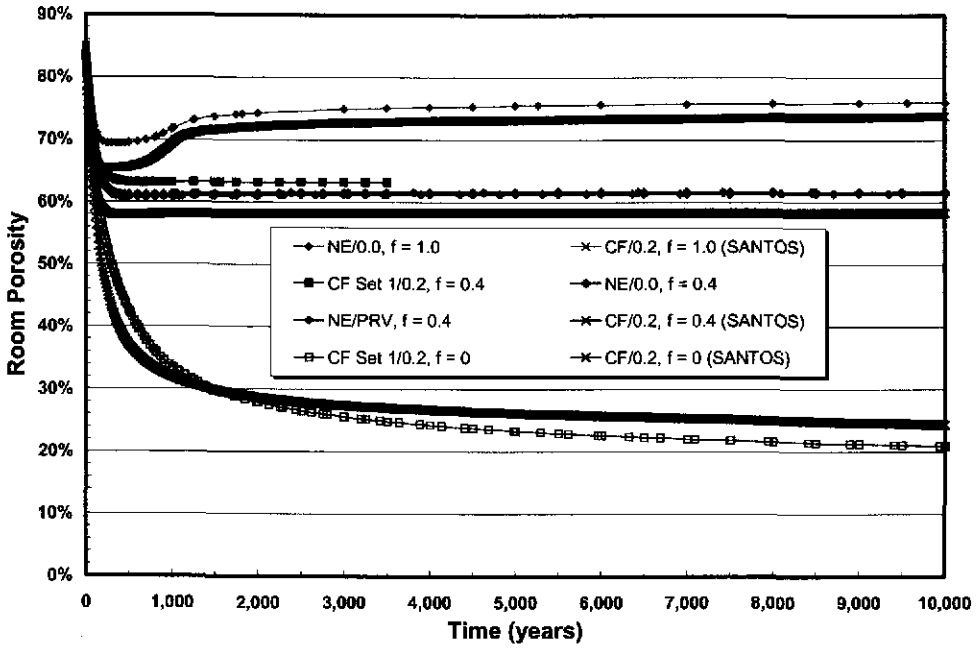

Figure 8-15. Comparison of Average Room Porosities With Gas Generation Through 10,000 Years.

RSI-1487-04-055

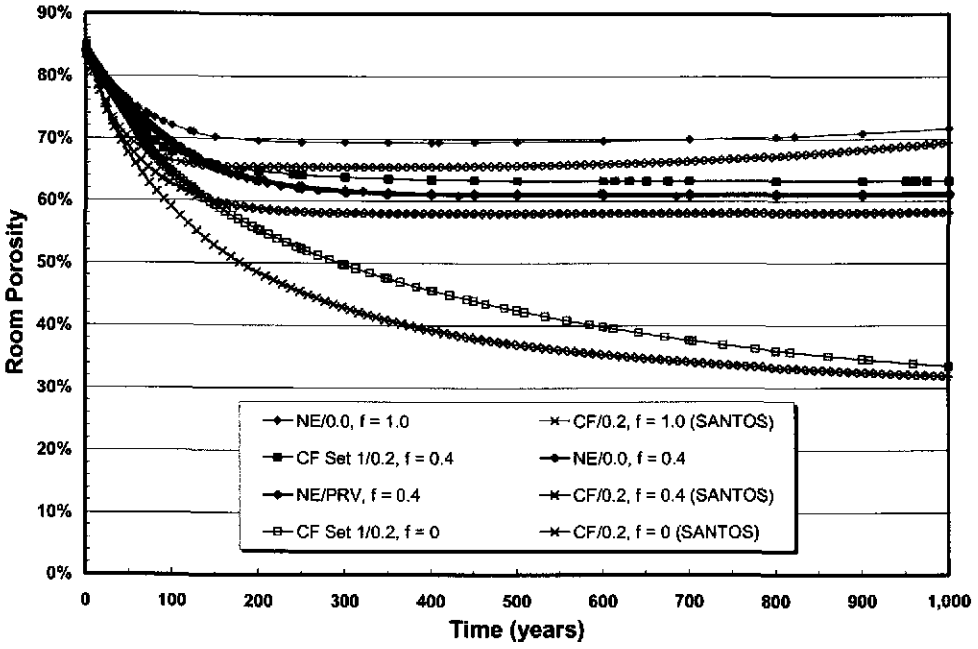

Figure 8-16. Comparison of Average Room Porosities With Gas Generation Through 1,000 Years.

RSI-1487-04-056

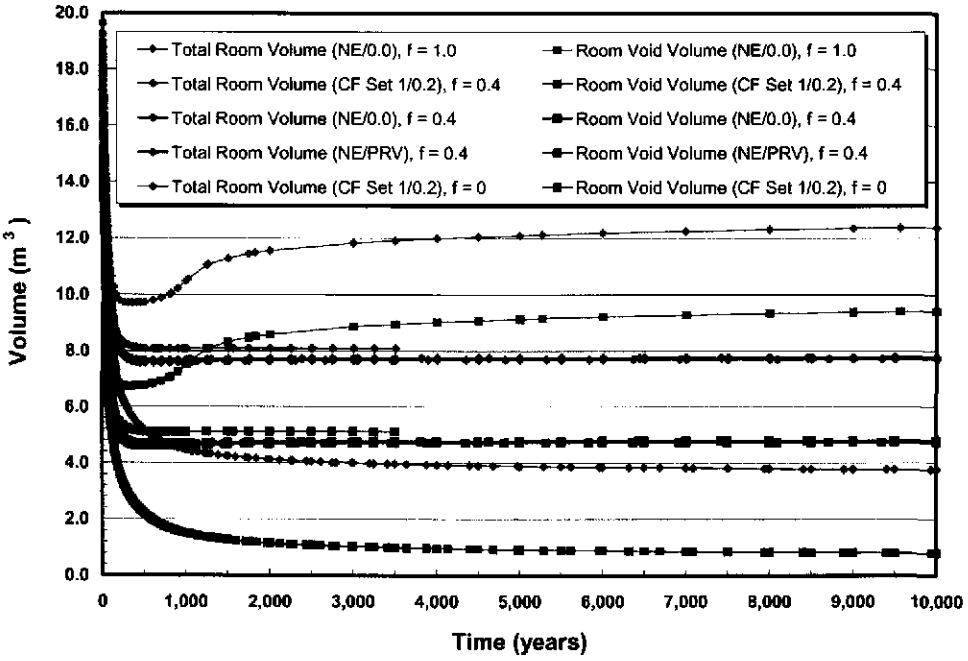

Figure 8-17. Comparison of Room Total and Void Volumes per Unit Depth With Gas Generation Through 10,000 Years.

RSI-1487-04-057

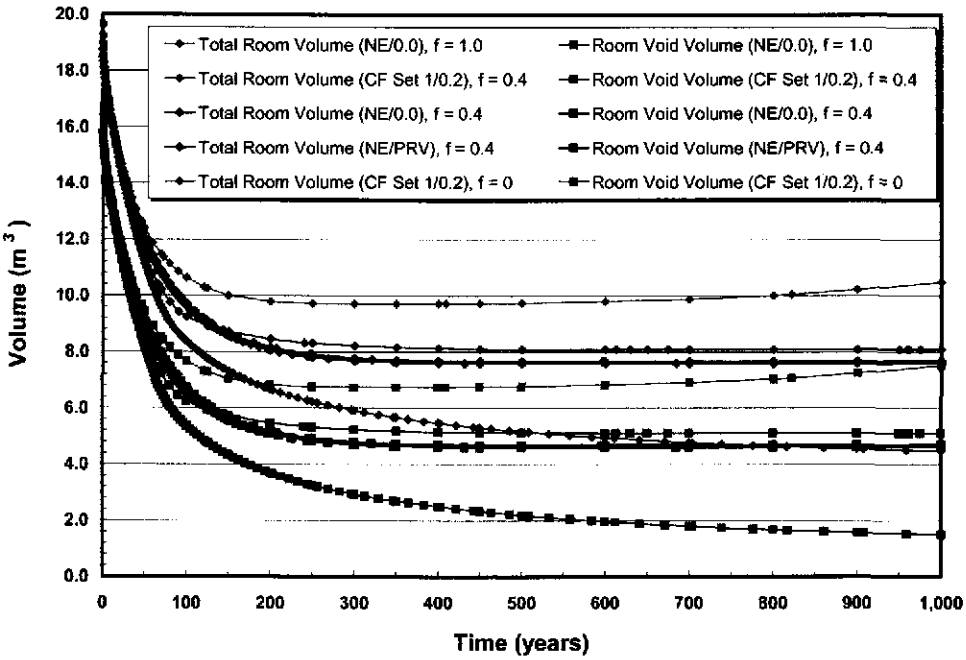

Figure 8-18. Comparison of Room Total and Void Volumes per Unit Depth With Gas Generation Through 1,000 Years.

RSI-1487-04-058

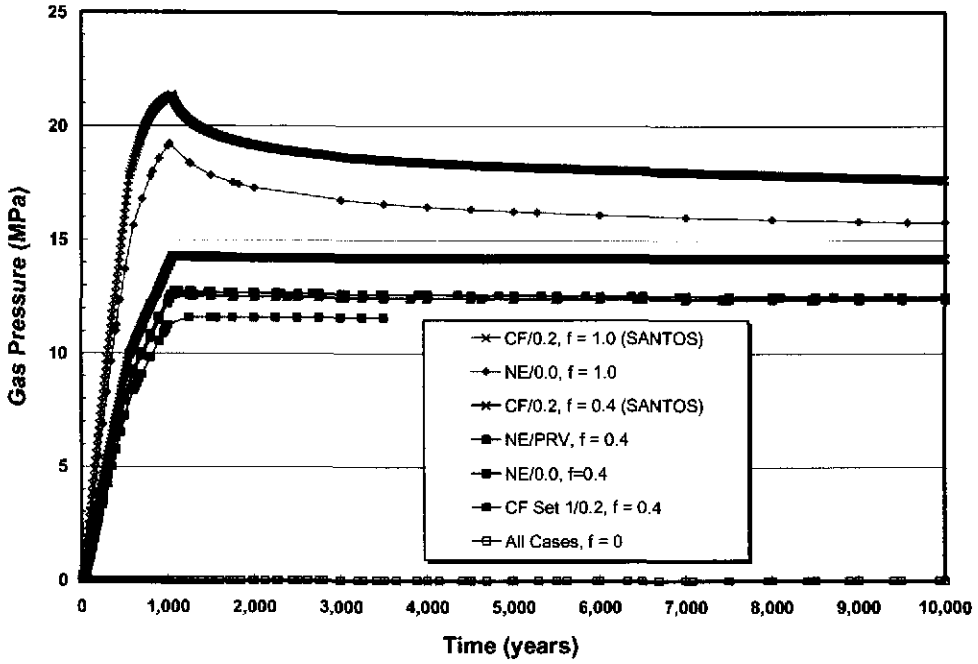

Figure 8-19. Comparison of Gas-Generated Room Pressures Through 10,000 Years.

RSI-1487-04-059

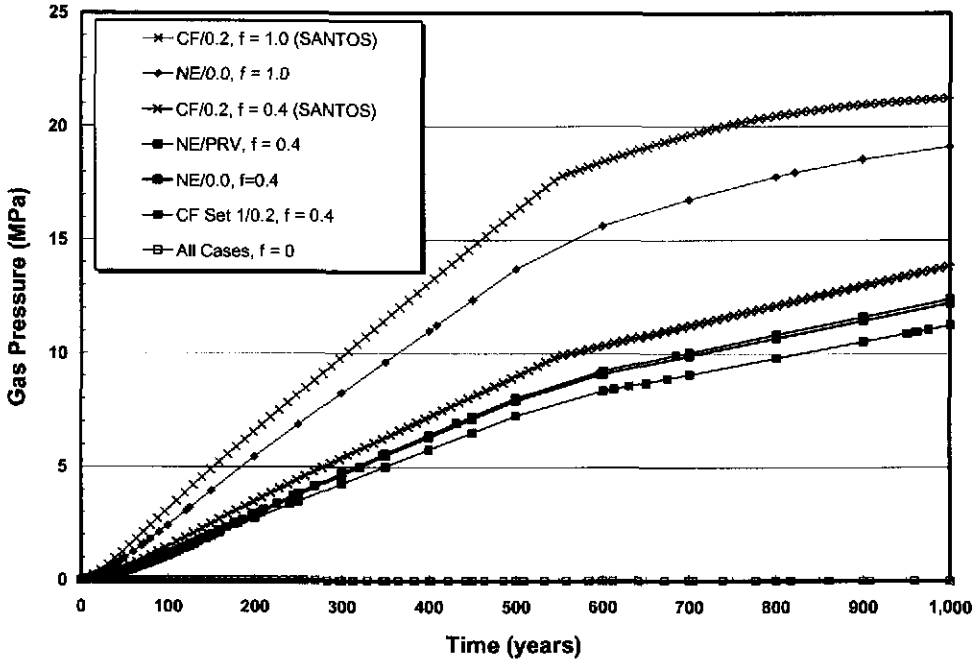

Figure 8-20. Comparison of Gas-Generated Room Pressures Through 1,000 Years.

The appendix includes plots of mean stress versus volumetric strain, mean stress versus time (excludes fluid), out-of-plane stress versus time (excludes fluid), elemental porosity (excludes fluid), and stress distributions from the centerline of the room to the centerline of the pillar near the pillar midheight for various times. Elemental porosity plots at different locations within the room are given for the crushable foam (Figures A-28 through A-32 and A-36) and nonlinear elastic (Figures A-33 through A-35 and A-37 through A-39) analyses. The crushable foam waste representation used a gap-element methodology where the room elements were initially air that converted to TRU waste after the appropriate porosity was reached (i.e., 68.2 percent). The nonlinear elastic model used a translated pressure-volumetric strain relationship for the TRU waste (see Table 4-1 and Figure 4-3) that reproduced the waste behavior after the appropriate porosity was reached. Room periphery plots are compared for each of the analyses at their final calculated configuration in Figure A-41. Deformed mesh configurations at the final recorded simulations times are also included in Appendix A (Figures A-42 through A-54) for each of the analyses.

9.0 SUMMARY

The crushable foam elastic-plastic, nonlinear elastic, and fluid material models used to model TRU waste compaction are presented as they were incorporated into **SPECTROM-32**. Simple example problems are included, which compare the nonlinear elastic and crushable foam plasticity models used to model TRU waste. The simple example problems show that the nonlinear elastic and crushable foam plasticity models produce the same volumetric behavior under the same loading conditions. WIPP disposal room analyses are compared to examine the differences in results produced by the different constitutive models assumed to represent the TRU waste. The three different TRU waste constitutive models examined provide distinct differences in their representation of the TRU waste. The volumetric behavior of the initially highly porous TRU waste is of primary interest, but its deviatoric response also affects the resulting deformation and stresses. The volumetric behavior for all three models used in this study is the same, i.e., the mean stress-volumetric strain description is essentially identical for every model. Therefore, differences in results obtained in the analyses are created exclusively by the model's prescribed deviatoric response along with any associated changes in mean stress, which affects the associated volumetric behavior.

The range in results obtained shows that the most important factor among the models is probably the resulting out-of-plane stress and its effect on the mean stress when no gas generation is included in the analyses. The two items that impact the out-of-plane stress most in these analyses are Poisson's ratio and the crushable foam deviatoric yield envelope. Calculations with the crushable foam model produced out-of-plane tensile stresses (as a product of the two-dimensional, plane-strain assumption) about the same magnitude as those calculated by **SANTOS**[2] when the equivalent crushable foam deviatoric model was used. However, the magnitude of the out-of-plane stresses can be controlled by changes in the crushable foam deviatoric plastic envelope and Poisson's ratio. Modification of Poisson's ratio and the crushable foam deviatoric parameters produces more realistic states of stress that include out-of-plane stresses that are not always tensile.

The alternative nonlinear elastic TRU waste model reproduced the volumetric behavior of the waste and did not produce out-of-plane tensile stresses. The magnitude of these out-of-plane stresses can also be controlled by changes in Poisson's ratio. The nonlinear elastic model produces more realistic states of stress in the waste, which results in higher mean stresses than the comparable crushable foam calculation. The higher mean stresses result in moderately lower room porosity values than those obtained with the crushable foam model in the **SANTOS** analyses without gas generation. However, when gas generation is included in the calculations, the importance of the mechanical behavior of the waste diminishes, and the

[2] Calculations performed using **SANTOS** for the Compliance Certification Application (CCA) as reported by Stone [1997].

nonlinear elastic model produces room porosity values about the same as those obtained with **SANTOS** and the crushable foam model.

Without gas generation, the stress states in the waste modeled with the nonlinear elastic constitutive relation show the same general trends and magnitudes as those computed using **SANTOS**. This stress state is reflected by the vertical stress being the largest compressive stress and closest to the lithostatic stress value, the horizontal stress perpendicular to the drift is the intermediate stress with a value about one-half the vertical stress, and the out-of-plane stress parallel to the drift is the smallest compressive stress value whose value may be as low as zero when Poisson's ratio is assumed to be zero. With gas generation, the stress levels in all directions within the waste are significantly diminished (only a few MPa when $f = 0.4$), but the same general stress component magnitude ordering and ratios are maintained among the stress components.

Improvement to the TRU waste model can be obtained by using the nonlinear elastic model, which eliminates the out-of-plane tensile stresses or by changing parameter values in the deviatoric portion of the crushable foam model, which can also eliminate the out-of-plane tensile stresses. Neither of these TRU waste model modifications changes the fundamental waste behavior; however, the global response of the pillar and drift would change resulting in moderately lower room porosities. The uncertainty in the constitutive model for the waste is minor and inconsequential in cases involving moderate gas generation because the presence of the waste is overshadowed by the support provided by the generated gas pressures.

Based on the results obtained for the different constitutive model representations of the TRU waste, the following observations are made:

Elastic-plastic crushable foam material (CF)

- Some of the analyses were conducted for a Poisson's ratio value of zero; thus, the room closure impingement and subsequent loading of the waste did not contribute to changes in the out-of-plane stress. The cases run with a Poisson's ratio of 0.2 reduce the magnitude of the out-of-plane tensile stresses, but the global change in the room and waste behavior is small (see Figures 8-7 through 8-12).
- The mean stresses for the TRU waste are always compressive; thus, the tensile limit portion of the model (Equation 3-11) was never activated and did not influence the results.
- All three deviatoric parameter value sets resulted in excursions of the out-of-plane stress into the tensile regime. This occurs because of the plane-strain analysis requirement that the total out-of-plane strain be zero (see Equation 1-1). The volumetric compaction portion of the model results in an elastic strain equal and opposite to the inelastic compaction strain causing the tensile stresses. The appearance of tensile stresses

increases the magnitude of the deviatoric stresses. The magnitude of the deviatoric stress along with the out-of-plane tensile stress is limited by the deviatoric envelope for the model (see Figure 3-1). Thus the deviatoric response of the waste alters the mean stress and influences the average room porosities. This is observed in the out-of-plane stress results in Figures A-12 through A-16 and the porosity results in Figures A-28 through A-32 for the three different assumed deviatoric parameter sets.

- The crushable foam model representation of the TRU waste model using Stone [1997] deviatoric parameters results in the largest average room porosity values.
- Differences in results compared to the nonlinear elastic model diminish as the gas generation rate increases.
- The mean stresses and porosities are variable throughout the disposal room.

Nonlinear elastic material (NE)

- Analyses were conducted for Poisson's ratio values of 0.0, 0.2, and a variable Poisson's ratio that changes as a function of the waste density. For Poisson's ratio equal to 0.0, the room closure loading did not contribute to changes in the out-of-plane stress. For Poisson's ratio equal to 0.2, out-of-plane stresses are generated by the room closure loading on the waste (cf., Figures A-17 and A-18). The out-of-plane stresses increase the mean stresses in the waste, resulting in more compaction of the waste and lower porosity values. Global room closure and porosities are virtually identical for the variable Poisson's ratio and Poisson's ratio equal to zero with or without gas generation (see Figures 8-7 though 8-20).
- The mean stresses for the TRU waste are always compressive.
- The out-of-plane stresses are never tensile.
- The nonlinear elastic model representation of the TRU waste results in lower average room porosity values than those obtained using the crushable foam representation when there is no gas generation.
- Differences in results compared to the crushable foam model diminish as the gas generation rate increases.
- The mean stresses and porosities are variable throughout the disposal room.

Fluid material (FL)

- The fluid model representation of the TRU waste removes all influences of out-of-plane stress and deviatoric waste response from the results.
- Mean stresses and out-of-plane stresses are nonexistent in the fluid model representation because the bulk waste behavior is simulated by a room periphery

traction equivalent to the pressure generated by the TRU waste pressure-volumetric strain relationship.

- The fluid model representation of the TRU waste results in the lowest average room porosity values.
- The fluid model representation of the TRU waste is implemented using extremely low stiffness elements ("air elements"). The combined effects of the low stiffness material and no deviatoric or out-of-plane stress influences result in an easily deformable material that rapidly experiences severe mesh distortion and halts execution.

The deviatoric response of the TRU waste appears to influence the calculational results. The volumetric response of the waste given by Stone [1997] and listed in Table 3-1 is attributed to data collected from uniaxial waste drum tests reported by Butcher [1997]. However, the last data point at 12 MPa is an extrapolation of Butcher's data. Unfortunately, the deviatoric response of the TRU waste has not received any experimental attention. Hansen and Mellegard [1998] conducted a laboratory investigation into the physical and mechanical properties of degraded waste surrogate materials, but the suite of tensile, uniaxial, and triaxial compression tests only included three triaxial tests, two of which were used for permeability testing. Despite the conductance of only a few triaxial tests and in the absence of any other experimental data, their collective test results could potentially be used to provide some guidance for refinement the crushable foam model.

Despite the fairly significant differences in the constitutive models, the ultimate total room and void volumes differences may not be significant from a performance assessment perspective. The example problems show that the crushable foam and nonlinear elastic models can produce the same results when subjected to the same stress fields. However, in plane-strain analyses, the out-of-plane stress varies considerably. A reasonable expectation is that as the TRU waste compresses, tensile stresses will not be generated in the waste along the length of the disposal room. Based on the expected behavior of the porous TRU waste and the results of this study, the nonlinear elastic model is probably more representative of the mechanical behavior of the TRU waste. Therefore, the average disposal room porosity values may be somewhat lower than the minimum porosity values computed earlier by Stone [1997]. However, this conclusion only applies to those cases where the gas generation rate is zero. Even with the alternate TRU waste models examined in this study, inclusion of gas generation serves to reduce room closure, results in increased room porosity values, and reduces the differences in results between the two waste models.

10.0 REFERENCES

Butcher, B. M., 1997. *A Summary of the Sources of Input Parameter Values for the WIPP Final Porosity Surface Calculations,* SAND97-0796, Sandia National Laboratories, Albuquerque, NM.

Callahan, G. D., 2002. *Documentation of SPECTROM-32: A Finite Element Thermomechanical Stress Analysis Program,* Revision 1, prepared by RESPEC, Rapid City, SD, Vol. I and II.

Callahan, G. D. and K. L. DeVries, 1991. *Analyses of Backfilled Transuranic Waste Storage Rooms,* SAND91-7052, prepared by RESPEC, Rapid City, SD, for Sandia National Laboratories, Albuquerque, NM.

Callahan, G. D., A. F. Fossum, and D. K. Svalstad, 1989. *Documentation of SPECTROM-32: A Finite Element Thermomechanical Stress Analysis Program,* DOE/CH/ 10378-2, prepared by RE/SPEC Inc., Rapid City, SD, for the U.S. Department of Energy, Chicago Operations Office, Argonne, IL, Vol. I and II.

Chen, W. F. and D. J. Han, 1988. *Plasticity for Structural Engineers,* Springer-Verglag, New York, NY.

Hansen, F. D. and K. D. Mellegard, 1998. "Physical and Mechanical Properties of Degraded Waste Surrogate Materials," *Proceedings, 3rd North American Rock Mechanics Symposium,* Cancún, Mexico, June 3–5, published in *International Journal of Rock Mechanics and Mining Sciences,* Vol. 35, No. 4/5, Paper No. 018.

Munson, D. E., and P. R. Dawson, 1982. *A Transient Creep Model for Salt During Stress Loading and Unloading,* SAND82-0962, Sandia National Laboratories, Albuquerque, NM.

Munson, D. E., A. F. Fossum, and P. E. Senseny 1989. *Advances in Resolution of Discrepancies Between Predicted and Measured In Situ WIPP Room Closures,* SAND88-2948, Sandia National Laboratories, Albuquerque, NM.

Sandler, I. S., F. L. DiMaggio, and G. Y. Baladi, 1976. "Generalized Cap Model for Geological Materials," *Journal of the Geotechnical Engineering Division,* ASCE, Vol. 102, No. GT7, July, pp. 683–699.

Stone, C. M., R. D. Krieg, and Z. E. Beisinger, 1985. *SANCHO: A Finite Element Computer Program for the Quasistatic, Large Deformation, Inelastic Response of Two-Dimensional Solids,* SAND84-2618, Sandia National Laboratories, Albuquerque, NM.

Stone, C. M., 1997. *Final Disposal Room Structural Response Calculations,* SAND97-0795, Sandia National Laboratories, Albuquerque, NM.

Stone, C. M., 1990. *SANTOS–A Two-Dimensional Finite Element Program for the Quasistatic, Large Deformation, Inelastic Response Solids,* SAND90-0543, Sandia National Laboratories, Albuquerque, NM.

APPENDIX A
ANALYSIS RESULTS

APPENDIX A
ANALYSIS RESULTS

Figure No.	Title
A-1	Mean Stress Versus Volumetric Strain at Five Locations Within the Room for the Crushable Foam Analysis (ν = 0.0) Using Parameter Set 1.
A-2	Mean Stress Versus Volumetric Strain at Five Locations Within the Room for the Crushable Foam Analysis (ν = 0.0) Using Parameter Set 2.
A-3	Mean Stress Versus Volumetric Strain at Five Locations Within the Room for the Crushable Foam Analysis (ν = 0.0) Using Parameter Set 3.
A-4	Mean Stress Versus Volumetric Strain at Five Locations Within the Room for the Nonlinear Elastic (ν = 0.0) Analysis.
A-5	Mean Stress Versus Volumetric Strain at Five Locations Within the Room for the Nonlinear Elastic (ν = 0.2) Analysis.
A-6	Average Room Pressure Versus Volumetric Strain for the Fluid Analysis.
A-7	Mean Stress Versus Time at Five Locations Within the Room for the Crushable Foam Analysis (ν = 0.0) Using Parameter Set 1.
A-8	Mean Stress Versus Time at Five Locations Within the Room for the Crushable Foam Analysis (ν = 0.0) Using Parameter Set 2.
A-9	Mean Stress Versus Time at Five Locations Within the Room for the Crushable Foam Analysis (ν = 0.0) Using Parameter Set 3.
A-10	Mean Stress Versus Time at Five Locations Within the Room for the Nonlinear Elastic (ν = 0.0) Analysis.
A-11	Mean Stress Versus Time at Five Locations Within the Room for the Nonlinear Elastic (ν = 0.2) Analysis.
A-12	Out-of-Plane Stress Versus Time at Five Locations Within the Room for the Crushable Foam Analysis (ν = 0.0) Using Parameter Set 1.
A-13	Out-of-Plane Stress Versus Time at Five Locations Within the Room for the Crushable Foam Analysis (ν = 0.0) Using Parameter Set 2.
A-14	Out-of-Plane Stress Versus Time at Five Locations Within the Room for the Crushable Foam Analysis (ν = 0.0) Using Parameter Set 3.
A-15	Out-of-Plane Stress Versus Time at Five Locations Within the Room for the Crushable Foam Analysis (ν = 0.2) Using Parameter Set 1.
A-16	Out-of-Plane Stress Versus Time at Five Locations Within the Room for the Crushable Foam Analysis (ν = 0.2) Using Parameter Set 3.
A-17	Out-of-Plane Stress Versus Time at Five Locations Within the Room for the Nonlinear Elastic (ν = 0.0) Analysis.

Figure No.	Title
A-18	Out-of-Plane Stress Versus Time at Five Locations Within the Room for the Nonlinear Elastic ($\nu = 0.2$) Analysis.
A-19	Horizontal Stress Distribution (σ_{xx}) From the Room Centerline to the Pillar Centerline at Room Midheight for the Crushable Foam Analysis Using Parameter Set 1, Poisson's Ratio Equal to 0.2, and Gas Generation ($f = 0.4$).
A-20	Vertical Stress Distribution (σ_{yy}) From the Room Centerline to the Pillar Centerline at Room Midheight for the Crushable Foam Analysis Using Parameter Set 1, Poisson's Ratio Equal to 0.2, and Gas Generation ($f = 0.4$).
A-21	Out-of-Plane Stress Distribution (σ_{zz}) From the Room Centerline to the Pillar Centerline at Room Midheight for the Crushable Foam Analysis using Parameter Set 1, Poisson's Ratio Equal to 0.2, and Gas Generation ($f = 0.4$).
A-22	Horizontal Stress Distribution (σ_{xx}) From the Room Centerline to the Pillar Centerline at Room Midheight for the Nonlinear Elastic Analysis With a Variable Poisson's Ratio and No Gas Generation ($f = 0$).
A-23	Vertical Stress Distribution (σ_{yy}) From the Room Centerline to the Pillar Centerline at Room Midheight for the Nonlinear Elastic Analysis With a Variable Poisson's Ratio and No Gas Generation ($f = 0$).
A-24	Out-of-Plane Stress Distribution (σ_{zz}) From the Room Centerline to the Pillar Centerline at Room Midheight for the Nonlinear Elastic Analysis With a Variable Poisson's Ratio and No Gas Generation ($f = 0$).
A-25	Horizontal Stress Distribution (σ_{xx}) From the Room Centerline to the Pillar Centerline at Room Midheight for the Nonlinear Elastic Analysis With a Variable Poisson's Ratio and Gas Generation ($f = 0.4$).
A-26	Vertical Stress Distribution (σ_{yy}) From the Room Centerline to the Pillar Centerline at Room Midheight for the Nonlinear Elastic Analysis With a Variable Poisson's Ratio and Gas Generation ($f = 0.4$).
A-27	Out-of-Plane Stress Distribution (σ_{zz}) From the Room Centerline to the Pillar Centerline at Room Midheight for the Nonlinear Elastic Analysis With a Variable Poisson's Ratio and Gas Generation ($f = 0.4$).
A-28	Elemental Porosity Versus Time at Five Locations Within the Room for the Crushable Foam Analysis ($\nu = 0.0$) Using Parameter Set 1.
A-29	Elemental Porosity Versus Time at Five Locations Within the Room for the Crushable Foam Analysis ($\nu = 0.2$) Using Parameter Set 1.
A-30	Elemental Porosity Versus Time at Five Locations Within the Room for the Crushable Foam Analysis ($\nu = 0.0$) Using Parameter Set 2.
A-31	Elemental Porosity Versus Time at Five Locations Within the Room for the Crushable Foam Analysis ($\nu = 0.0$) Using Parameter Set 3.

Figure No.	Title
A-32	Elemental Porosity Versus Time at Five Locations Within the Room for the Crushable Foam Analysis ($\nu = 0.2$) Using Parameter Set 3.
A-33	Elemental Porosity Versus Time at Five Locations Within the Room for the Nonlinear Elastic ($\nu = 0.0$) Analysis.
A-34	Elemental Porosity Versus Time at Five Locations Within the Room for the Nonlinear Elastic ($\nu = 0.2$) Analysis.
A-35	Elemental Porosity Versus Time at Five Locations Within the Room for the Nonlinear Elastic (ν = Variable) Analysis.
A-36	Elemental Porosity Versus Time at Five Locations Within the Room for the Crushable Foam Analysis ($\nu = 0.2$) Using Parameter Set 1 With Gas Generation Rate $f = 0.4$.
A-37	Elemental Porosity Versus Time at Five Locations Within the Room for the Nonlinear Elastic ($\nu = 0.0$) Analysis With Gas Generation Rate $f = 1$.
A-38	Elemental Porosity Versus Time at Five Locations Within the Room for the Nonlinear Elastic ($\nu = 0.0$) Analysis With Gas Generation Rate $f = 0.4$.
A-39	Elemental Porosity Versus Time at Five Locations Within the Room for the Nonlinear Elastic (ν = Variable) Analysis With Gas Generation Rate $f = 0.4$.
A-40	Elemental Porosity Versus Time at Five Locations Within the Room for the Fluid Material Analysis.
A-41	Comparison of the Room Peripheries at Their Final Calculated Configuration for Each of the Analyses.
A-42	*Deformed Mesh Configuration for the Crushable Foam* Analysis Using Parameter Set 1 at 10,000 Years.
A-43	Deformed Mesh Configuration for the Crushable Foam Analysis Using Parameter Set 2 at 10,000 Years.
A-44	Deformed Mesh Configuration for the Crushable Foam Analysis Using Parameter Set 3 at 10,000 Years.
A-45	Deformed Mesh Configuration for the Crushable Foam Analysis Using Parameter Set 1 With Poisson's Ratio Equal to 0.2 at 10,000 Years.
A-46	Deformed Mesh Configuration for the Crushable Foam Analysis Using Parameter Set 3 With Poisson's Ratio Equal to 0.2 at 10,000 Years.
A-47	Deformed Mesh Configuration for the Crushable Foam Analysis Using Parameter Set 1 With Poisson's Ratio Equal to 0.0 Including Gas Generation ($f = 0.4$) at 3,500 Years.
A-48	Deformed Mesh Configuration for the Nonlinear Elastic ($\nu = 0.0$) Analysis at 3,000 Years.

Figure No.	Title
A-49	Deformed Mesh Configuration for the Nonlinear Elastic (ν = 0.2) Analysis at 4,443 Years.
A-50	Deformed Mesh Configuration for the Nonlinear Elastic Analysis With Variable Poisson's Ratio Including No Gas Generation (f = 0) at 4,000 Years.
A-51	Deformed Mesh Configuration for the Nonlinear Elastic Analysis With Poisson's Ratio Equal to 0.0 Including Gas Generation (f = 1) at 10,000 Years.
A-52	Deformed Mesh Configuration for the Nonlinear Elastic Analysis With Poisson's Ratio Equal to 0.0 Including Gas Generation (f = 0.4) at 10,000 Years.
A-53	Deformed Mesh Configuration for the Nonlinear Elastic Analysis With Variable Poisson's Ratio Including Gas Generation (f = 0.4) at 10,000 Years.
A-54	Deformed Mesh Configuration for the Fluid Analysis at 150 Years.

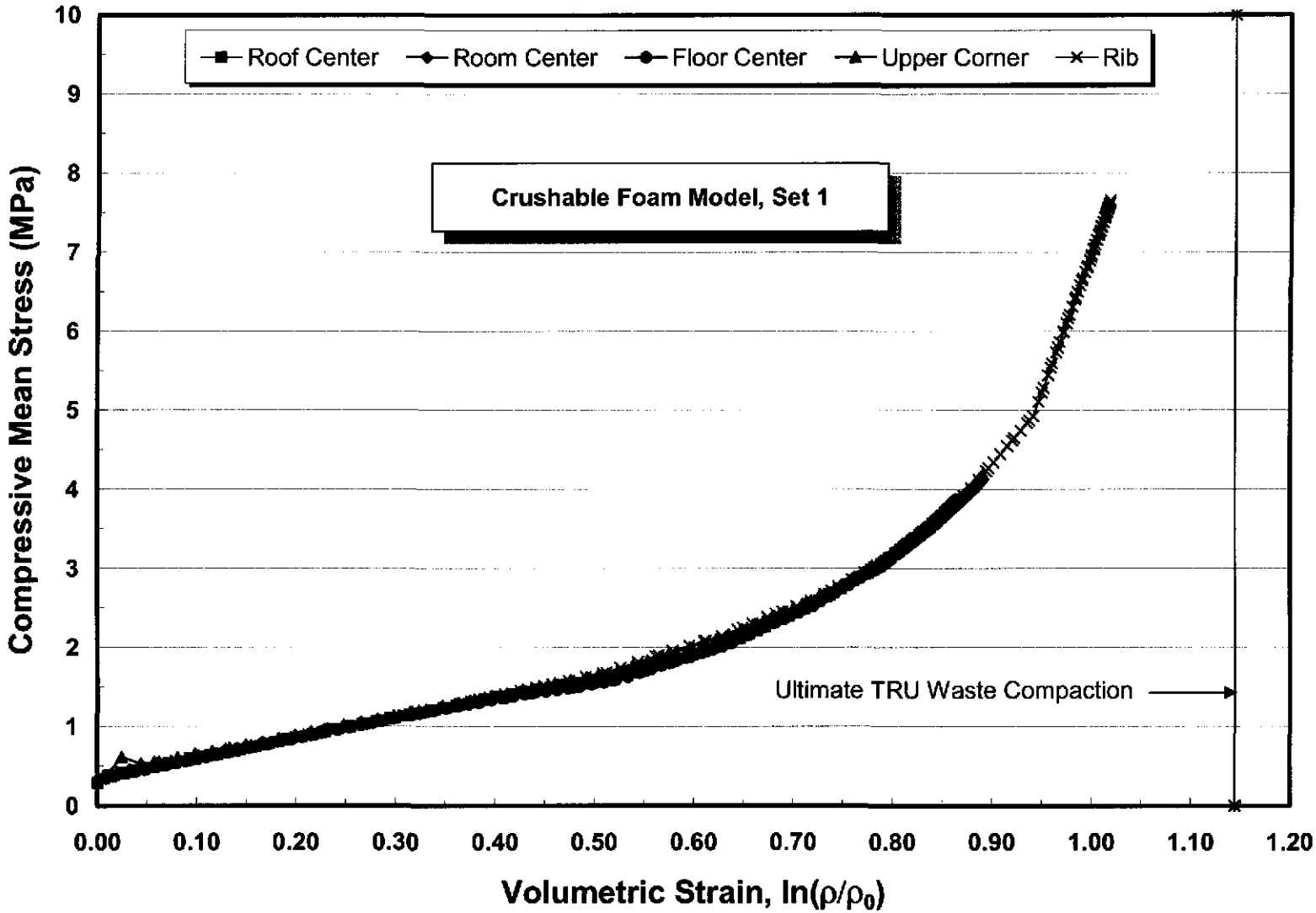

RSI-1487-04-013

Figure A-1. Mean Stress Versus Volumetric Strain at Five Locations Within the Room for the Crushable Foam Analysis (ν = 0.0) Using Parameter Set 1.

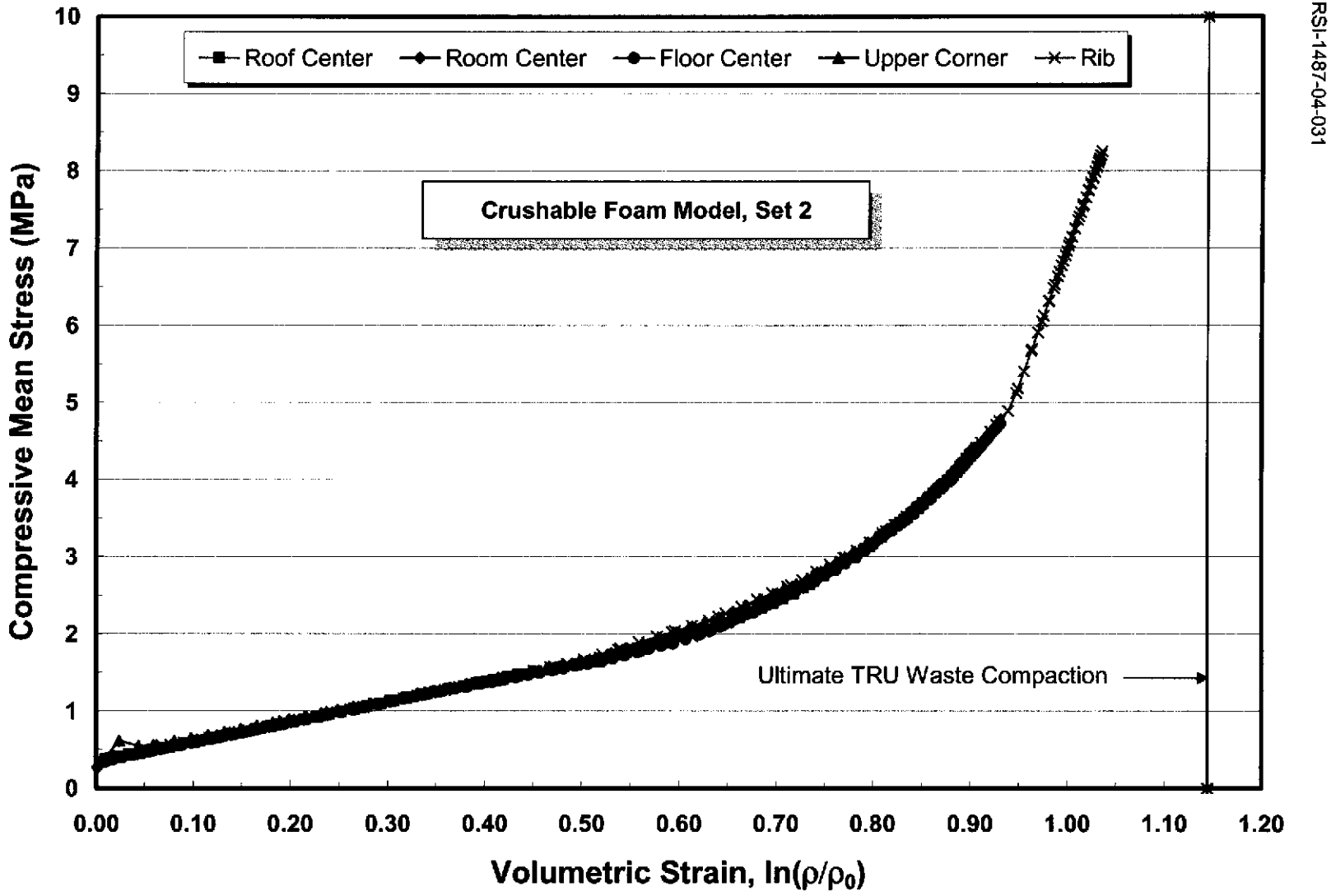

RSI-1487-04-031

Figure A-2. Mean Stress Versus Volumetric Strain at Five Locations Within the Room for the Crushable Foam Analysis (ν = 0.0) Using Parameter Set 2.

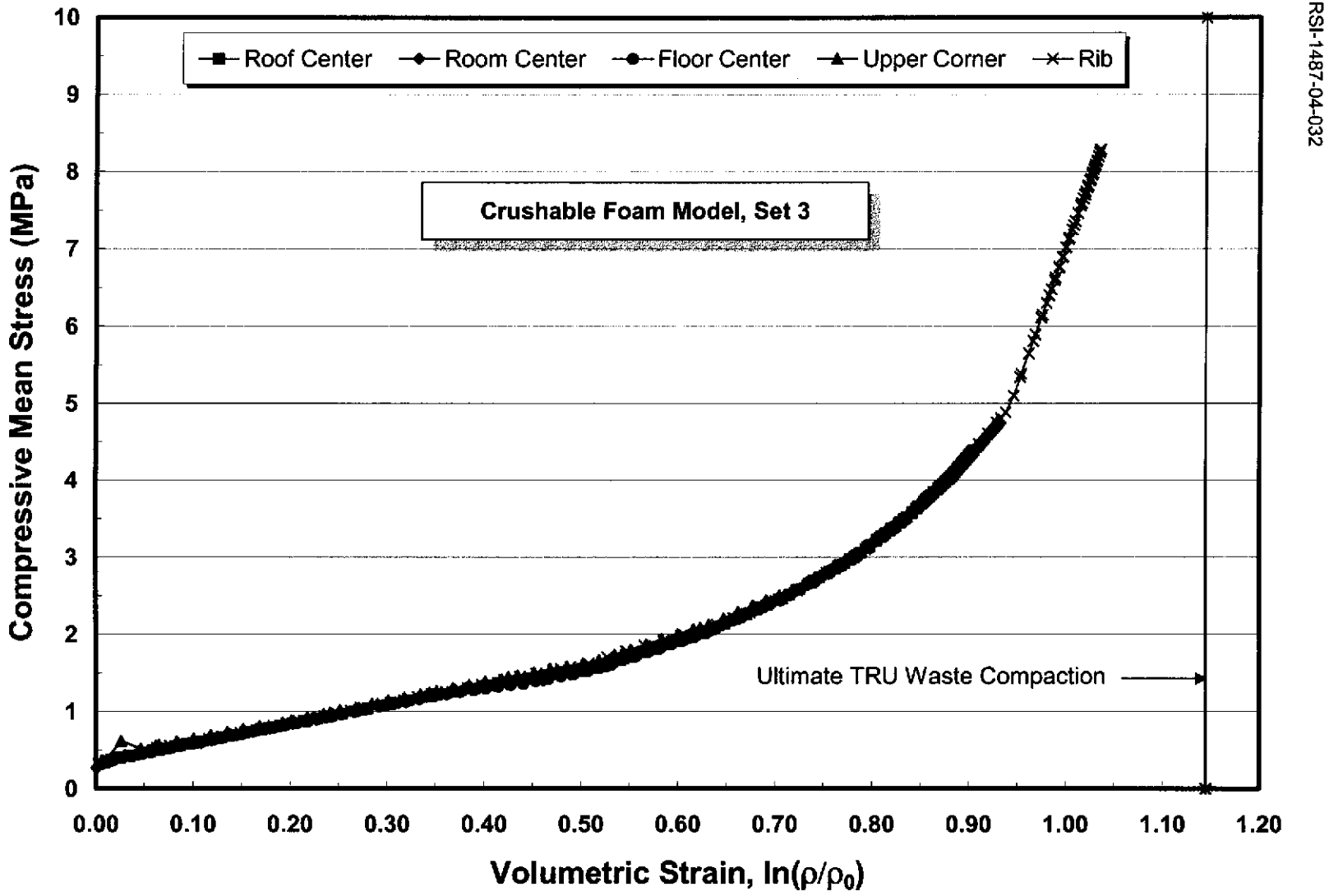

RSI-1487-04-032

Figure A-3. Mean Stress Versus Volumetric Strain at Five Locations Within the Room for the Crushable Foam Analysis (ν = 0.0) Using Parameter Set 3.

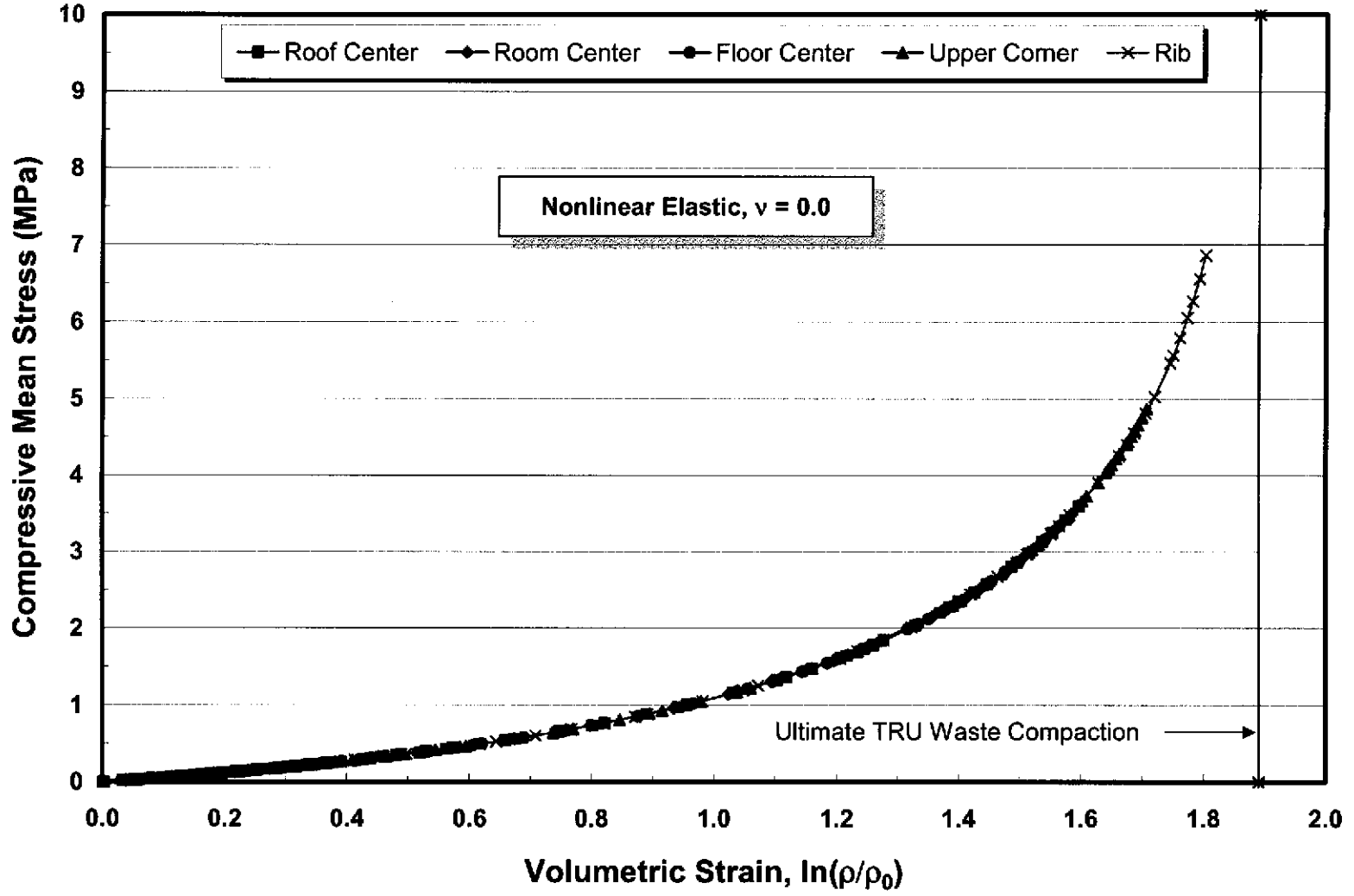

Figure A-4. Mean Stress Versus Volumetric Strain at Five Locations Within the Room for the Nonlinear Elastic (ν = 0.0) Analysis.

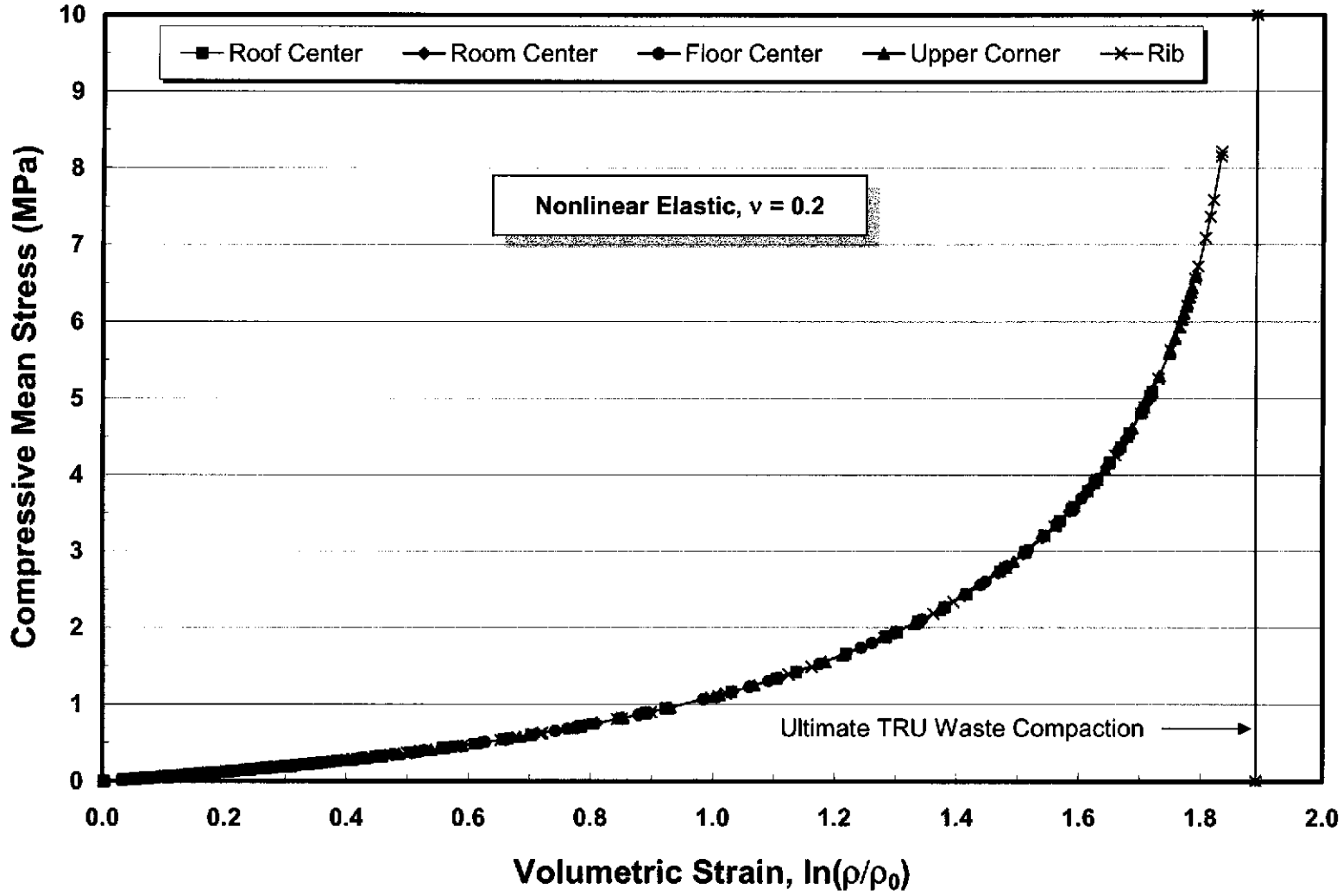

Figure A-5. Mean Stress Versus Volumetric Strain at Five Locations Within the Room for the Nonlinear Elastic (ν = 0.2) Analysis.

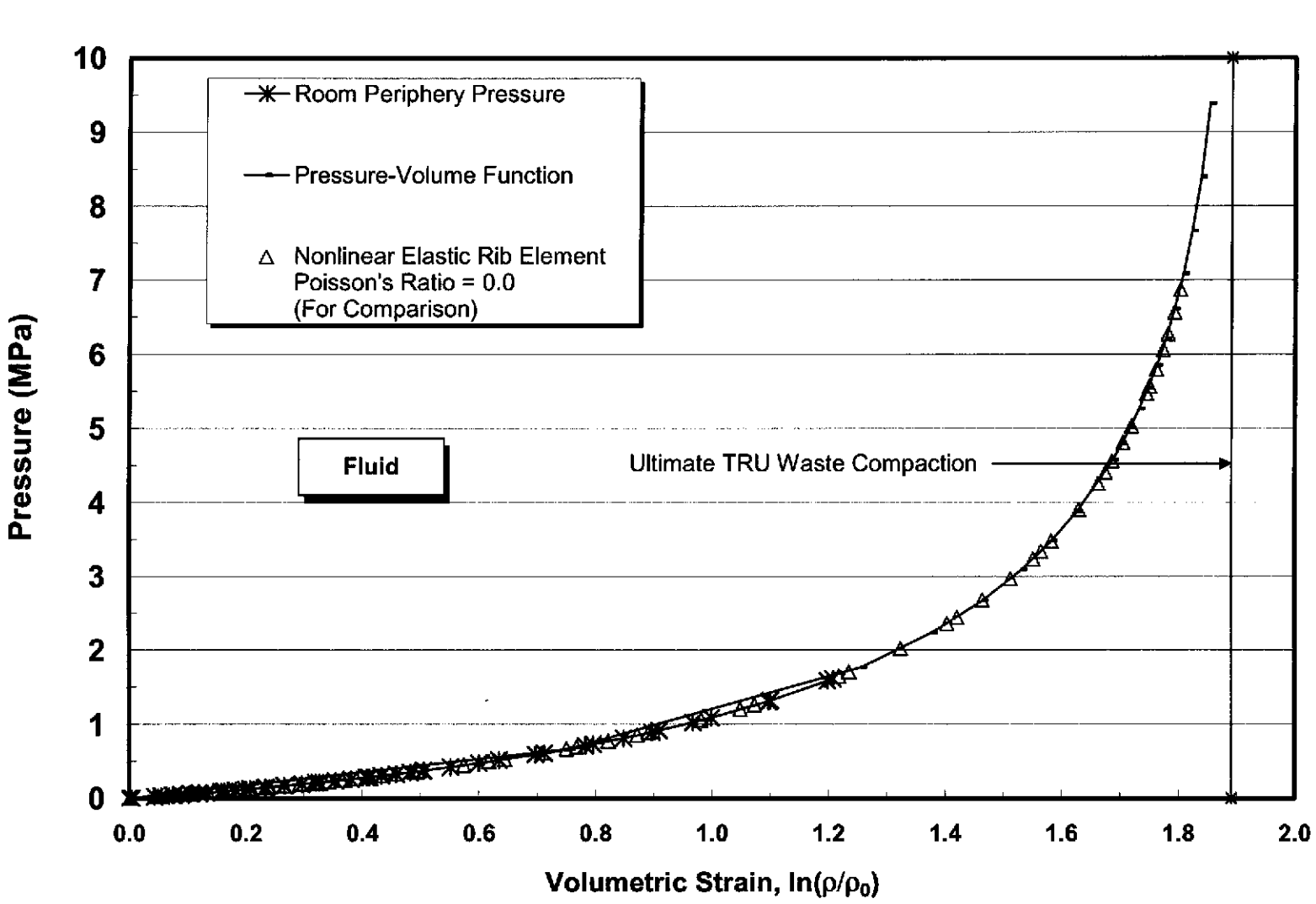

Figure A-6. Average Room Pressure Versus Volumetric Strain for the Fluid Analysis.

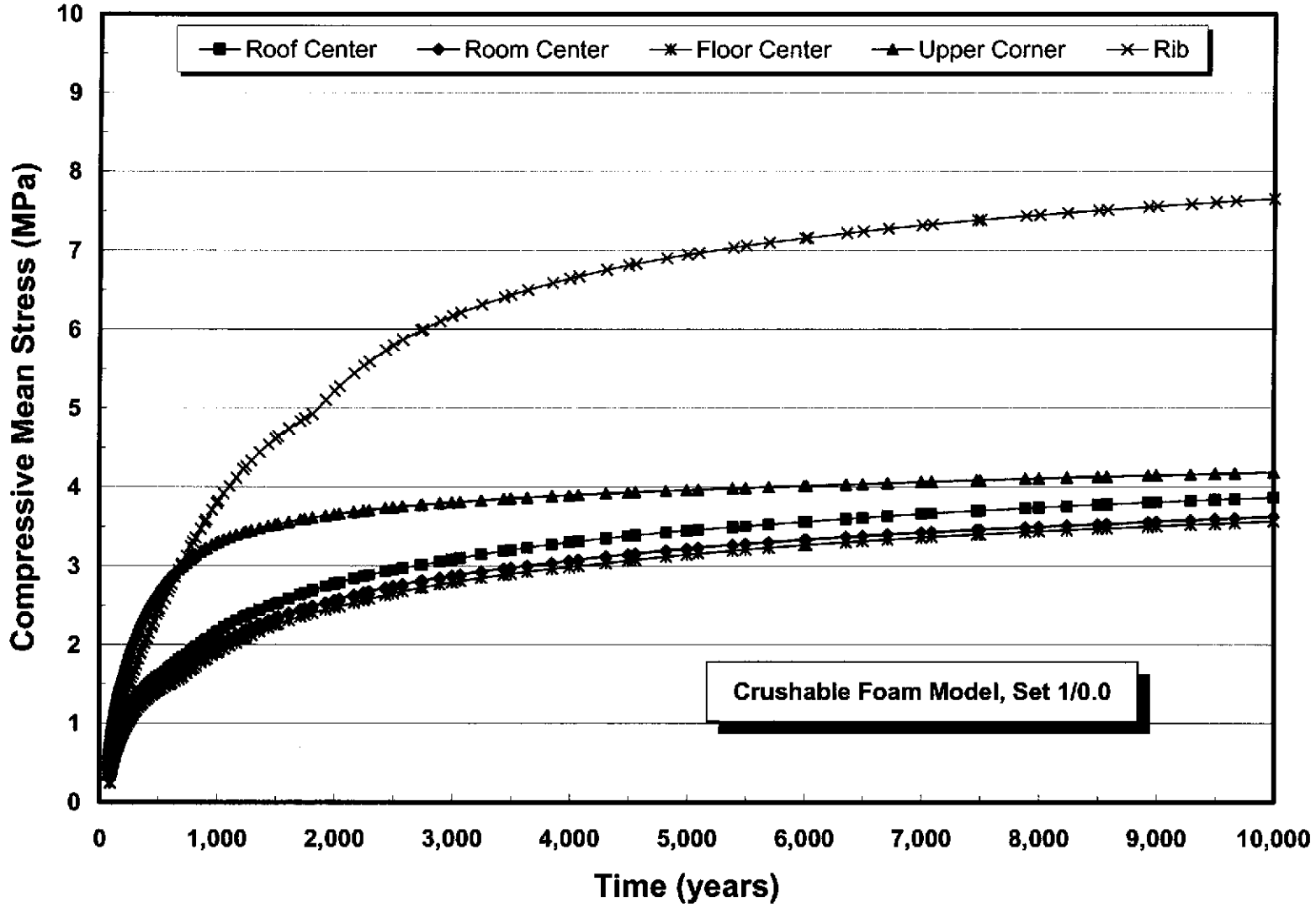

Figure A-7. Mean Stress Versus Time at Five Locations Within the Room for the Crushable Foam Analysis (ν = 0.0) Using Parameter Set 1.

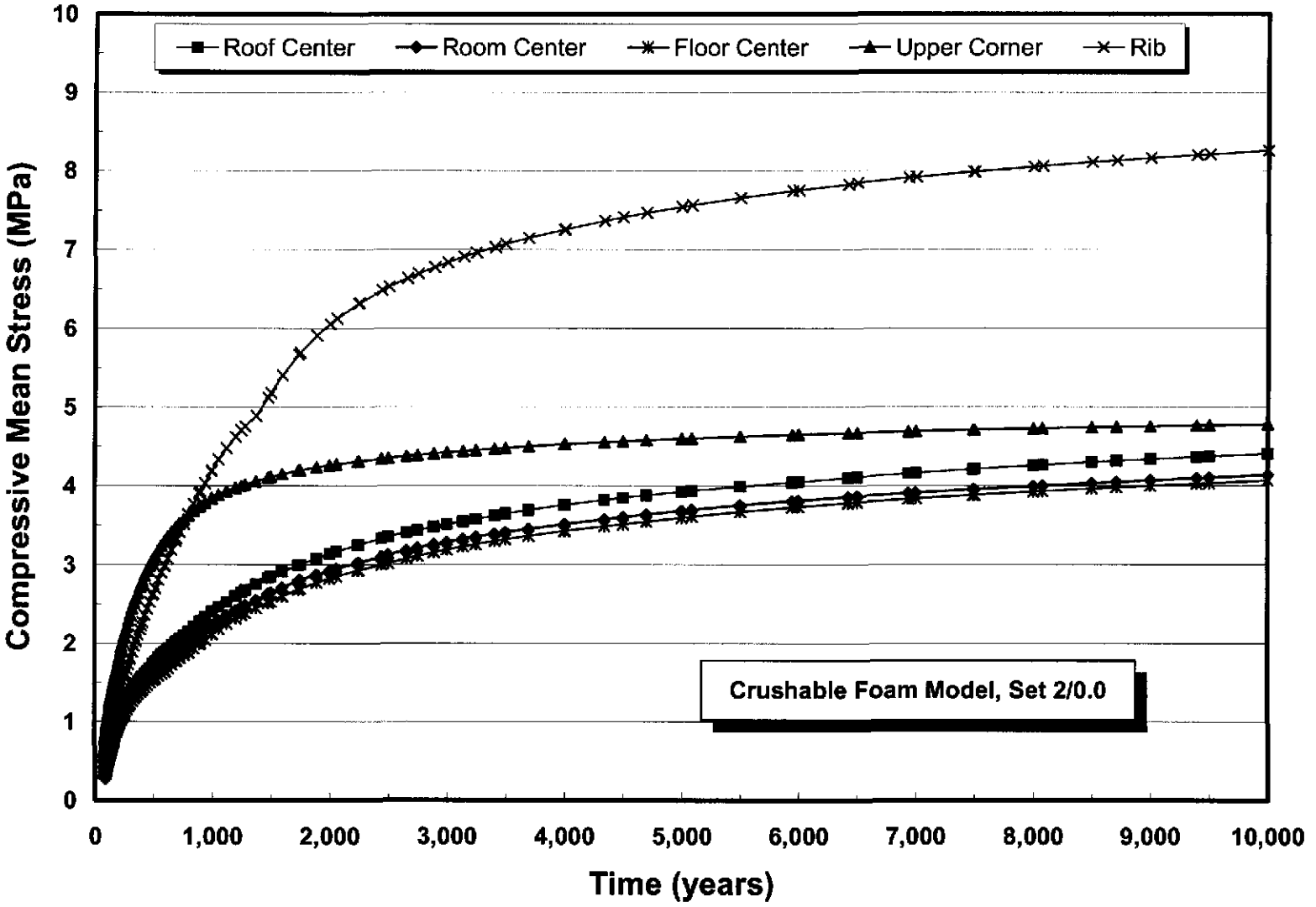

Figure A-8. Mean Stress Versus Time at Five Locations Within the Room for the Crushable Foam Analysis (ν = 0.0) Using Parameter Set 2.

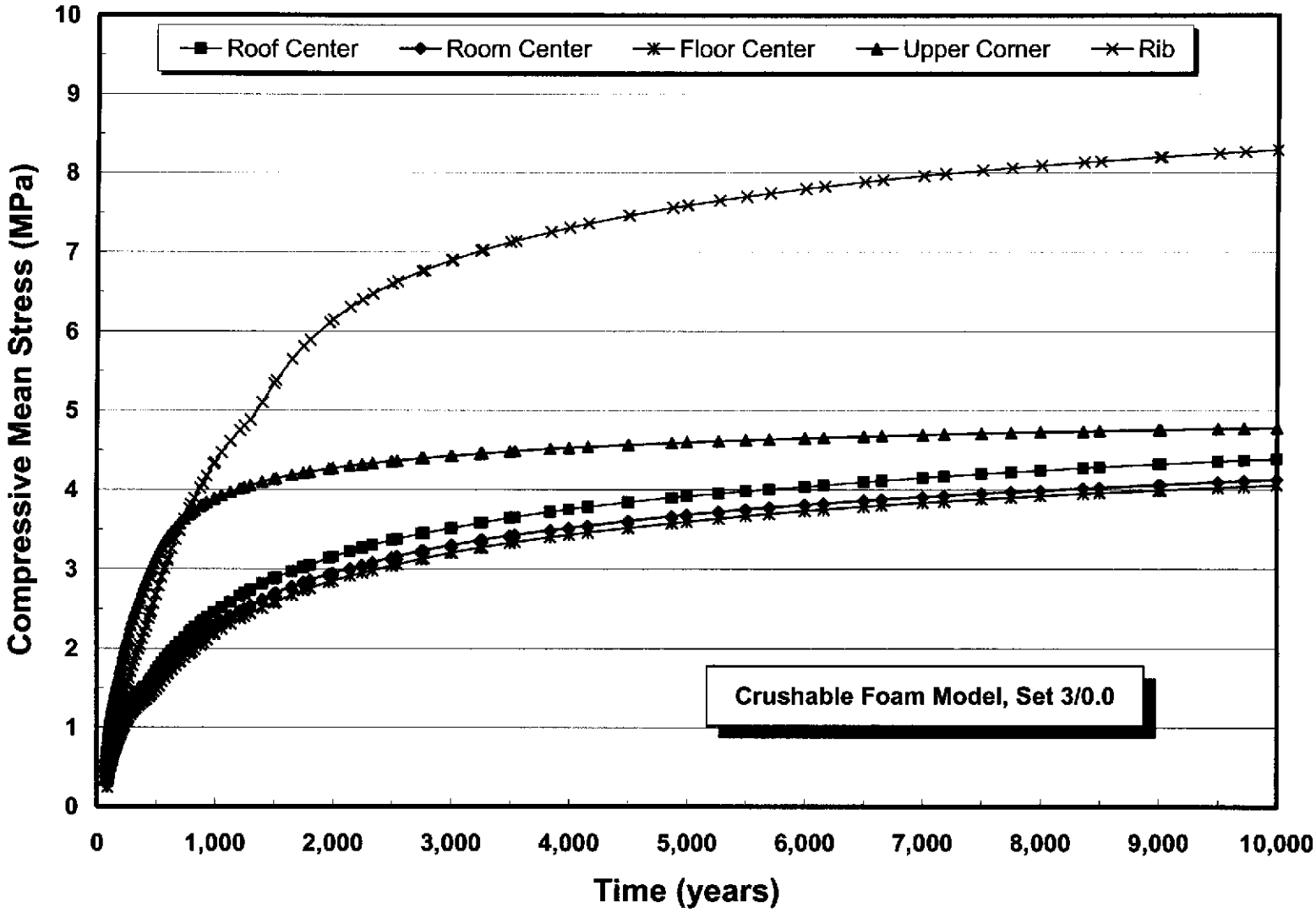

RSI-1487-04-034

Figure A-9. Mean Stress Versus Time at Five Locations Within the Room for the Crushable Foam Analysis (ν = 0.0) Using Parameter Set 3.

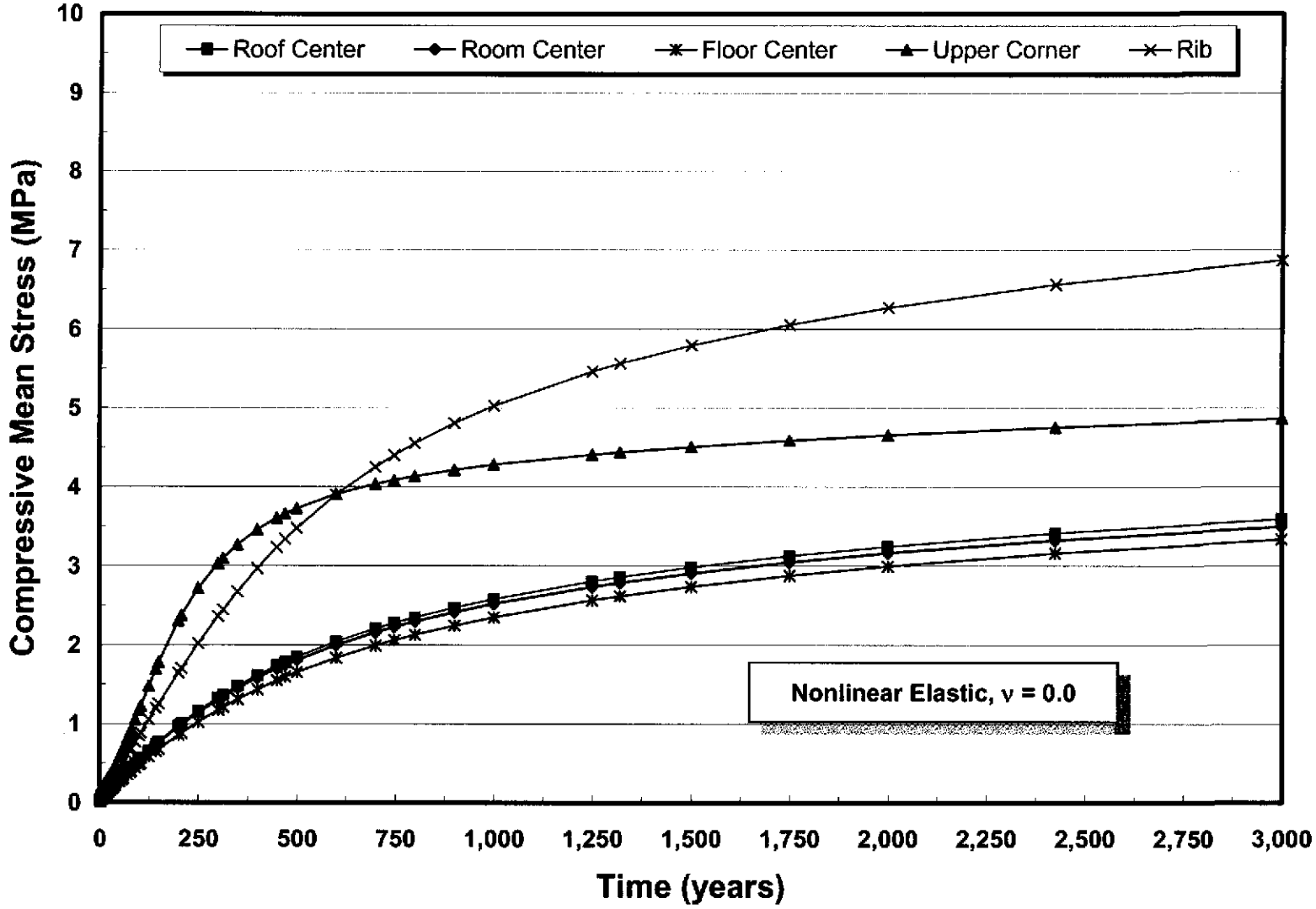

Figure A-10. Mean Stress Versus Time at Five Locations Within the Room for the Nonlinear Elastic (ν = 0.0) Analysis.

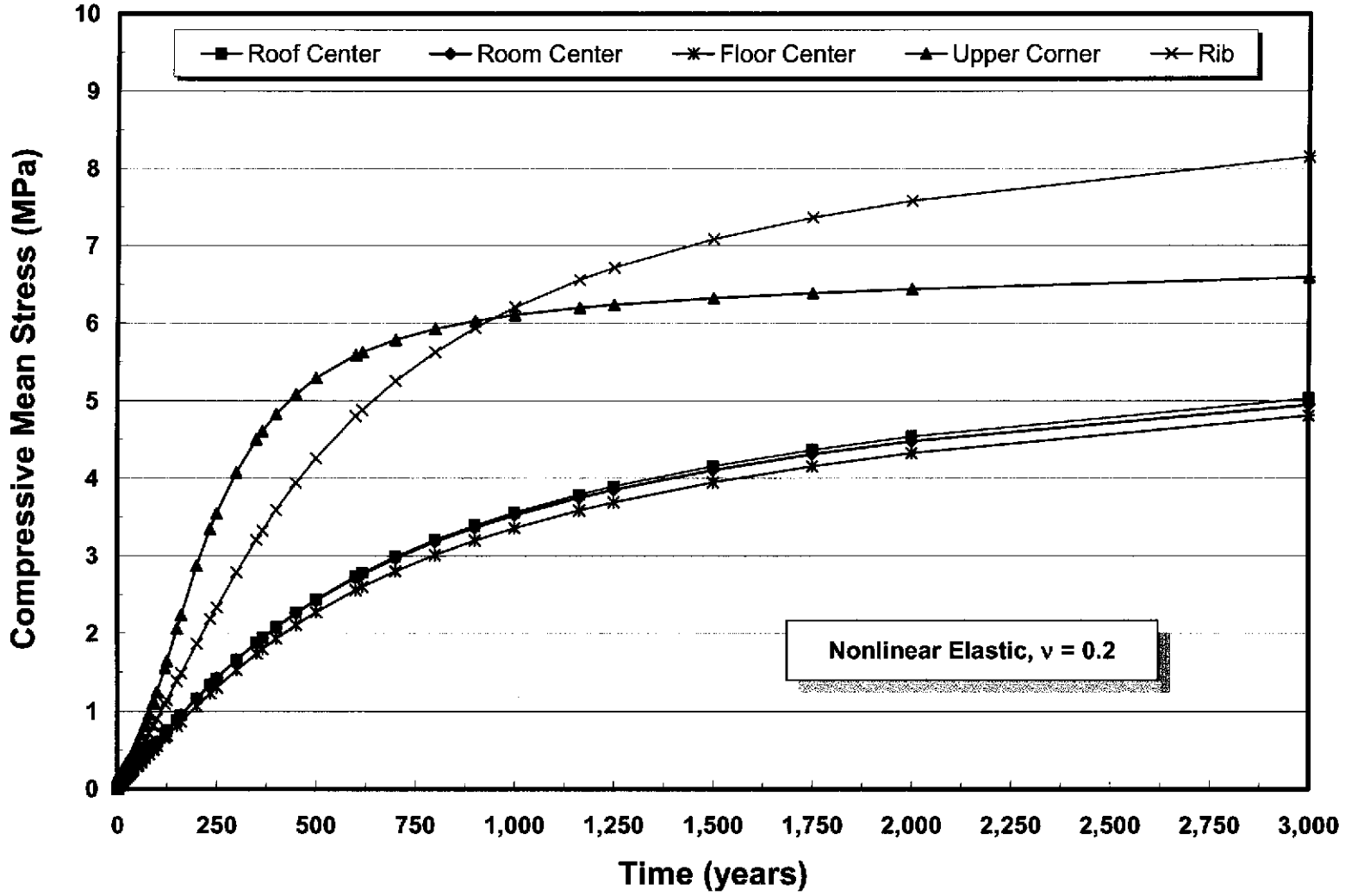

Figure A-11. Mean Stress Versus Time at Five Locations Within the Room for the Nonlinear Elastic ($\nu = 0.2$) Analysis.

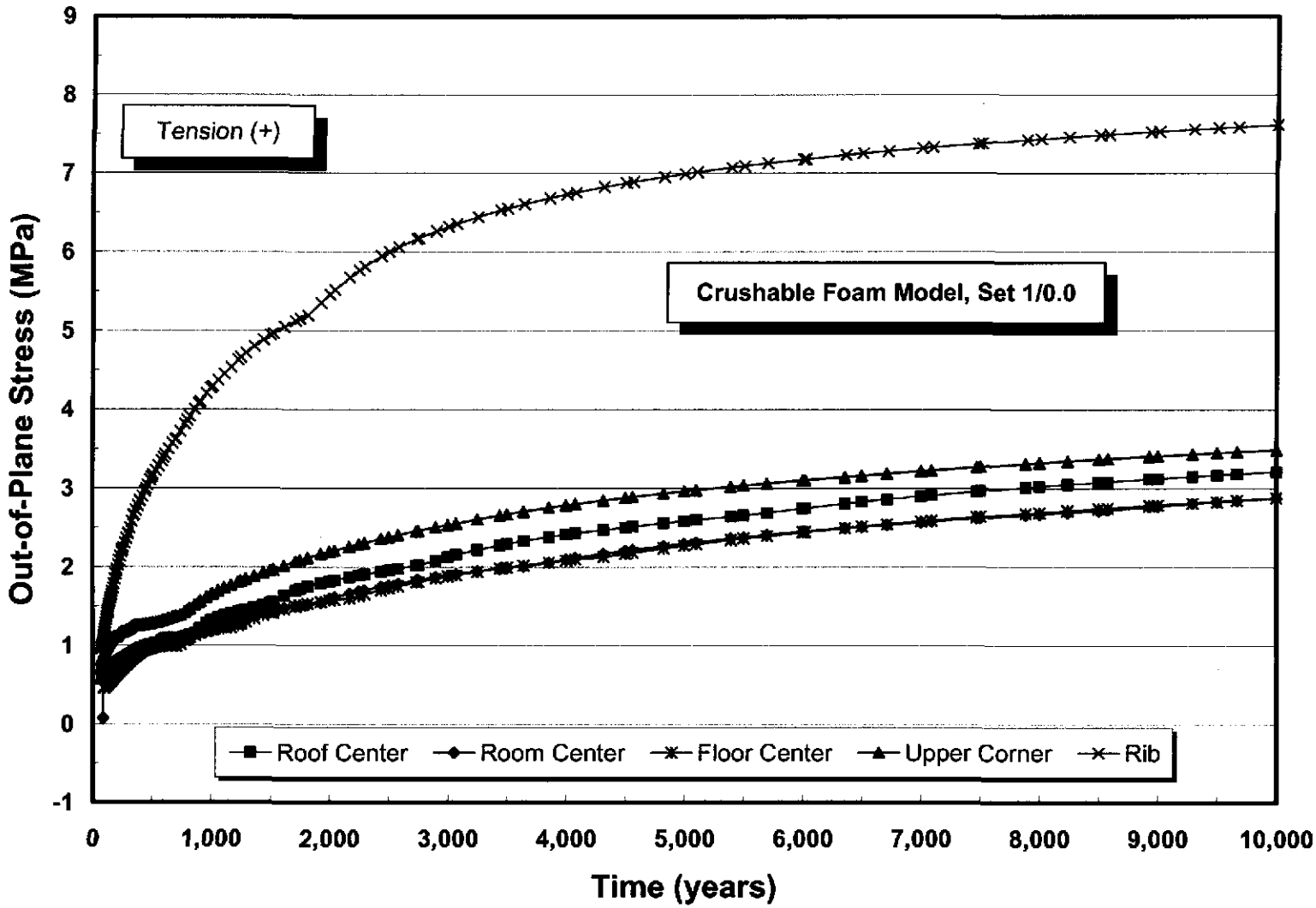

Figure A-12. Out-of-Plane Stress Versus Time at Five Locations Within the Room for the Crushable Foam Analysis (ν = 0.0) Using Parameter Set 1.

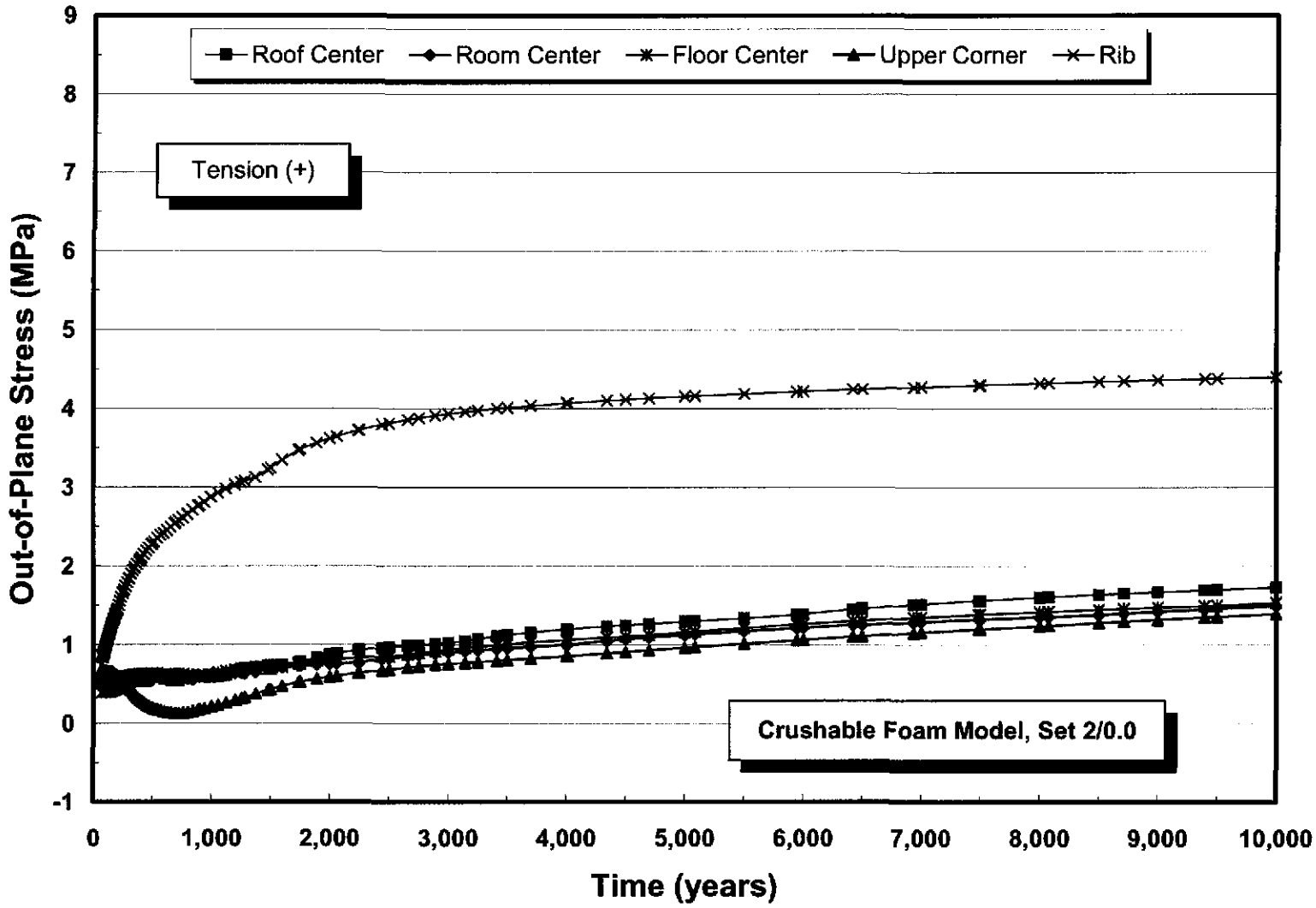

Figure A-13. Out-of-Plane Stress Versus Time at Five Locations Within the Room for the Crushable Foam Analysis (ν = 0.0) Using Parameter Set 2.

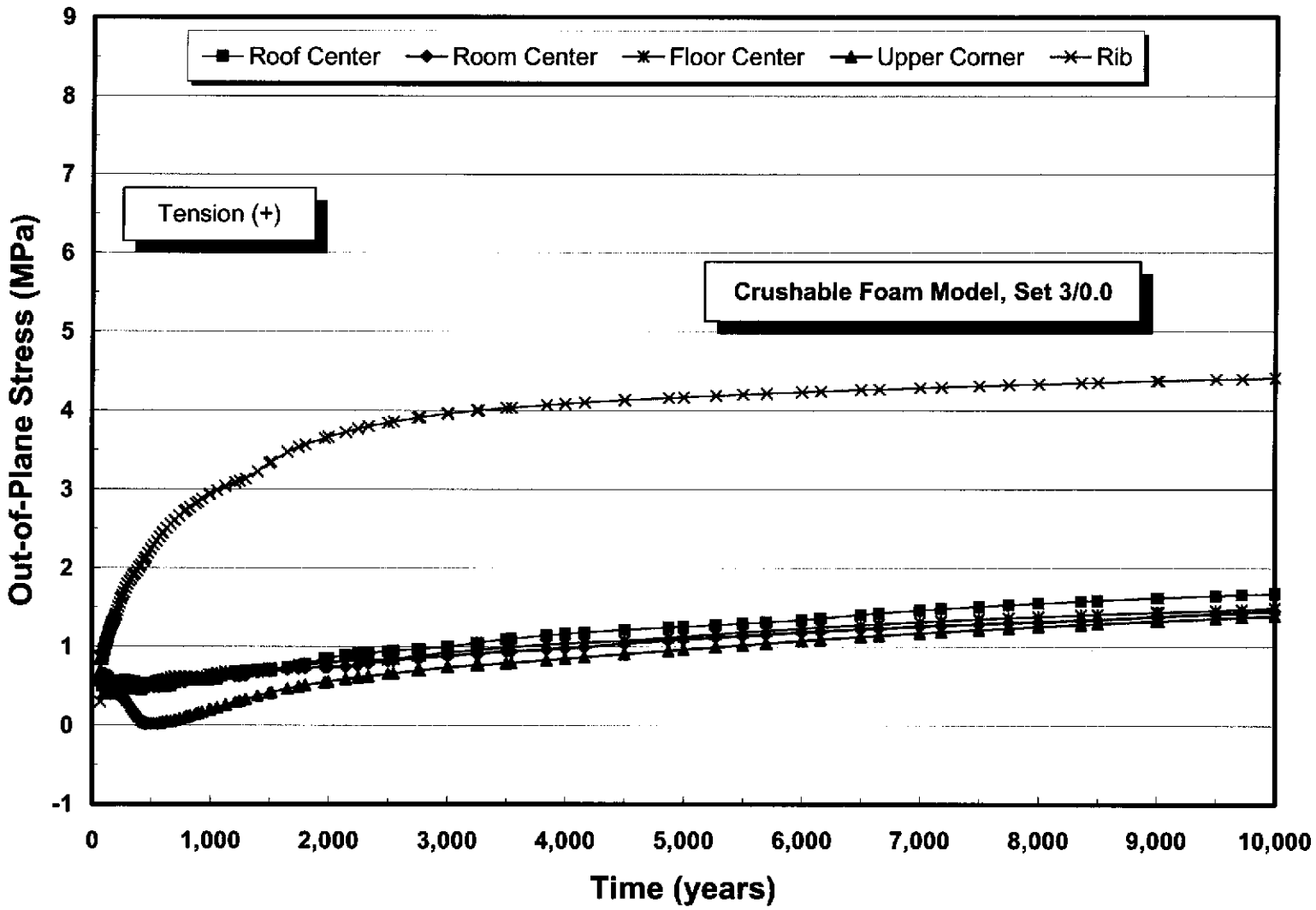

Figure A-14. Out-of-Plane Stress Versus Time at Five Locations Within the Room for the Crushable Foam Analysis (ν = 0.0) Using Parameter Set 3.

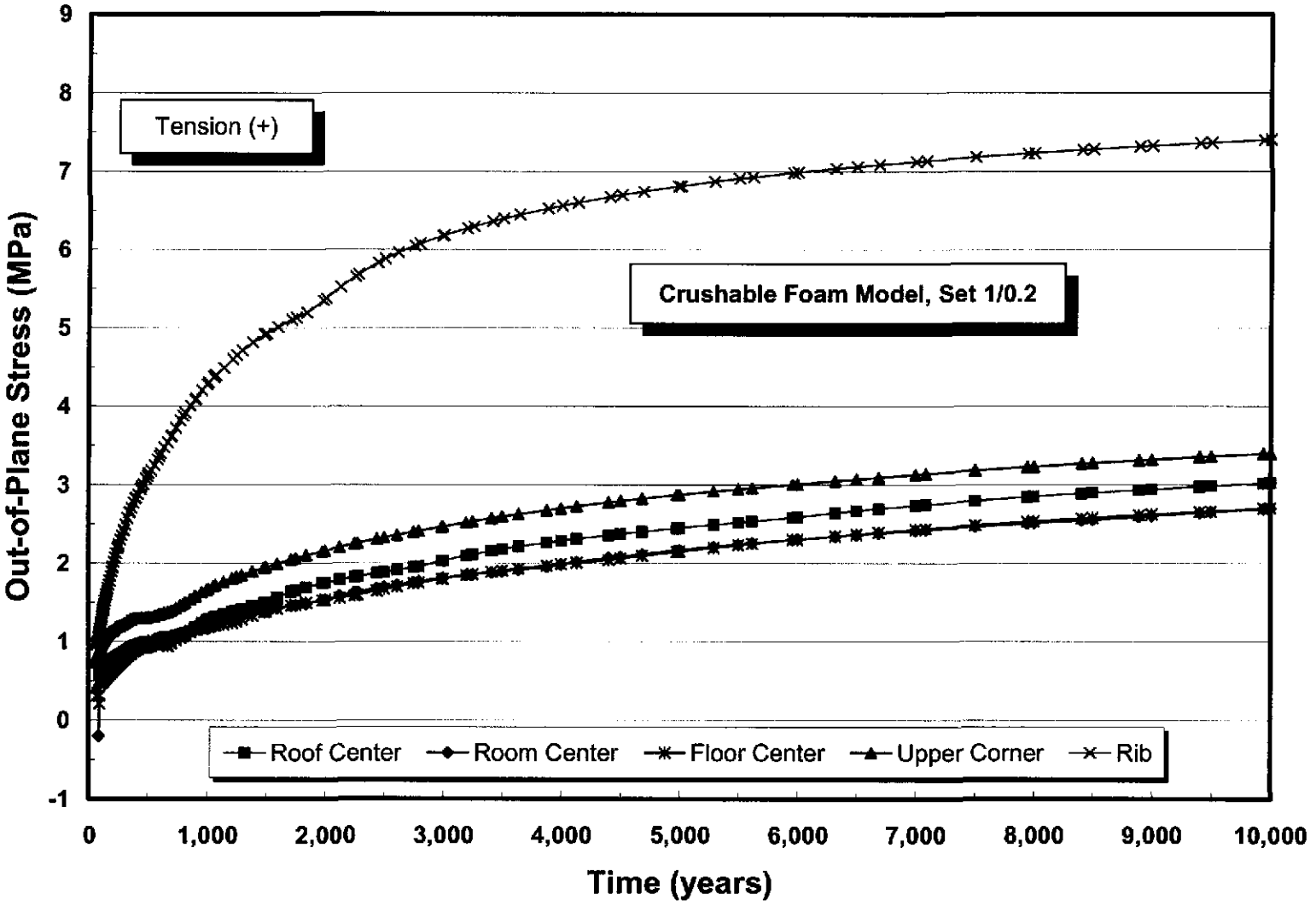

Figure A-15. Out-of-Plane Stress Versus Time at Five Locations Within the Room for the Crushable Foam Analysis ($\nu = 0.2$) Using Parameter Set 1.

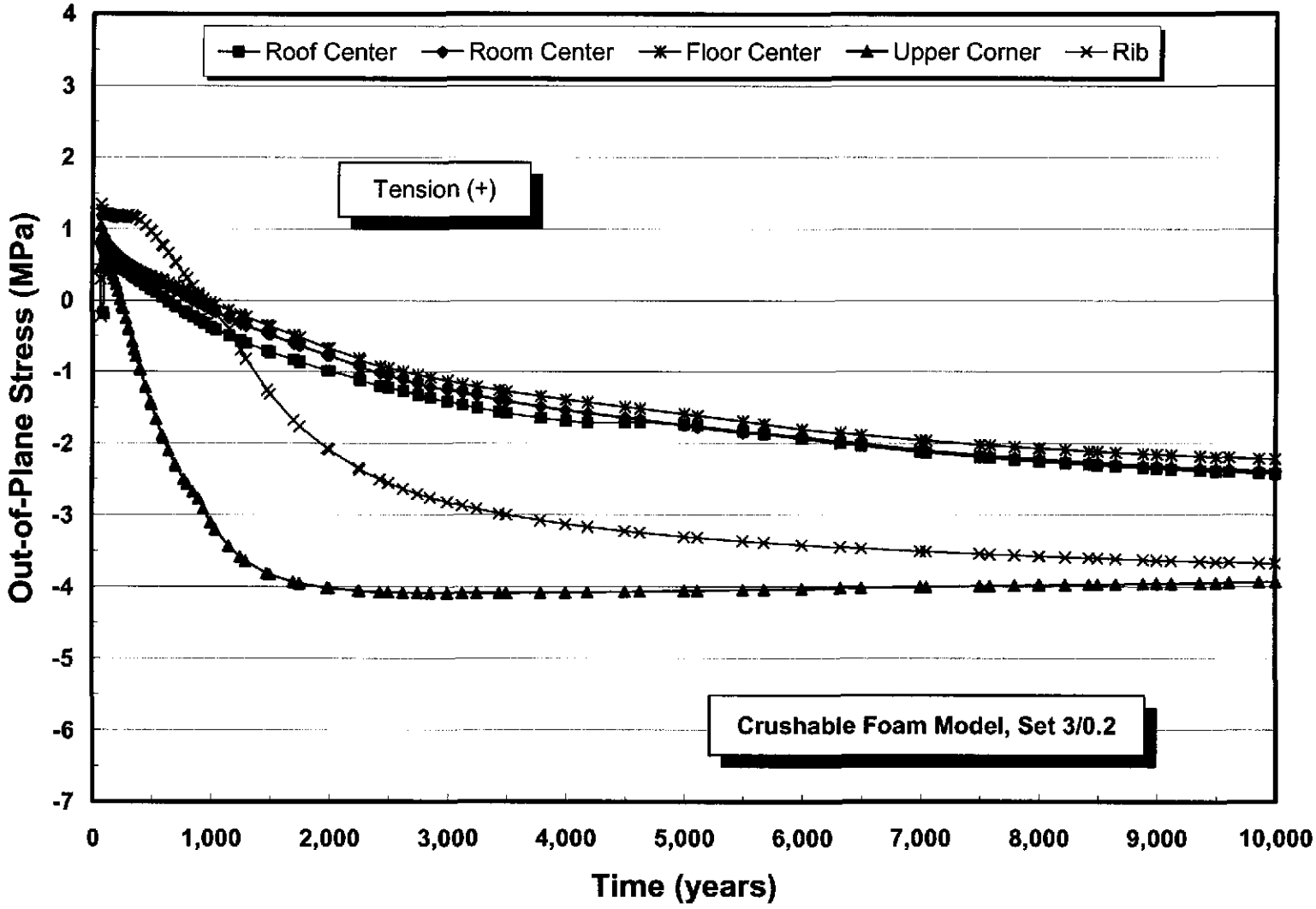

Figure A-16. Out-of-Plane Stress Versus Time at Five Locations Within the Room for the Crushable Foam Analysis (ν = 0.2) Using Parameter Set 3.

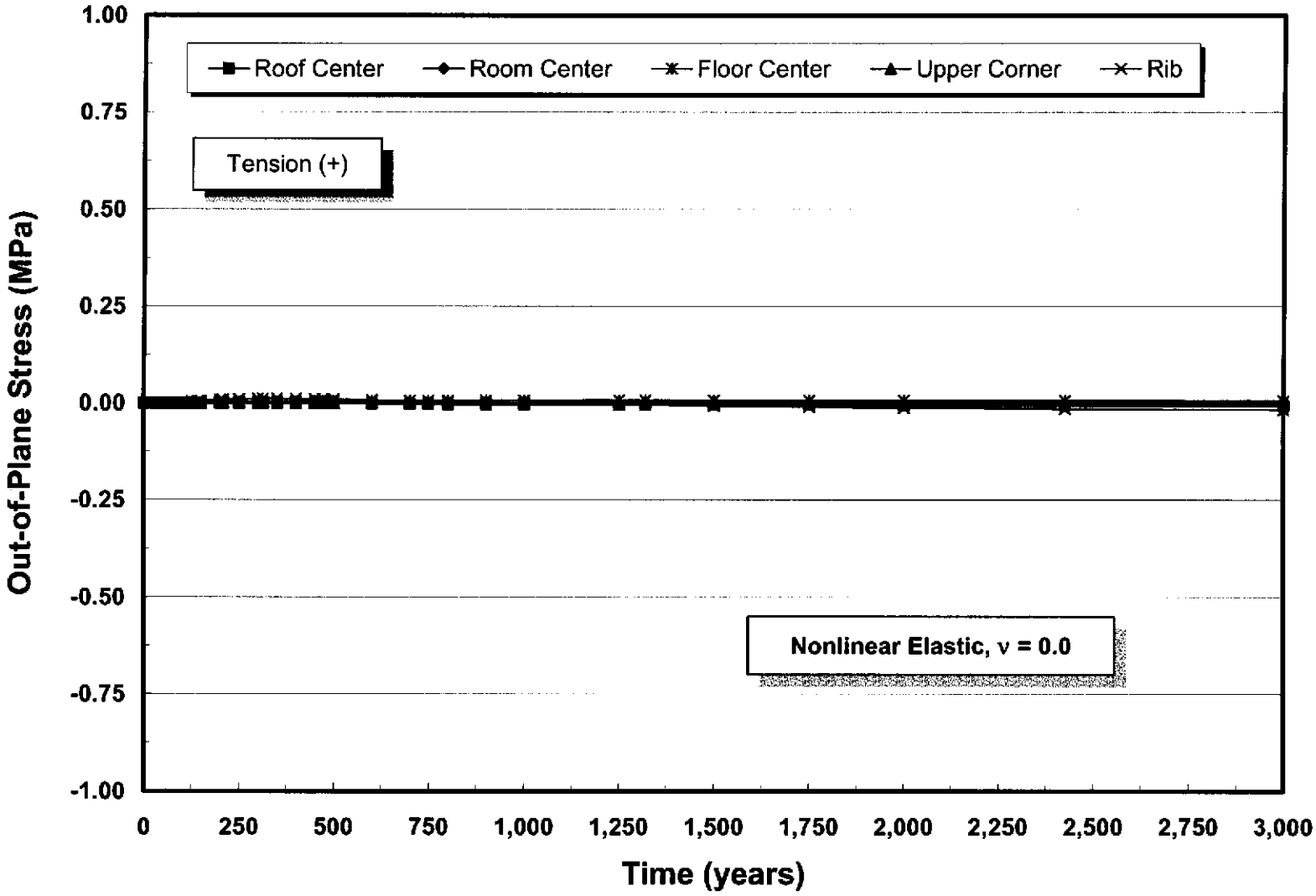

Figure A-17. Out-of-Plane Stress Versus Time at Five Locations Within the Room for the Nonlinear Elastic (ν = 0.0) Analysis.

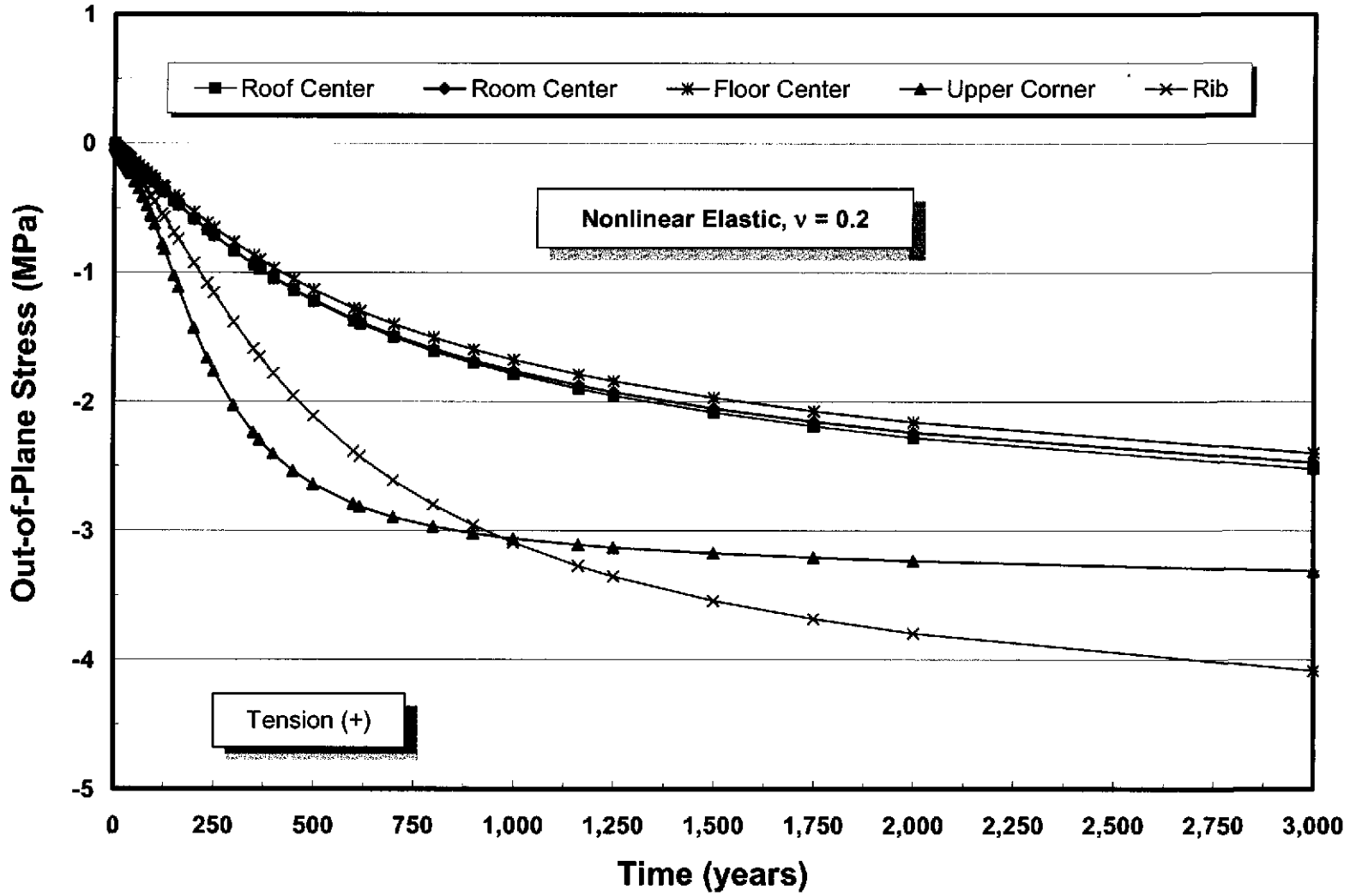

Figure A-18. Out-of-Plane Stress Versus Time at Five Locations Within the Room for the Nonlinear Elastic (ν = 0.2) Analysis.

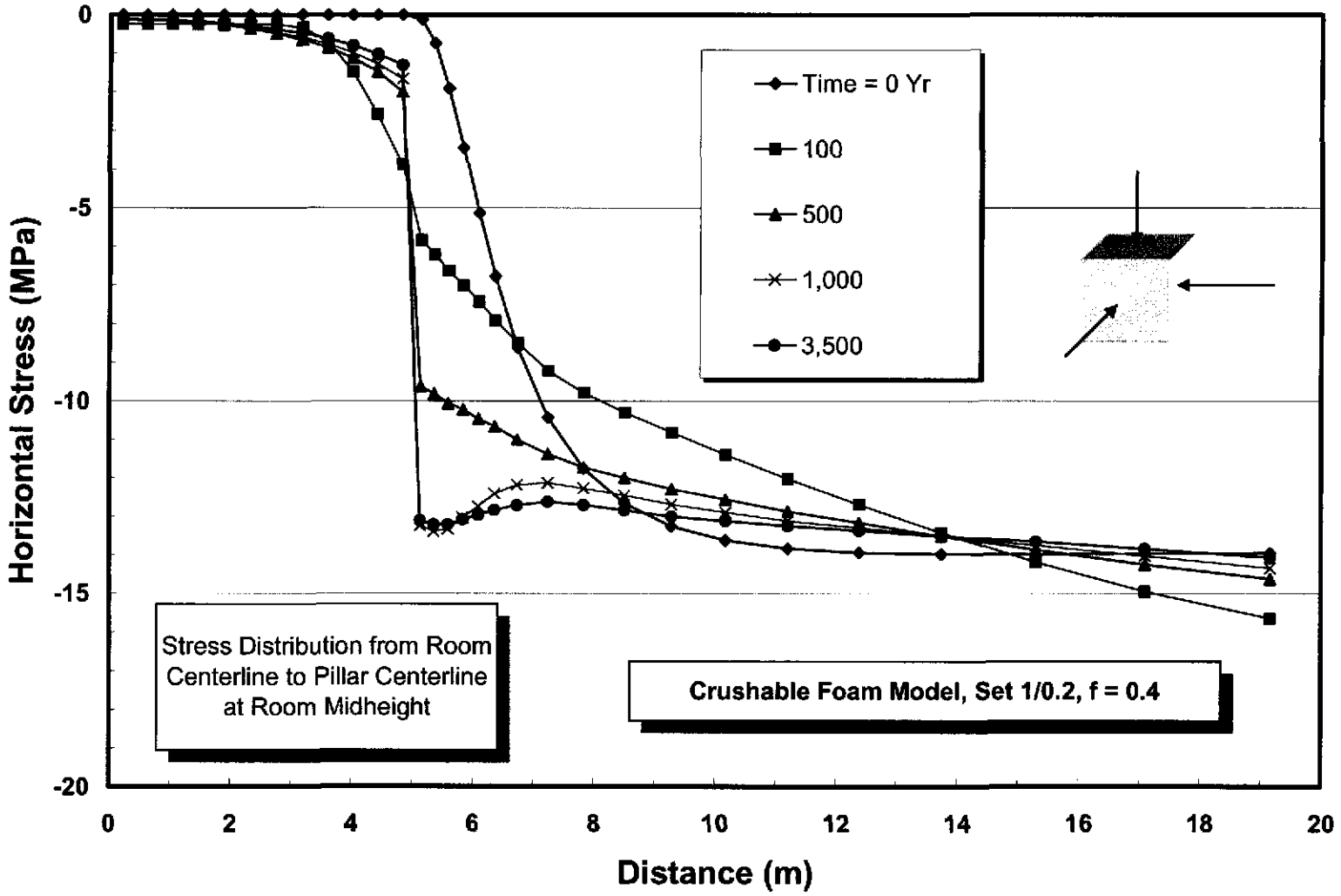

Figure A-19. Horizontal Stress Distribution (σ_{xx}) From the Room Centerline to the Pillar Centerline at Room Midheight for the Crushable Foam Analysis Using Parameter Set 1, Poisson's Ratio Equal to 0.2, and Gas Generation (f = 0.4).

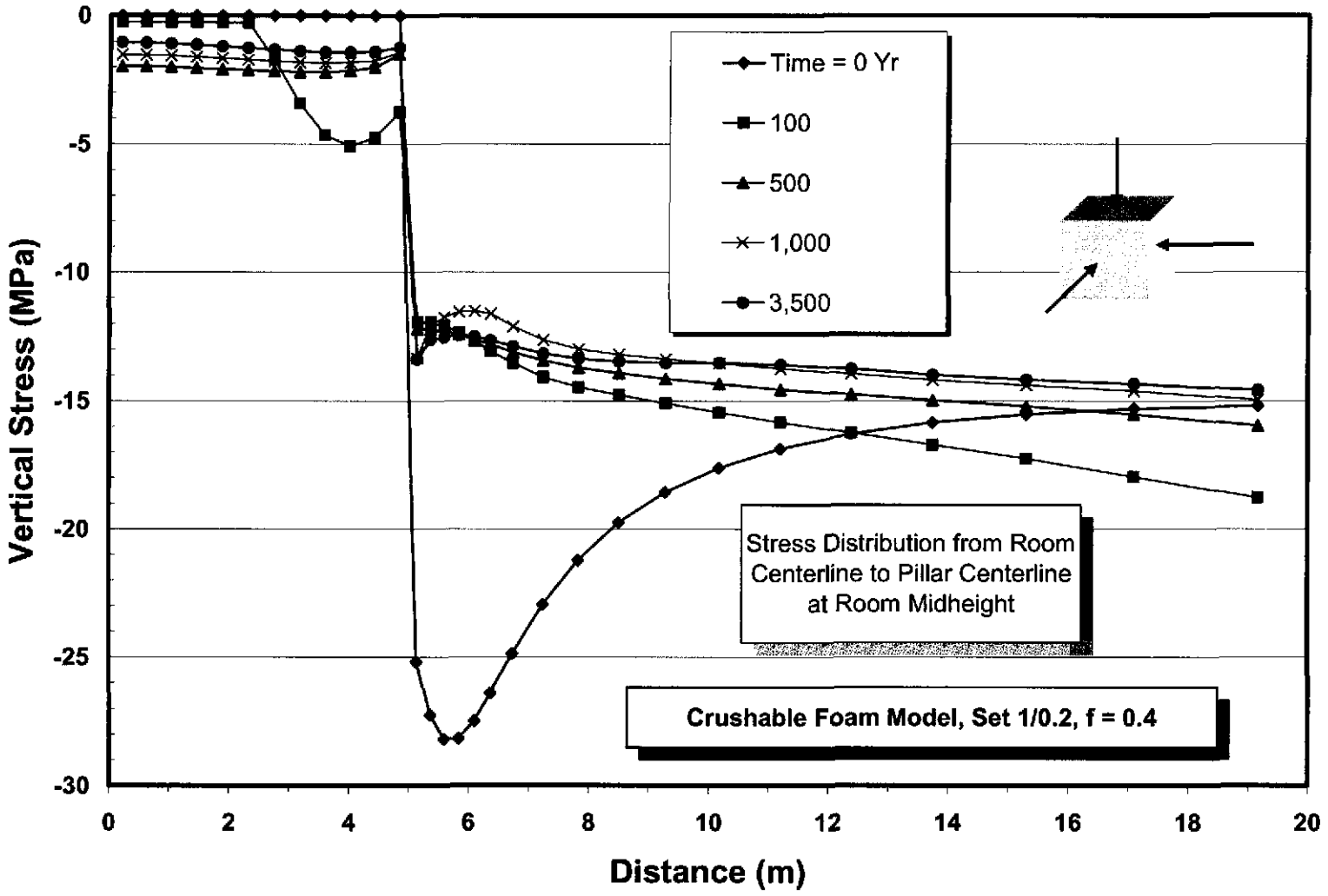

Figure A-20. Vertical Stress Distribution (σ_{yy}) From the Room Centerline to the Pillar Centerline at Room Midheight for the Crushable Foam Analysis Using Parameter Set 1, Poisson's Ratio Equal to 0.2, and Gas Generation ($f = 0.4$).

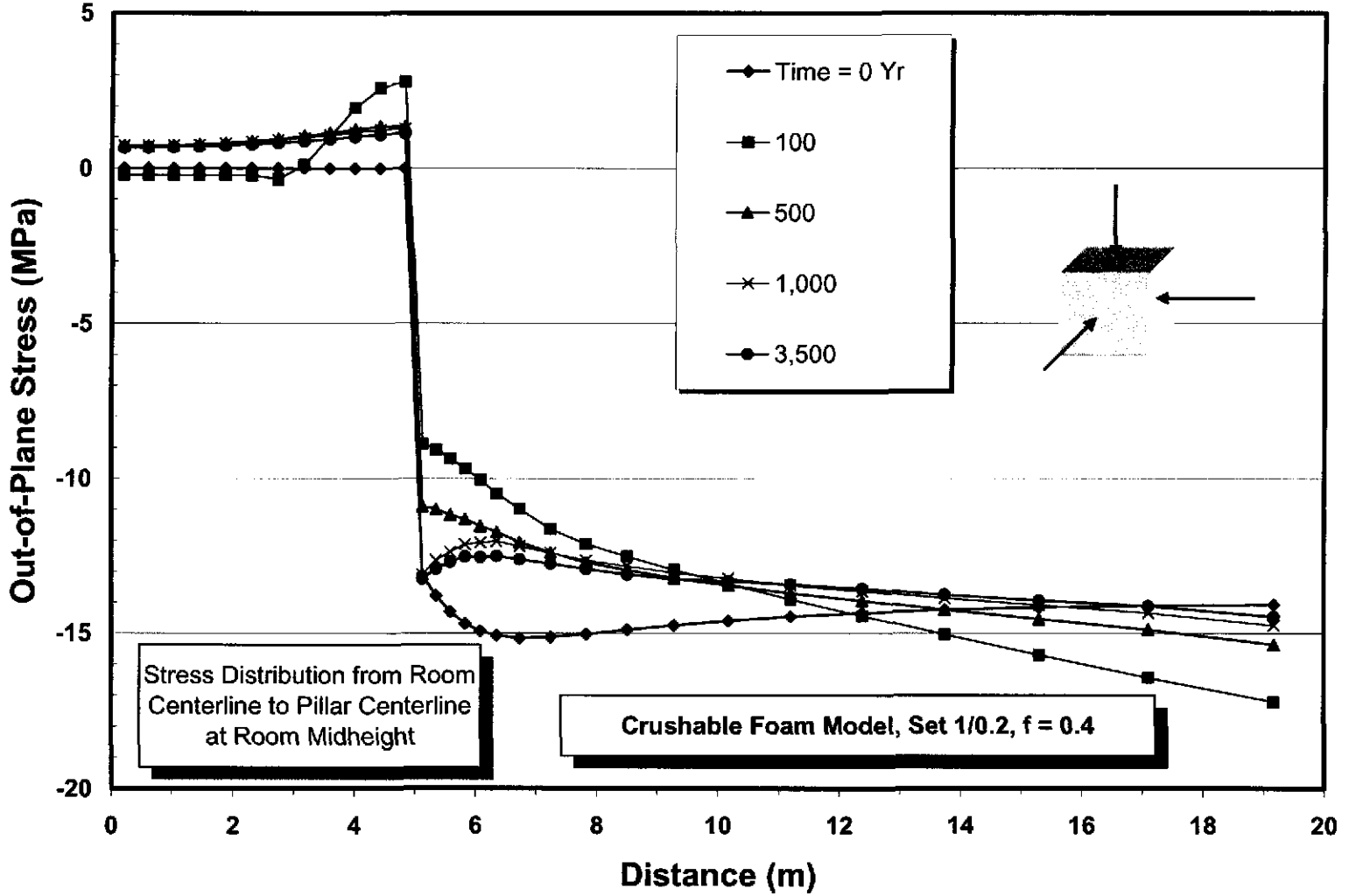

Figure A-21. Out-of-Plane Stress Distribution (σ_{zz}) From the Room Centerline to the Pillar Centerline at Room Midheight for the Crushable Foam Analysis Using Parameter Set 1, Poisson's Ratio Equal to 0.2, and Gas Generation ($f = 0.4$).

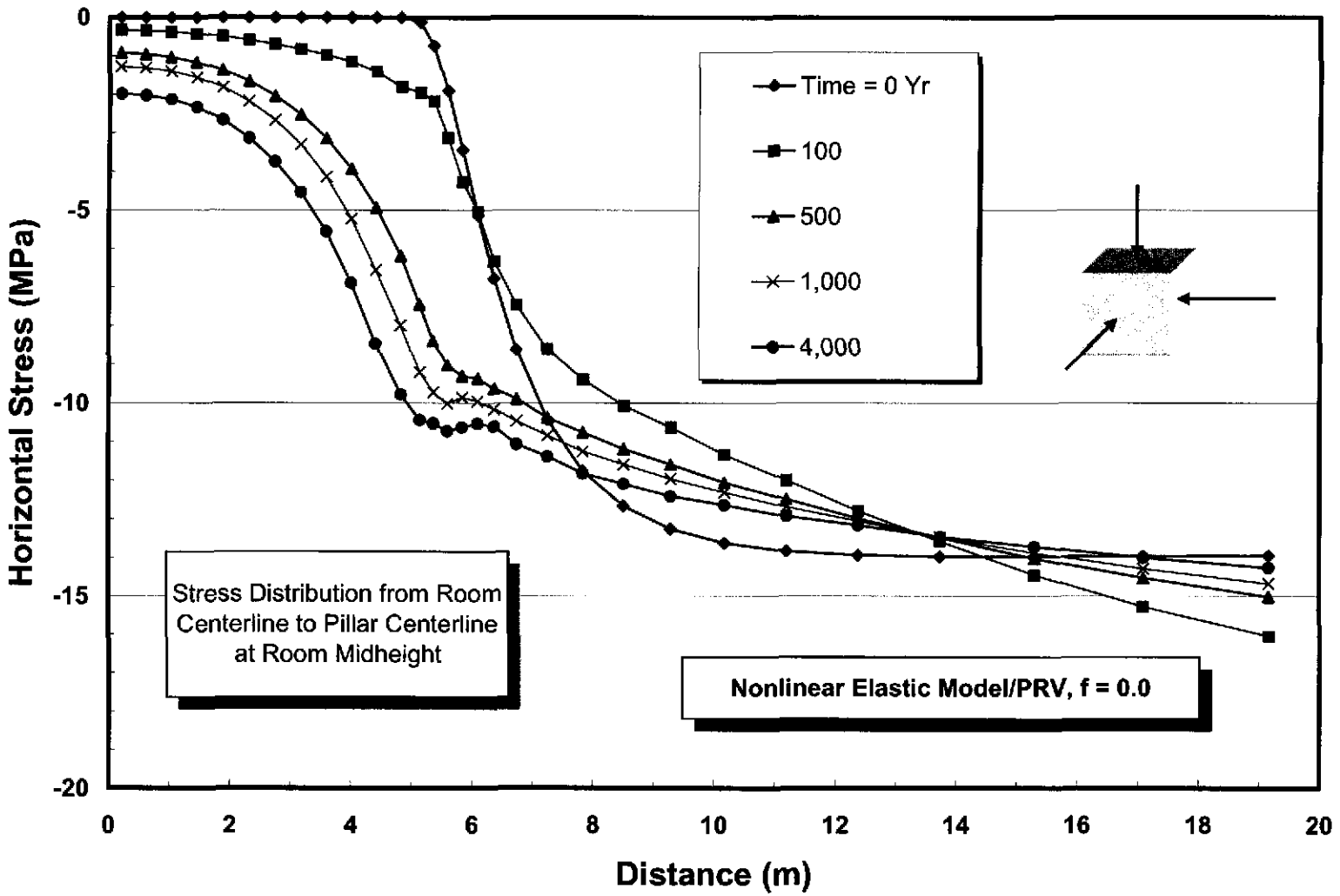

Figure A-22. Horizontal Stress Distribution (σ_{xx}) From the Room Centerline to the Pillar Centerline at Room Midheight for the Nonlinear Elastic Analysis With a Variable Poisson's Ratio and No Gas Generation ($f = 0$).

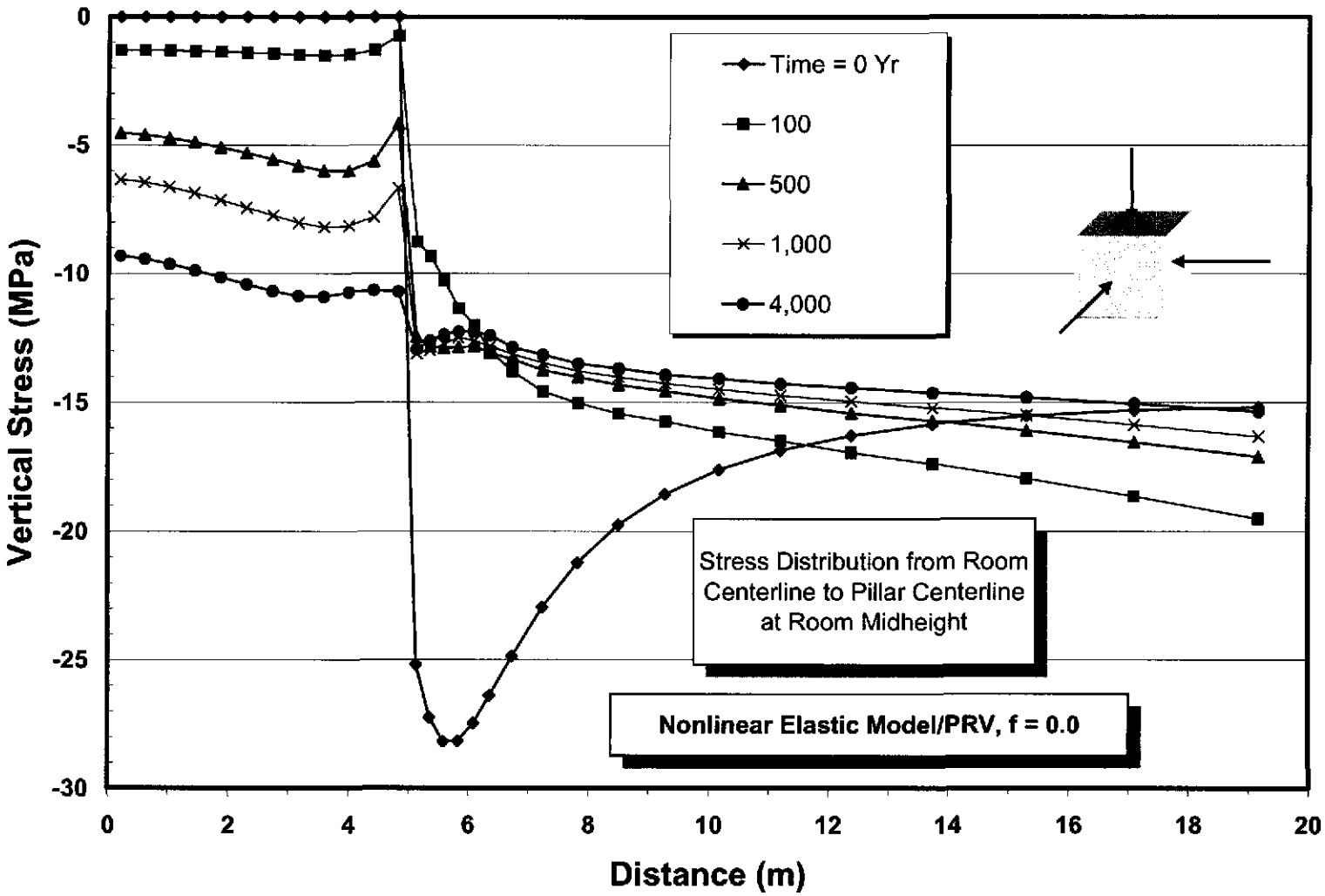

Figure A-23. Vertical Stress Distribution (σ_{yy}) From the Room Centerline to the Pillar Centerline at Room Midheight for the Nonlinear Elastic Analysis With a Variable Poisson's Ratio and No Gas Generation ($f = 0$).

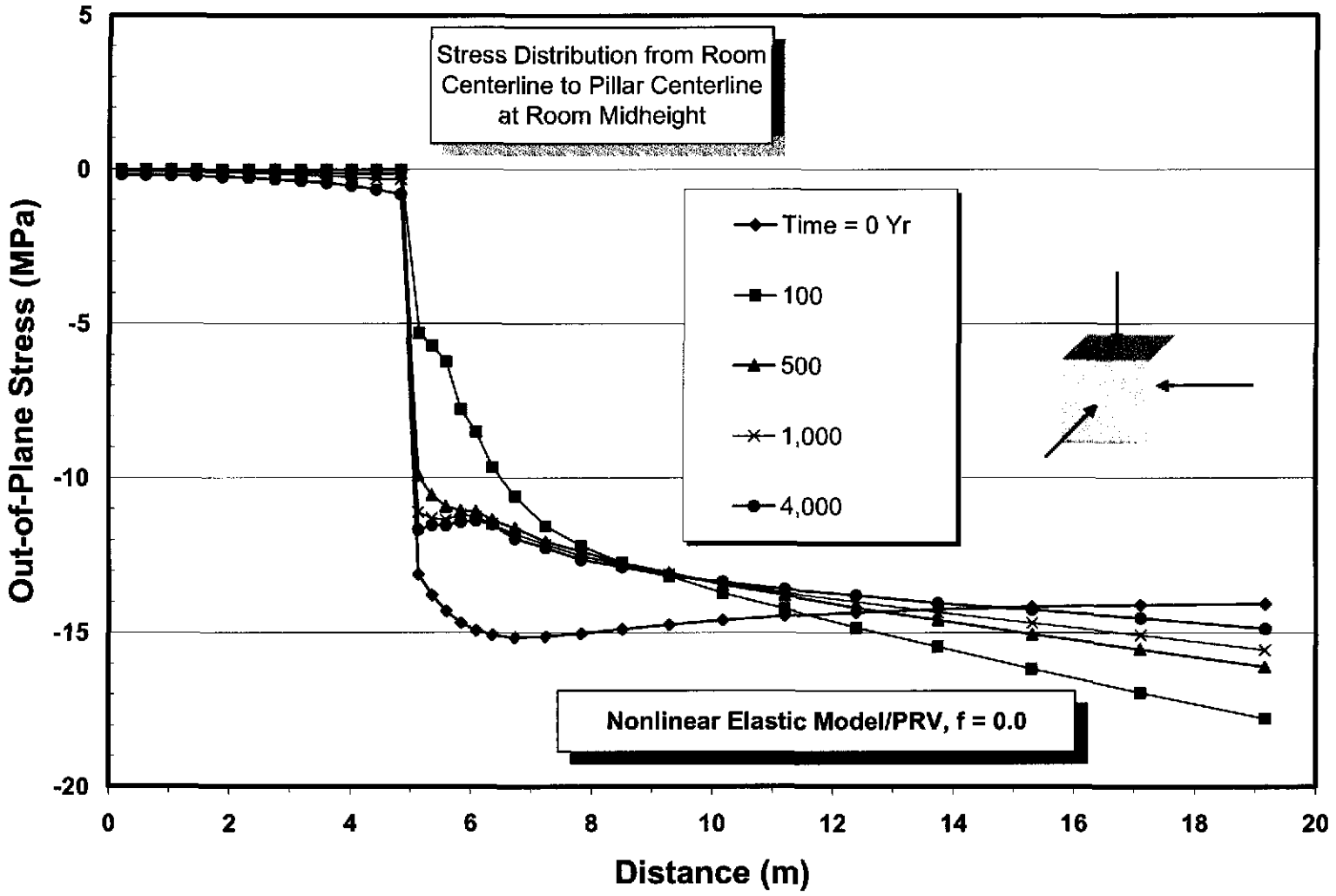

Figure A-24. Out-of-Plane Stress Distribution (σ_{zz}) From the Room Centerline to the Pillar Centerline at Room Midheight for the Nonlinear Elastic Analysis With a Variable Poisson's Ratio and No Gas Generation ($f = 0$).

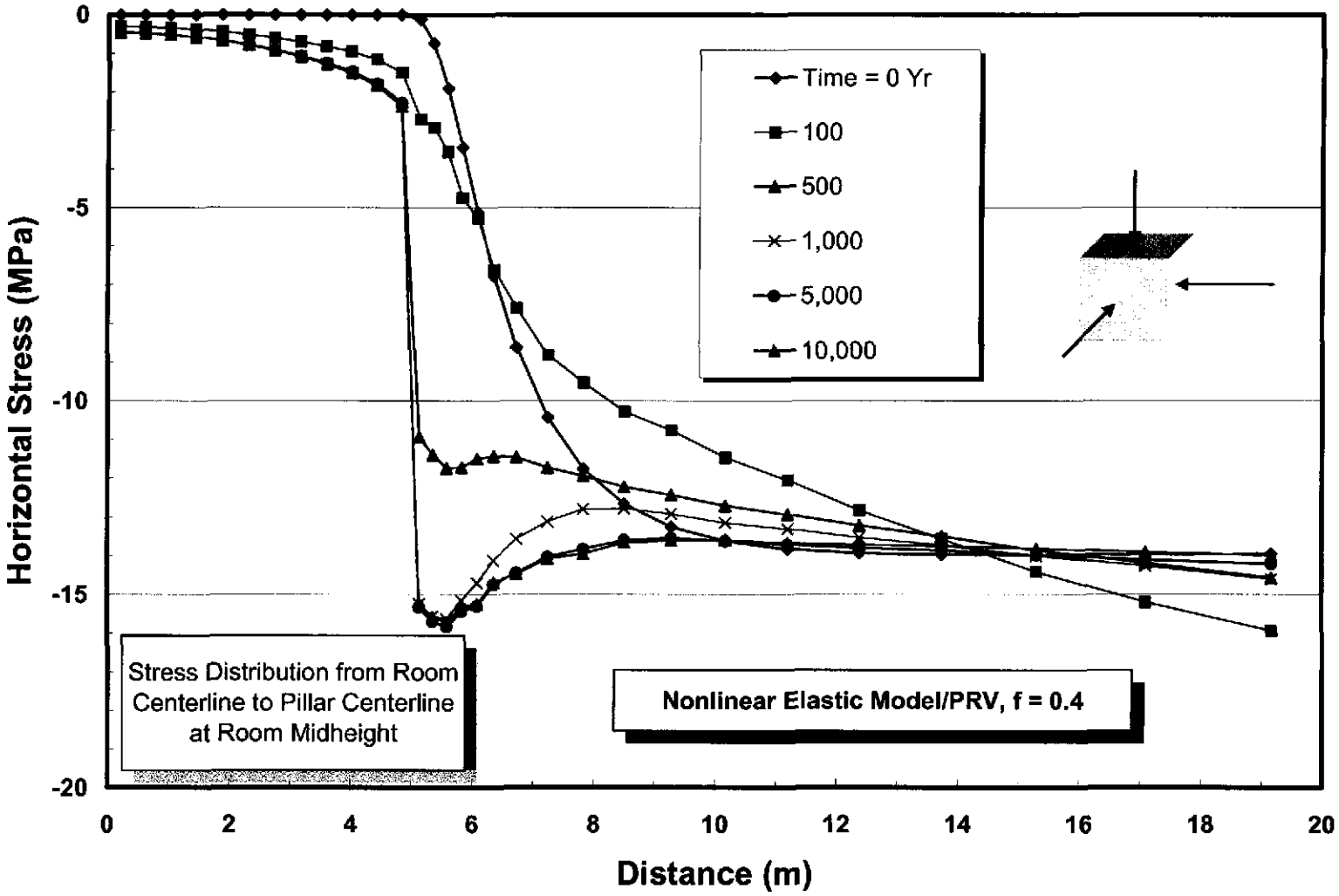

Figure A-25. Horizontal Stress Distribution (σ_{xx}) From the Room Centerline to the Pillar Centerline at Room Midheight for the Nonlinear Elastic Analysis With a Variable Poisson's Ratio and Gas Generation ($f = 0.4$).

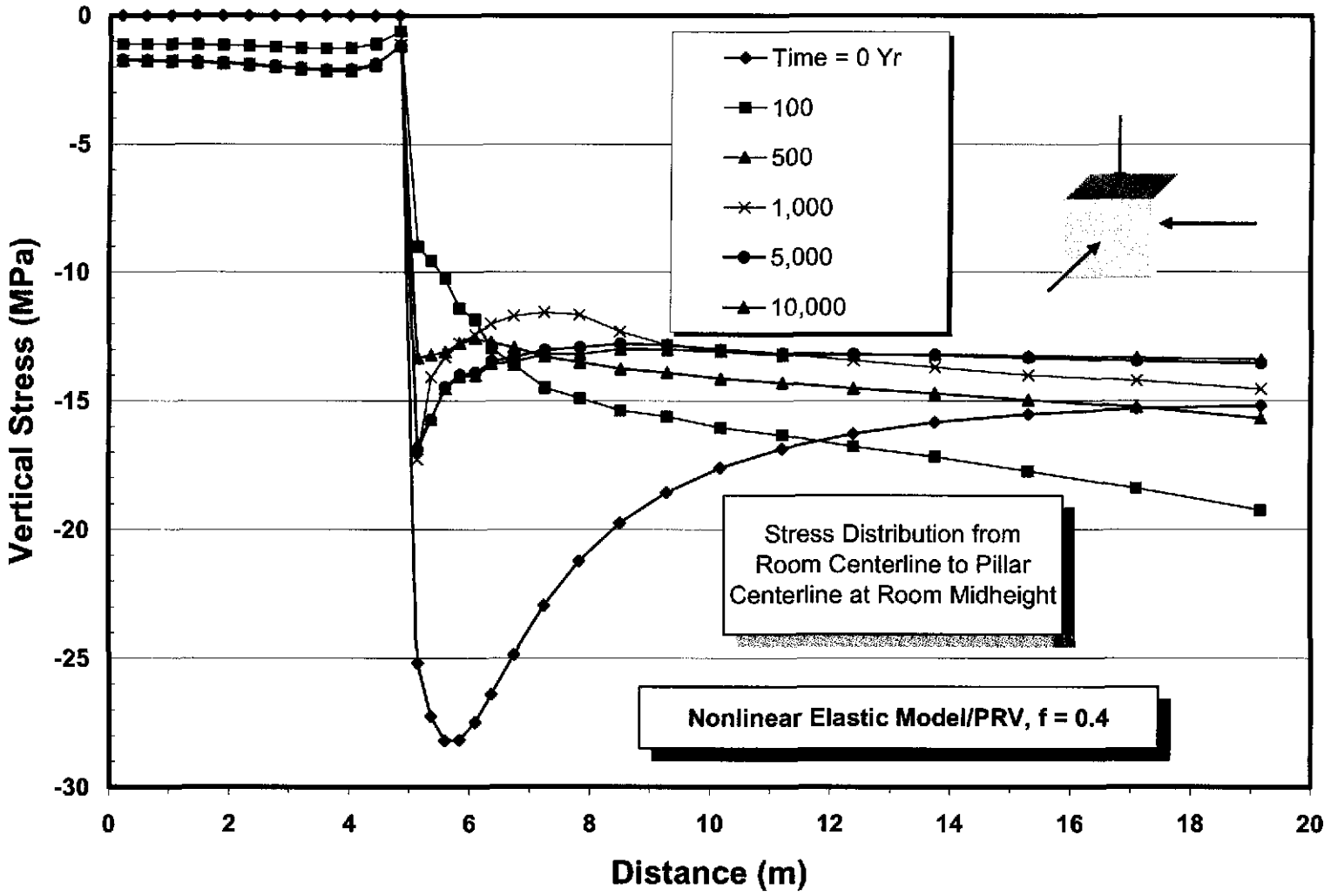

Figure A-26. Vertical Stress Distribution (σ_{yy}) From the Room Centerline to the Pillar Centerline at Room Midheight for the Nonlinear Elastic Analysis With a Variable Poisson's Ratio and Gas Generation ($f = 0.4$).

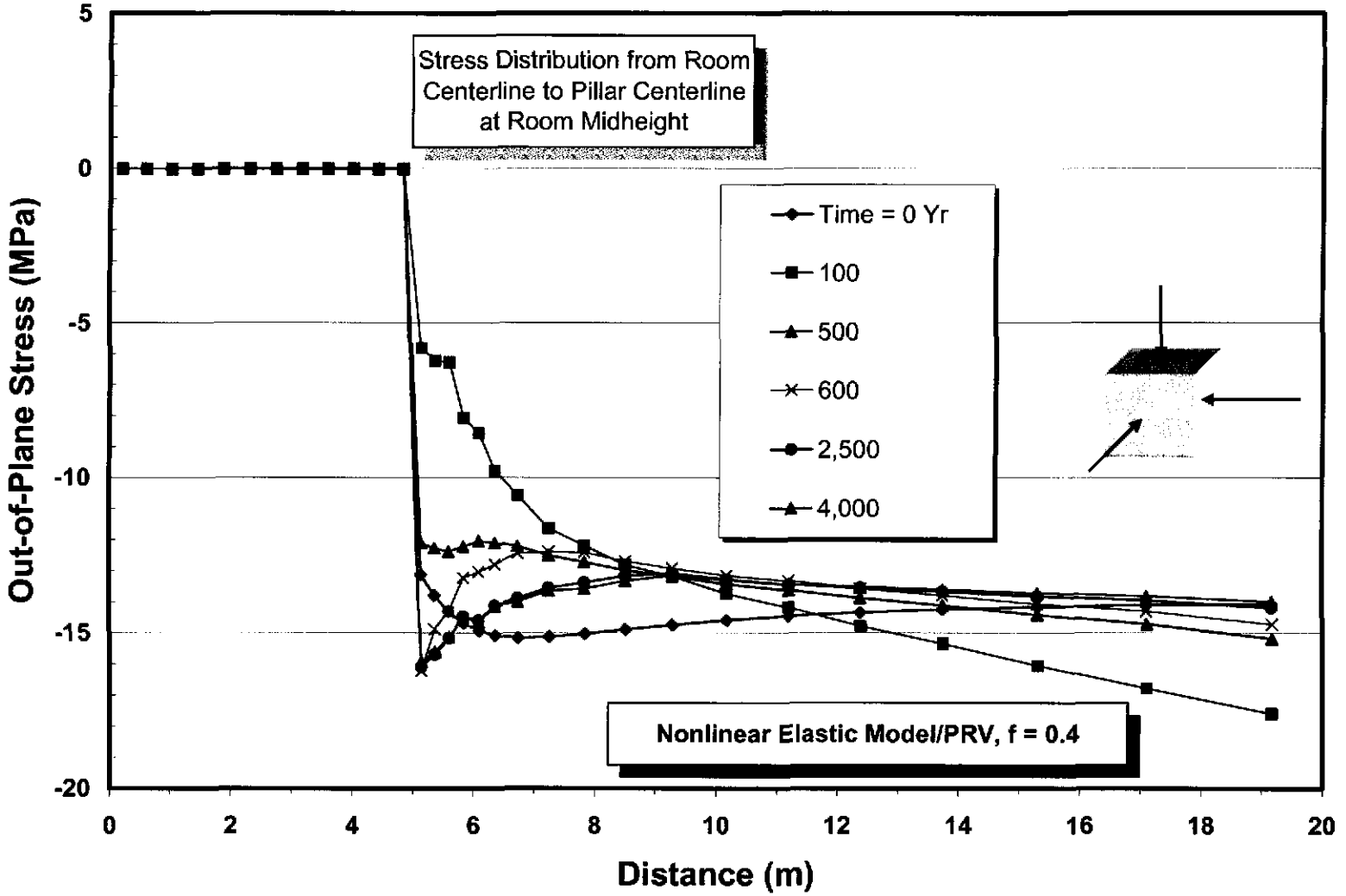

Figure A-27. Out-of-Plane Stress Distribution (σ_{zz}) From the Room Centerline to the Pillar Centerline at Room Midheight for the Nonlinear Elastic Analysis With a Variable Poisson's Ratio and Gas Generation ($f = 0.4$).

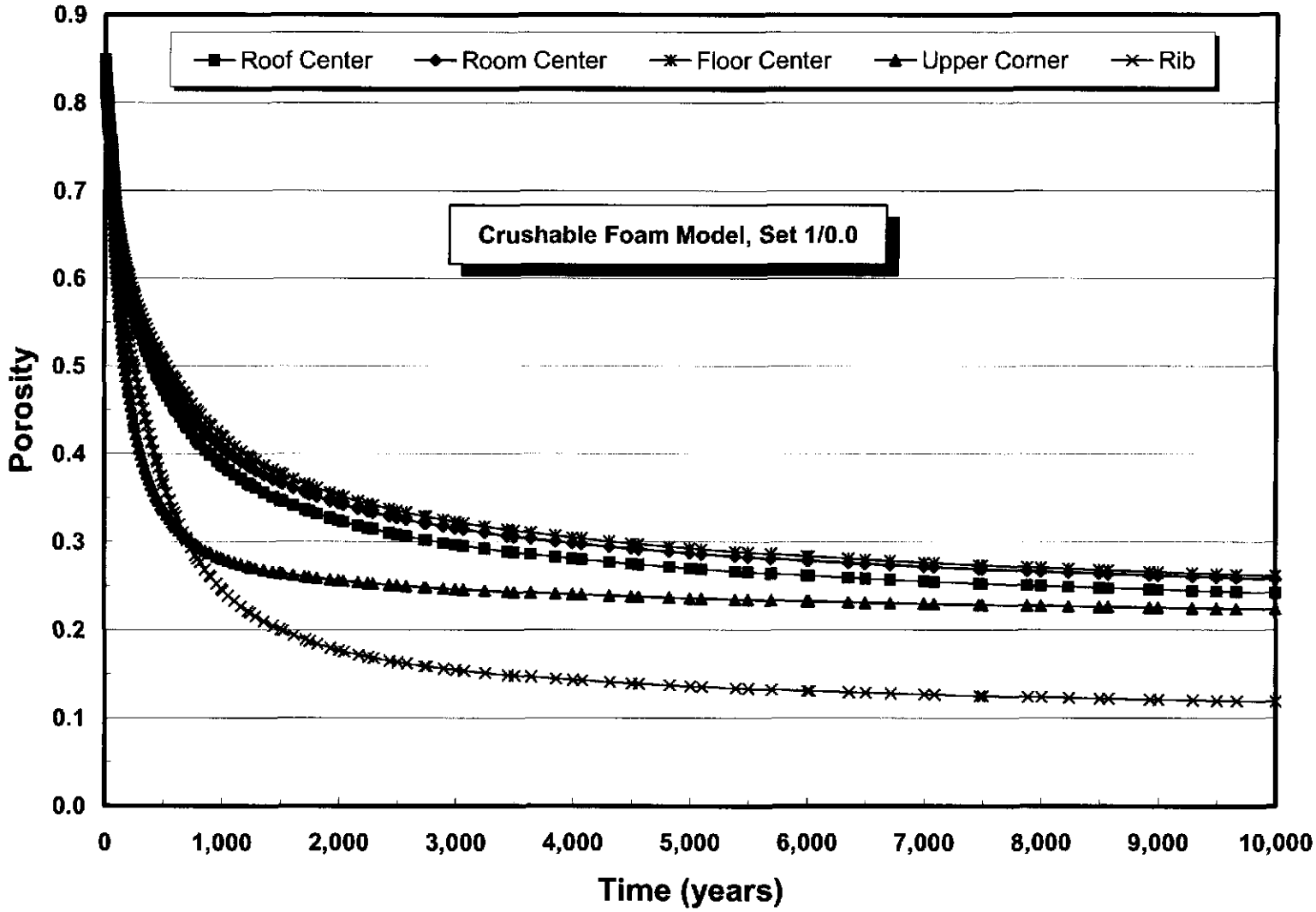

RSI-1487-04-023

Figure A-28. Elemental Porosity Versus Time at Five Locations Within the Room for the Crushable Foam Analysis (v = 0.0) Using Parameter Set 1.

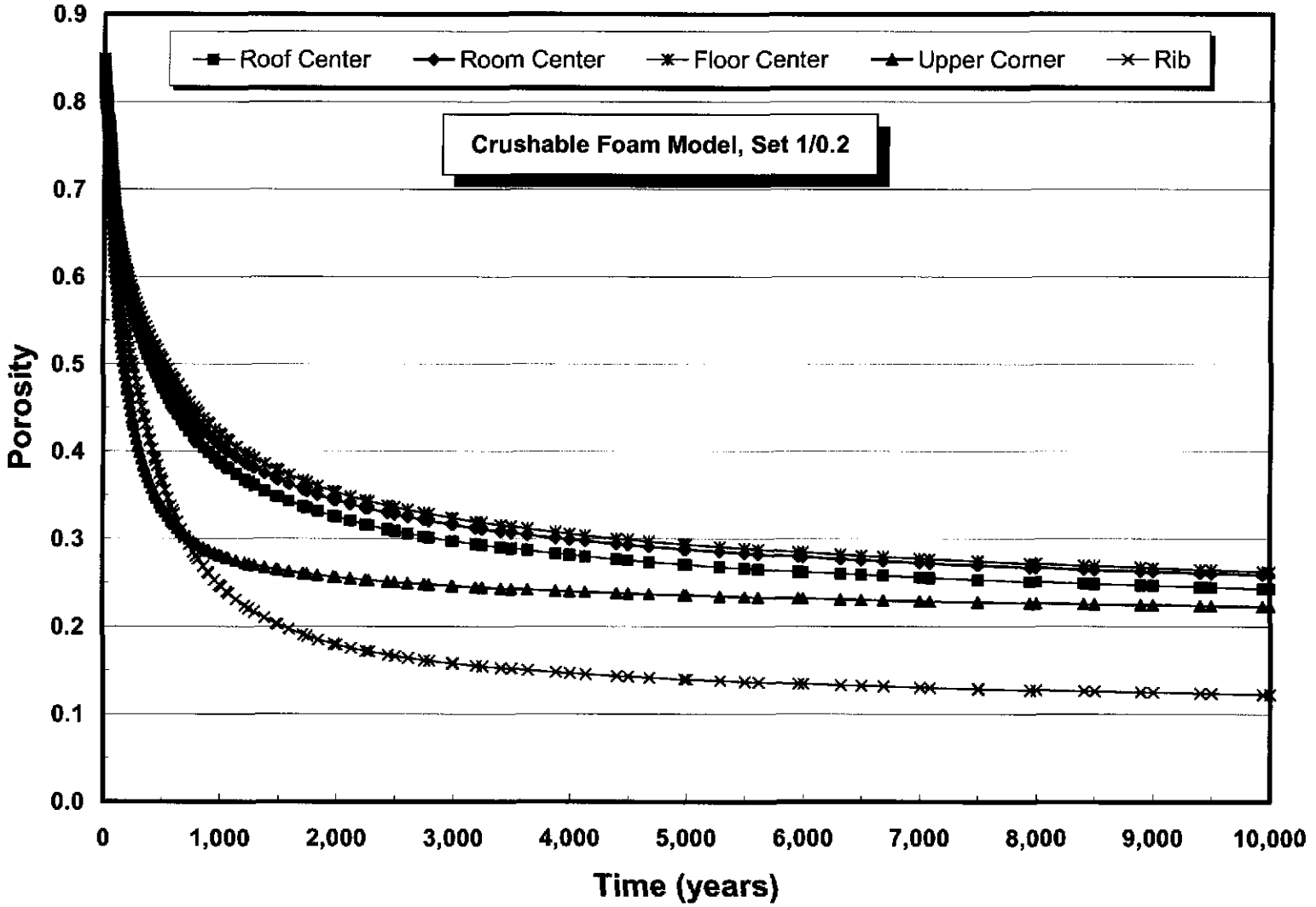

RSI-1487-04-077

Figure A-29. Elemental Porosity Versus Time at Five Locations Within the Room for the Crushable Foam Analysis ($\nu = 0.2$) Using Parameter Set 1.

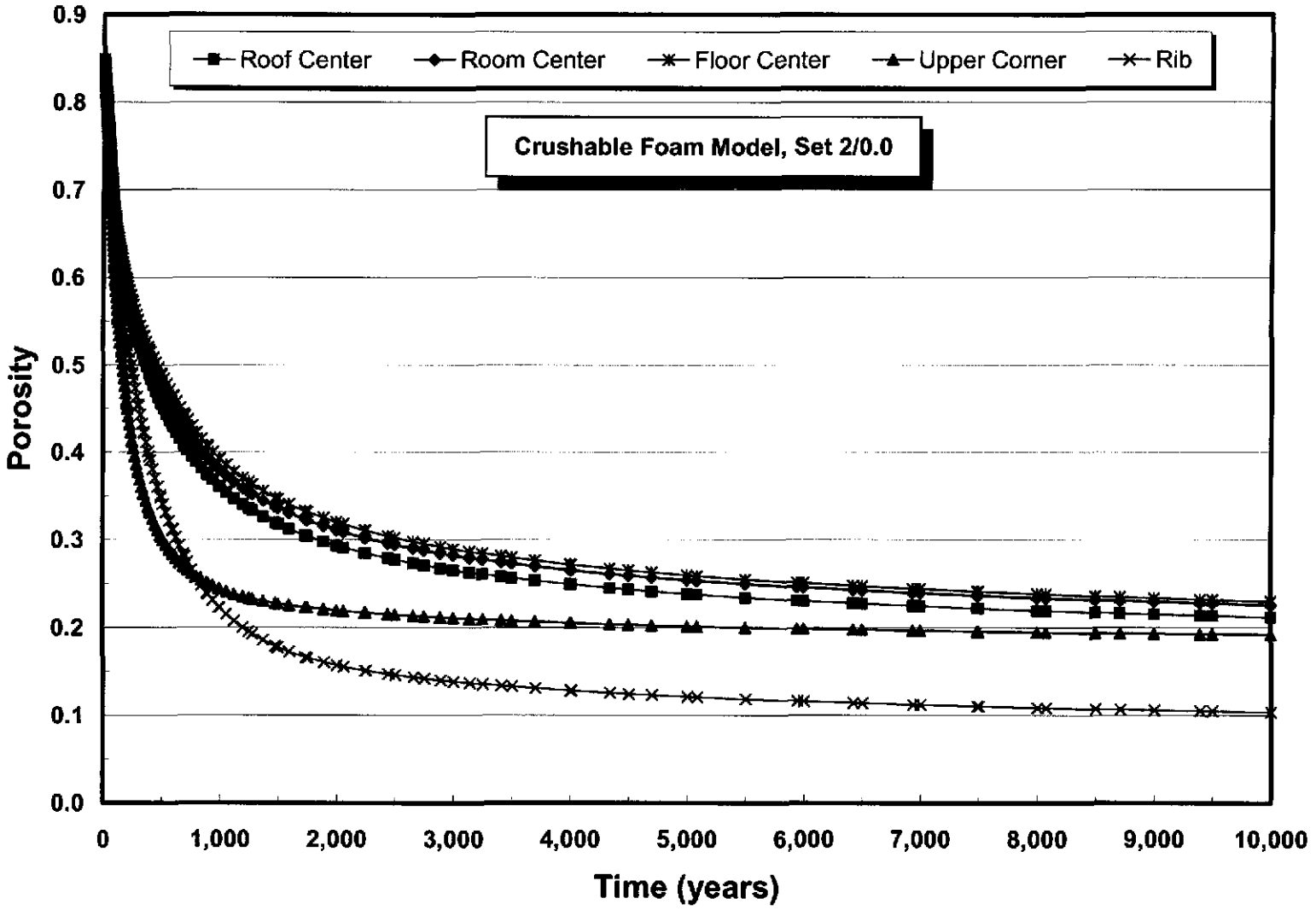

Figure A-30. Elemental Porosity Versus Time at Five Locations Within the Room for the Crushable Foam Analysis (ν = 0.0) Using Parameter Set 2.

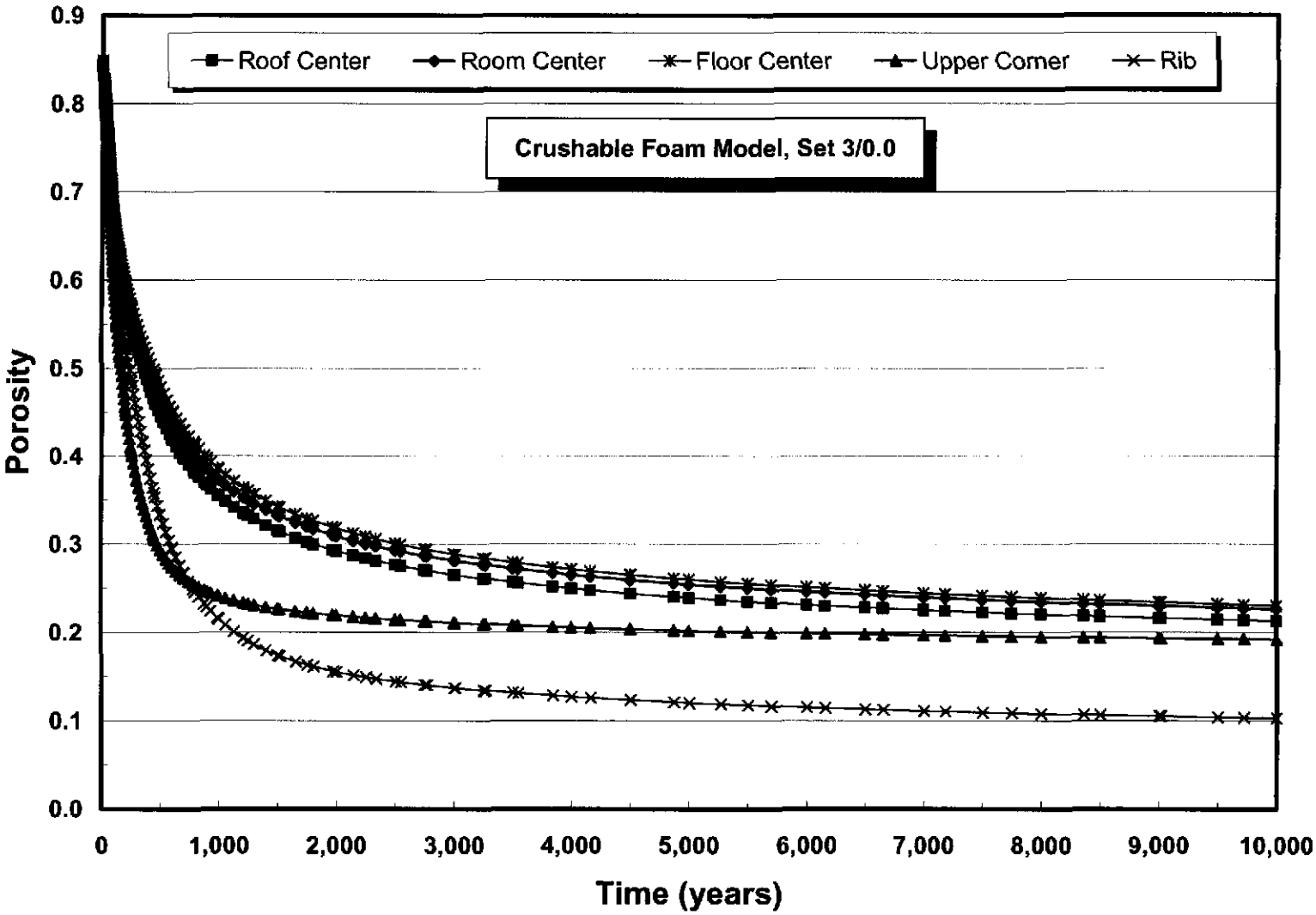

RSI-1487-04-038

Figure A-31. Elemental Porosity Versus Time at Five Locations Within the Room for the Crushable Foam Analysis (ν = 0.0) Using Parameter Set 3.

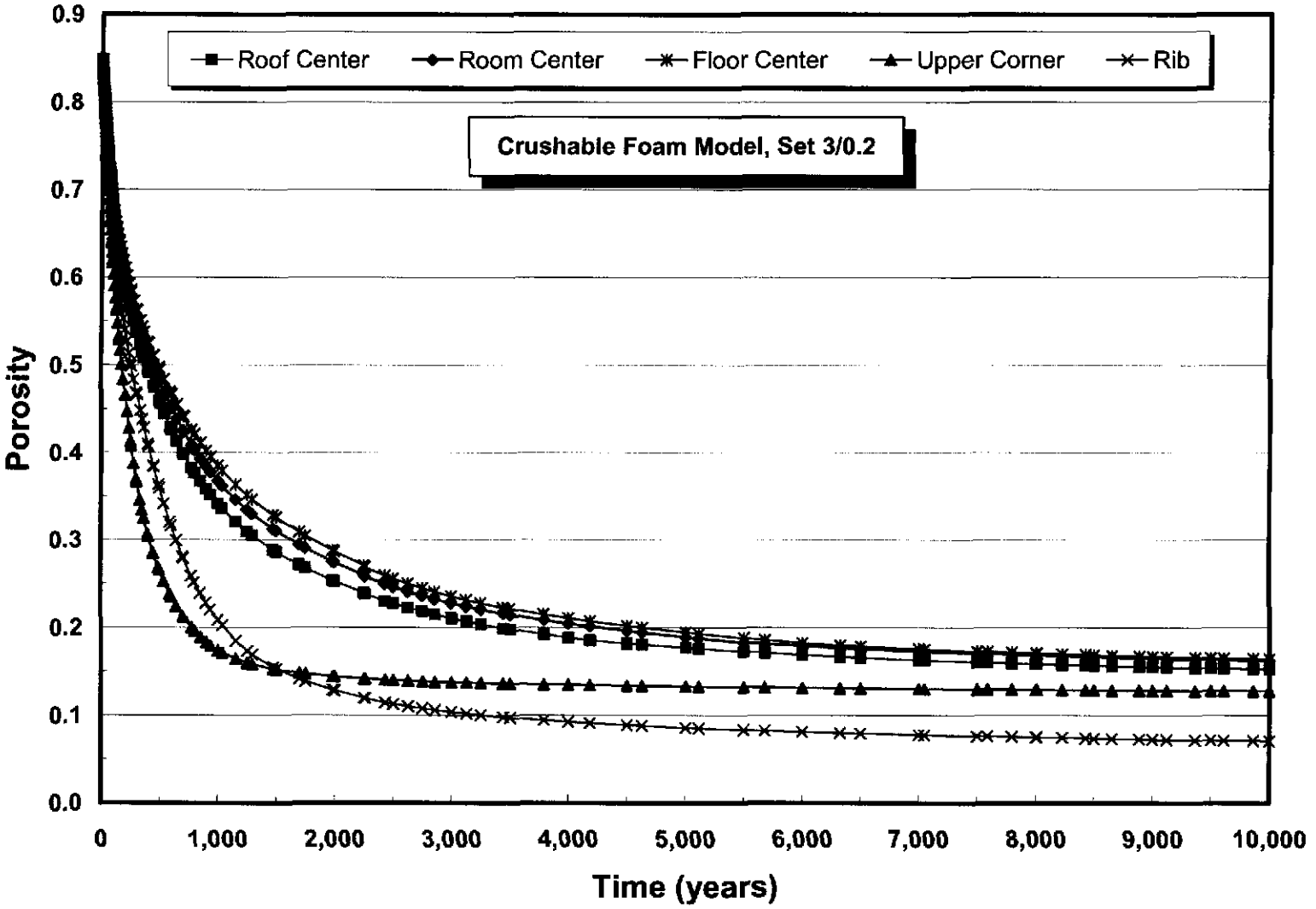

Figure A-32. Elemental Porosity Versus Time at Five Locations Within the Room for the Crushable Foam Analysis (ν = 0.2) Using Parameter Set 3.

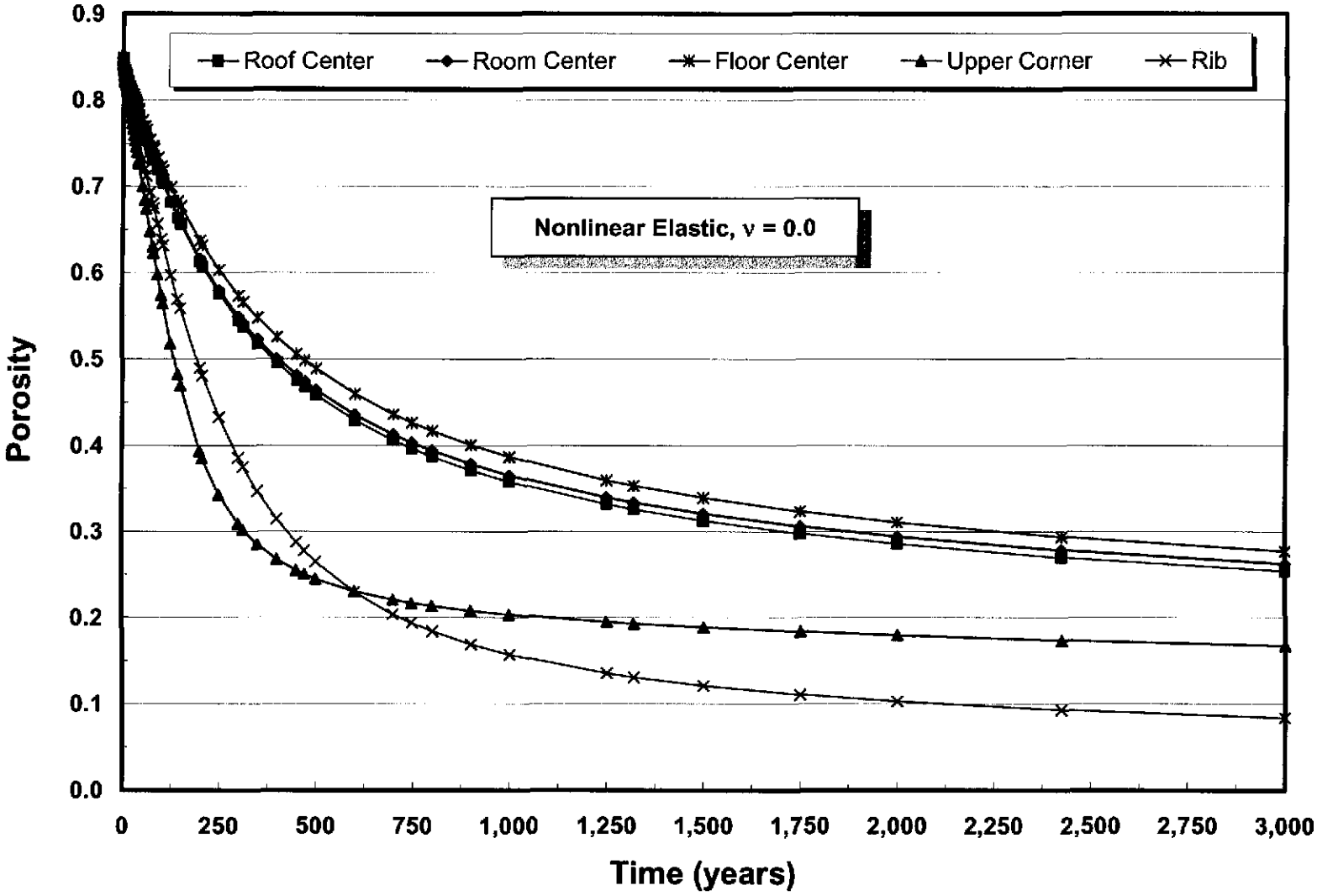

Figure A-33. Elemental Porosity Versus Time at Five Locations Within the Room for the Nonlinear Elastic (ν = 0.0) Analysis.

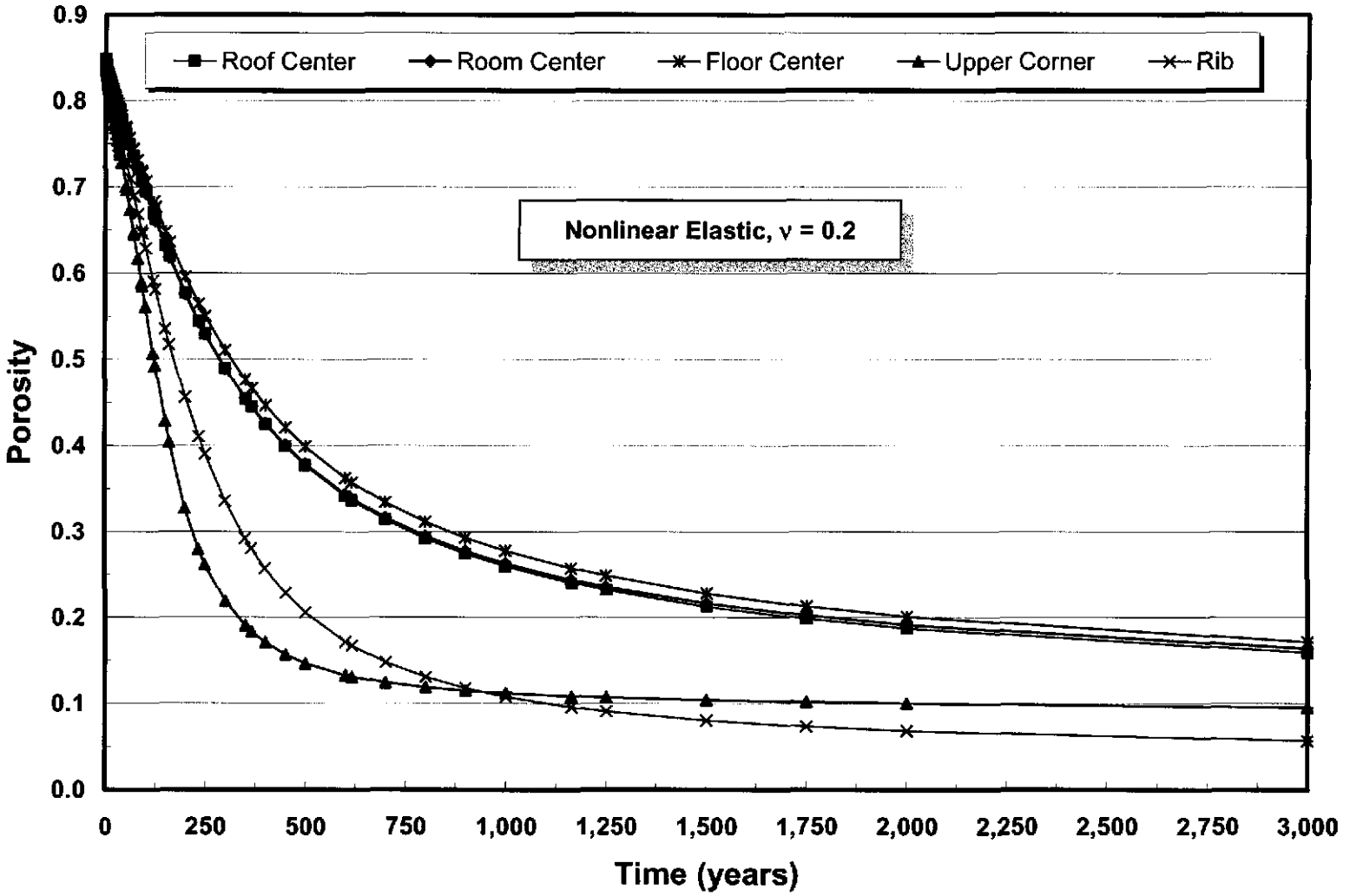

Figure A-34. Elemental Porosity Versus Time at Five Locations Within the Room for the Nonlinear Elastic (ν = 0.2) Analysis.

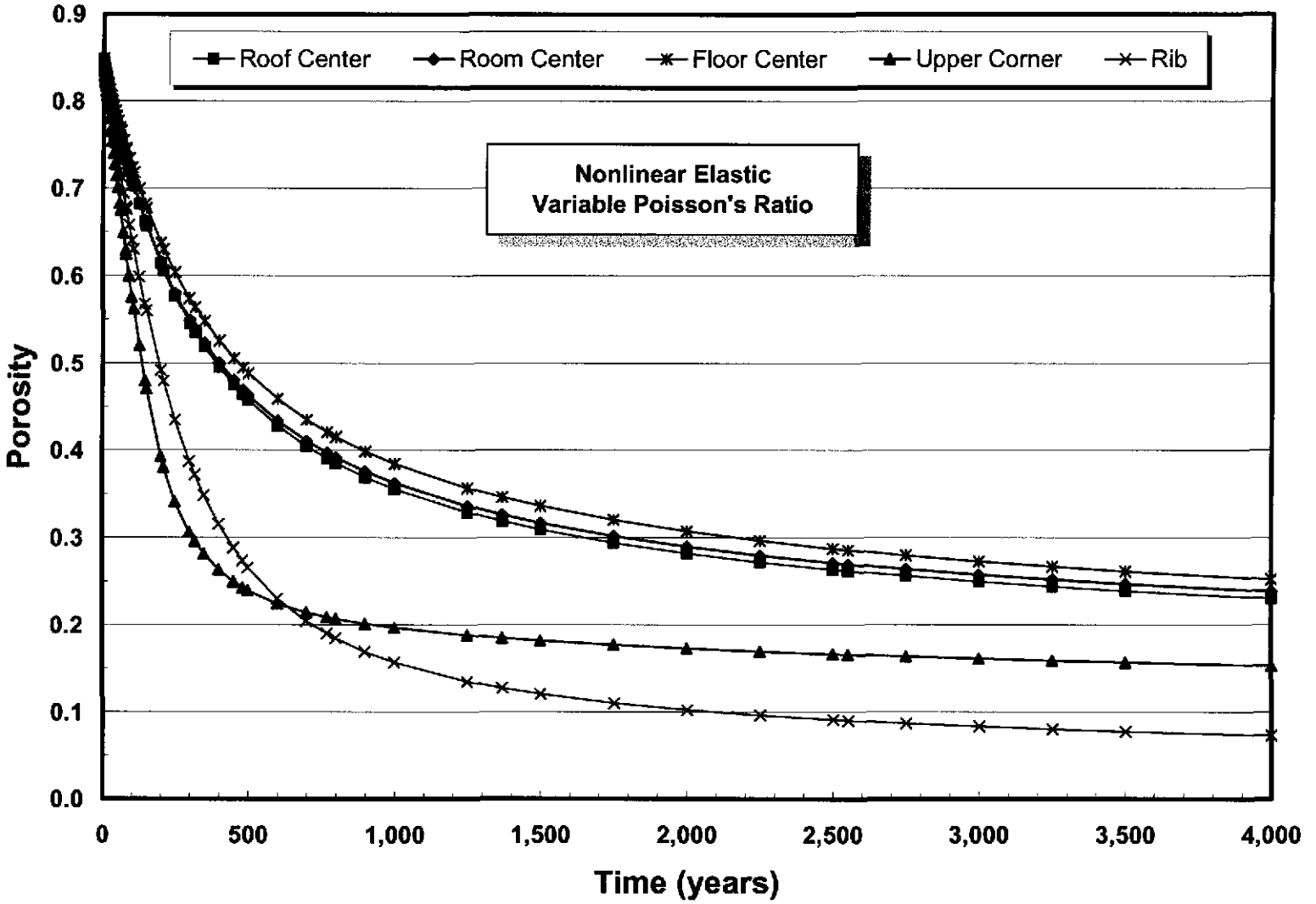

RSI-1487-04-080

Figure A-35. Elemental Porosity Versus Time at Five Locations Within the Room for the Nonlinear Elastic (ν = Variable) Analysis.

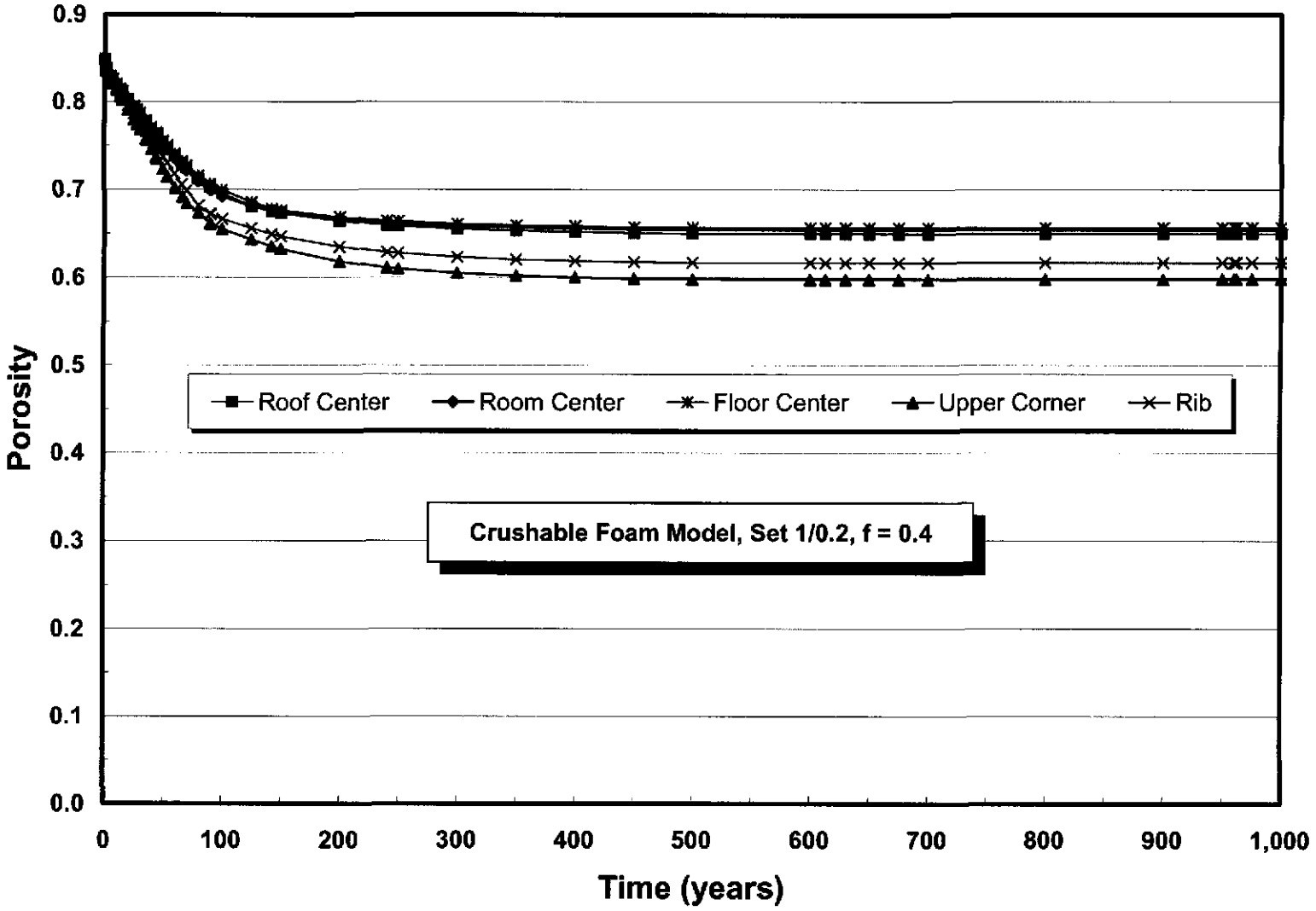

Figure A-36. Elemental Porosity Versus Time at Five Locations Within the Room for the Crushable Foam Analysis (ν = 0.2) Using Parameter Set 1 With Gas Generation Rate $f = 0.4$.

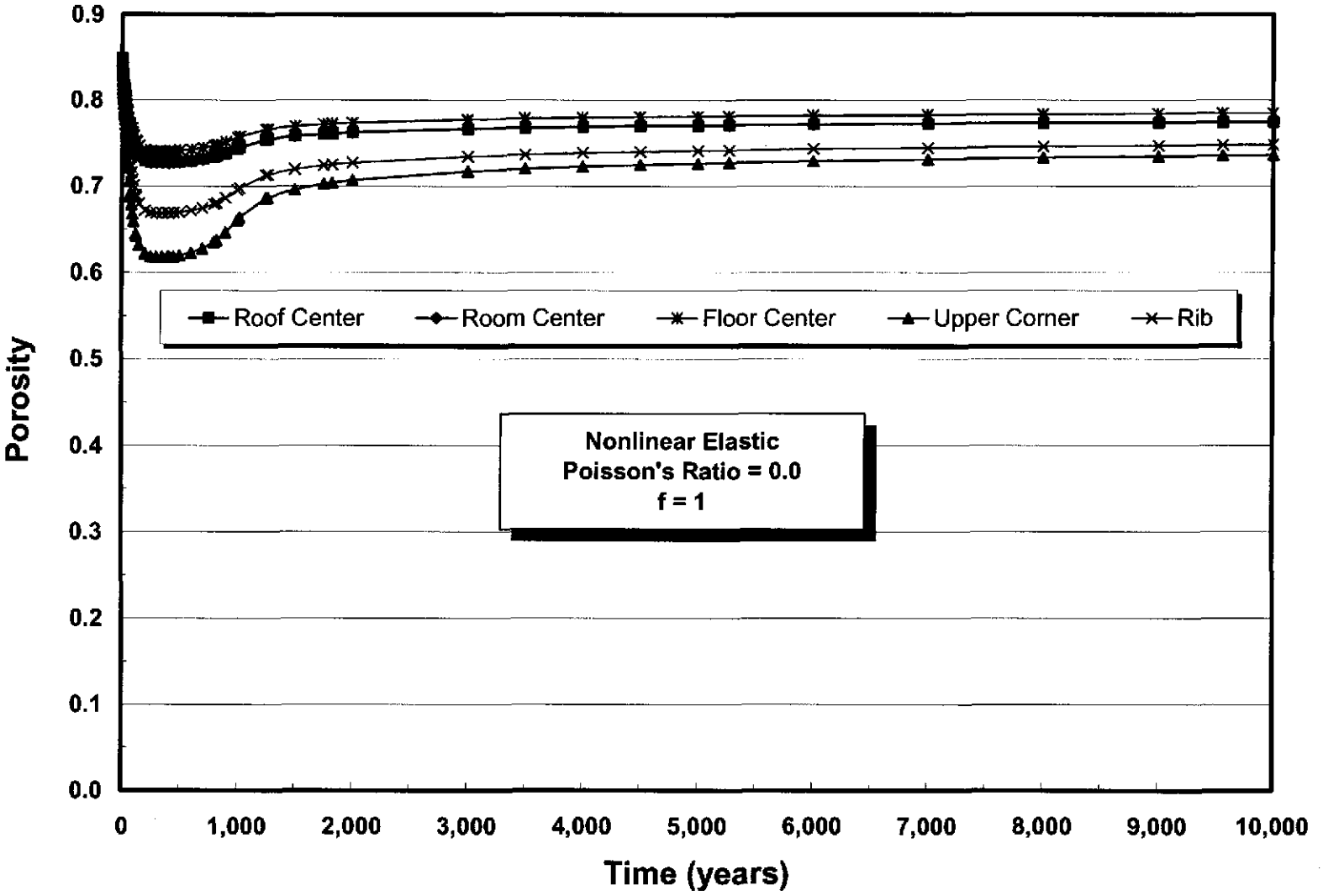

Figure A-37. Elemental Porosity Versus Time at Five Locations Within the Room for the Nonlinear Elastic ($\nu = 0.0$) Analysis With Gas Generation Rate $f = 1$.

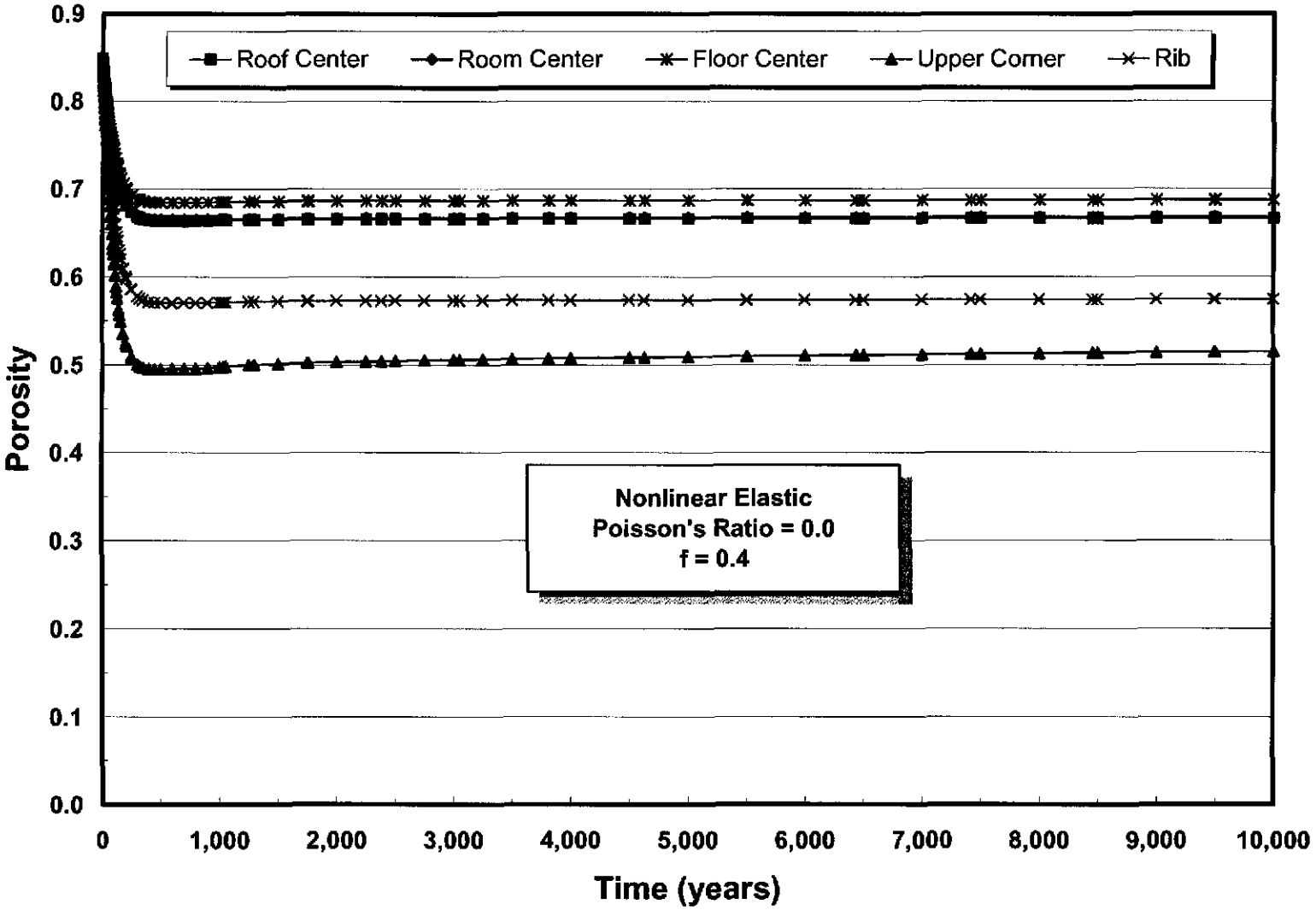

Figure A-38. Elemental Porosity Versus Time at Five Locations Within the Room for the Nonlinear Elastic ($\nu = 0.0$) Analysis With Gas Generation Rate $f = 0.4$.

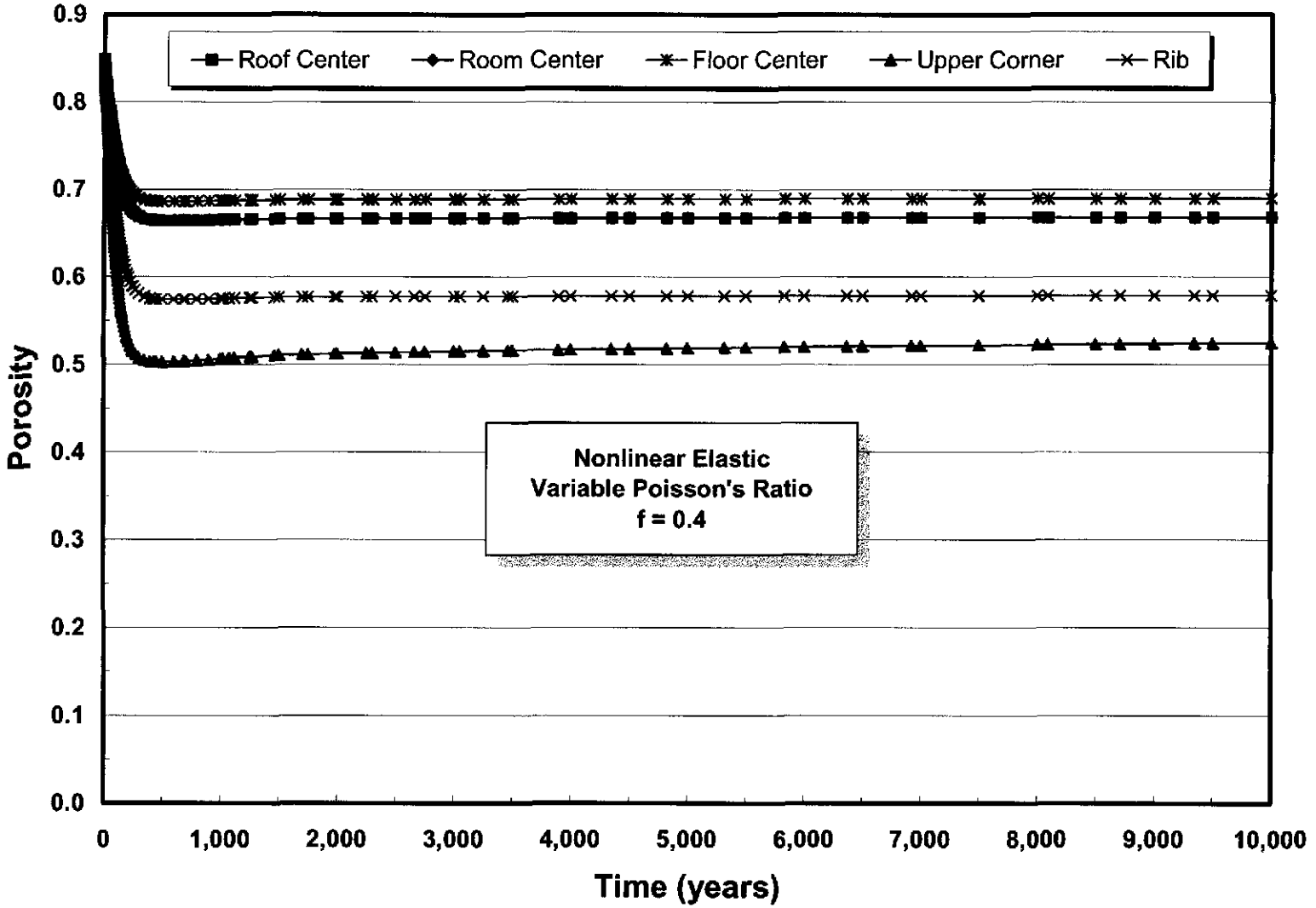

Figure A-39. Elemental Porosity Versus Time at Five Locations Within the Room for the Nonlinear Elastic (ν = Variable) Analysis With Gas Generation Rate $f = 0.4$.

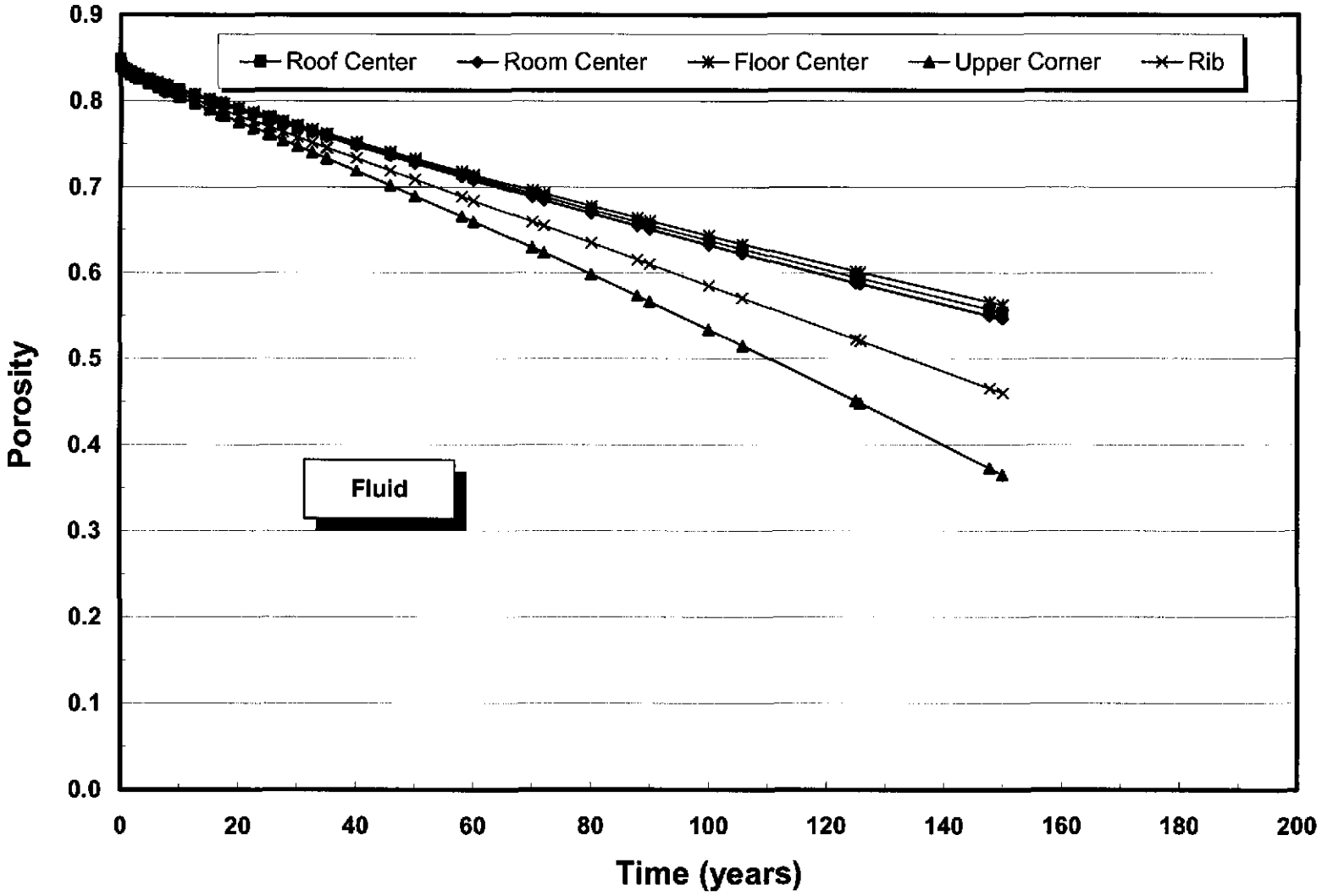

Figure A-40. Elemental Porosity Versus Time at Five Locations Within the Room for the Fluid Material Analysis.

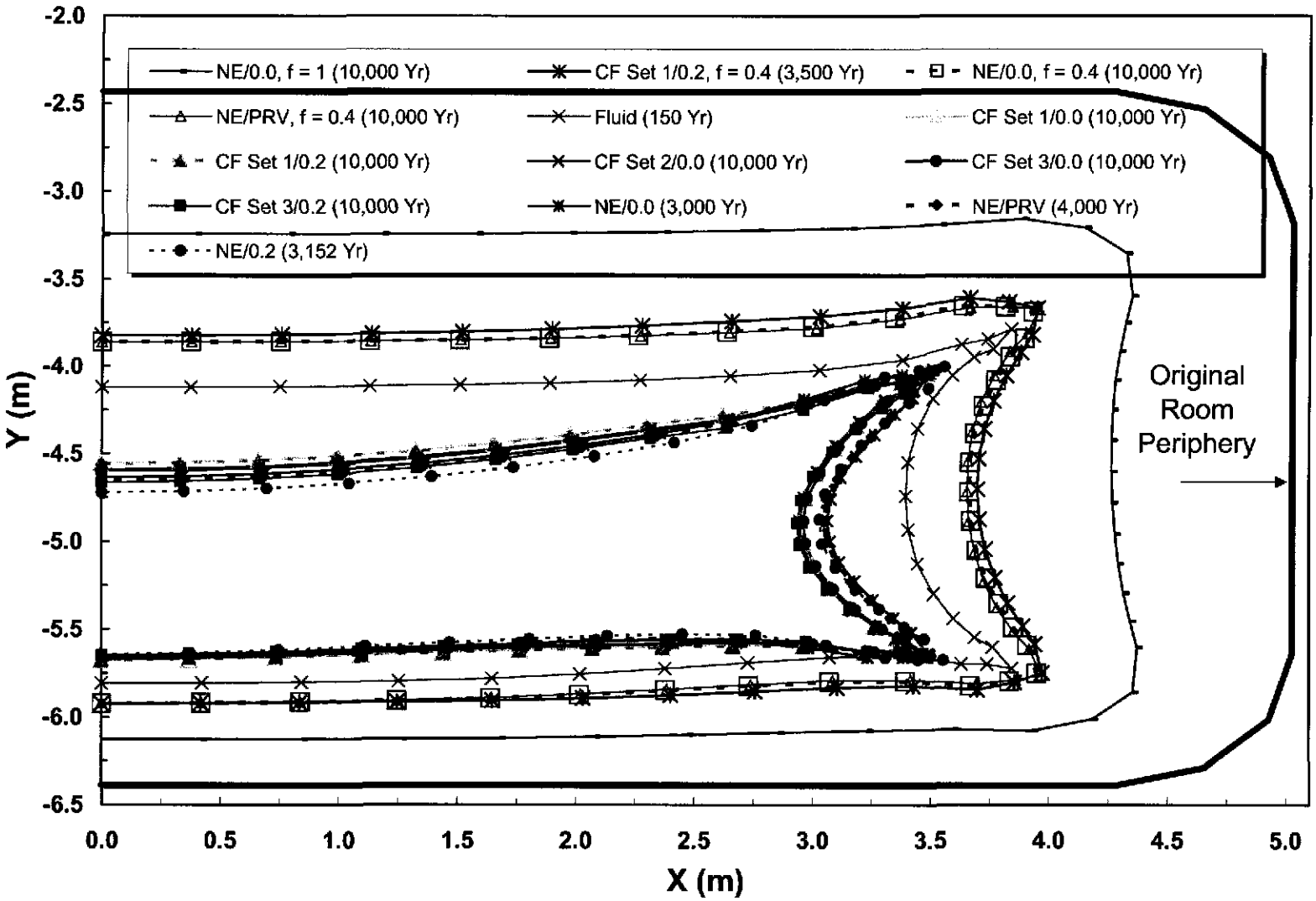

RSI-1487-04-041

Figure A-41. Comparison of the Room Peripheries at Their Final Calculated Configuration for Each of the Analyses.

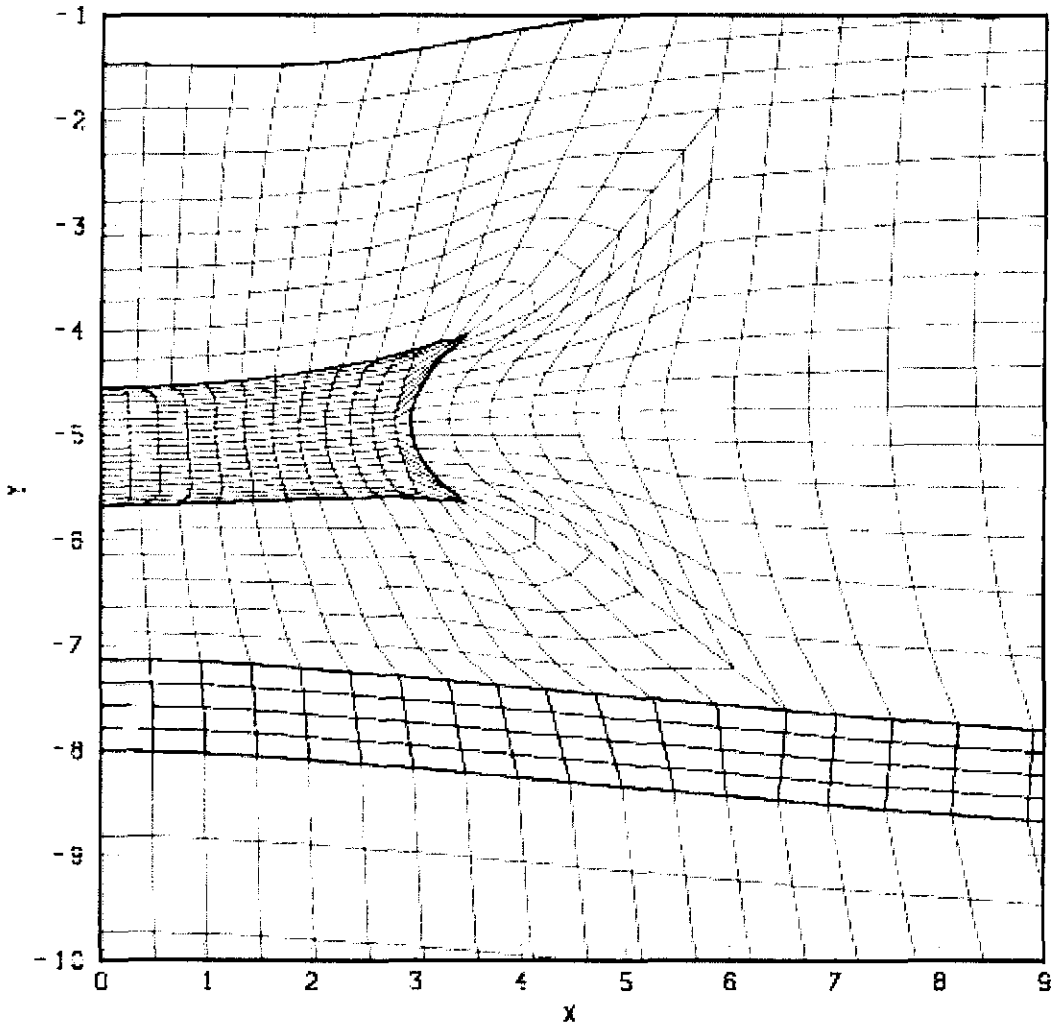

Figure A-42. Deformed Mesh Configuration for the Crushable Foam Analysis Using Parameter Set 1 at 10,000 Years.

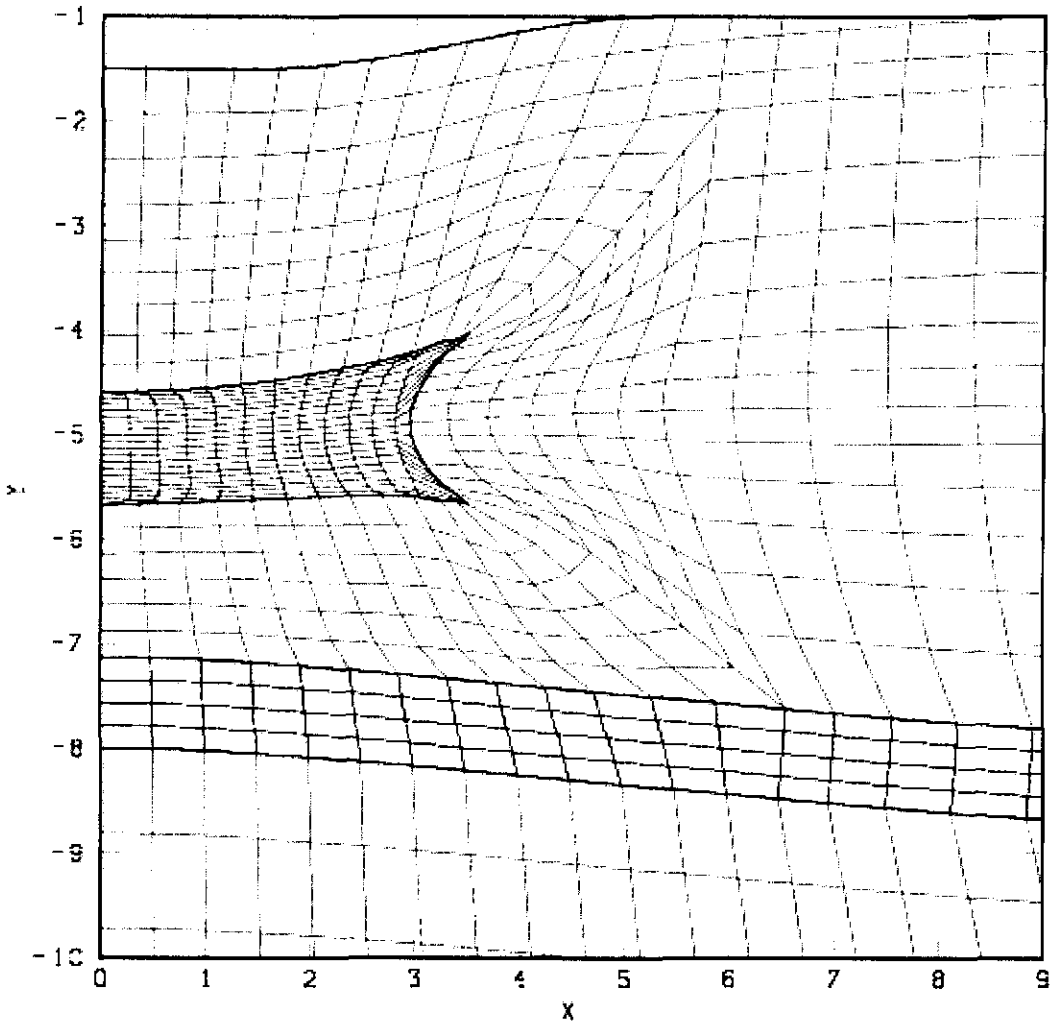

Figure A-43. Deformed Mesh Configuration for the Crushable Foam Analysis Using Parameter Set 2 at 10,000 Years.

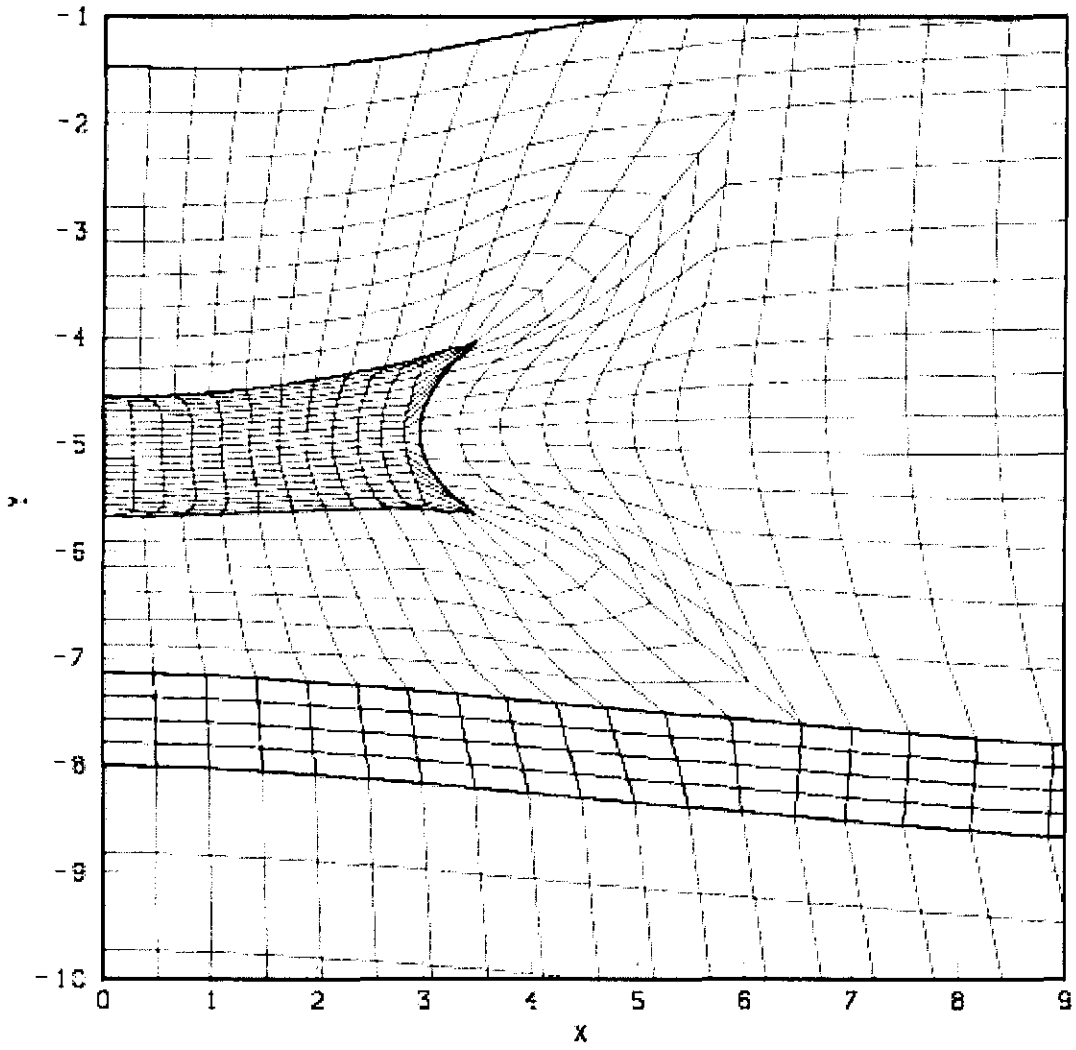

Figure A-44. Deformed Mesh Configuration for the Crushable Foam Analysis Using Parameter Set 3 at 10,000 Years.

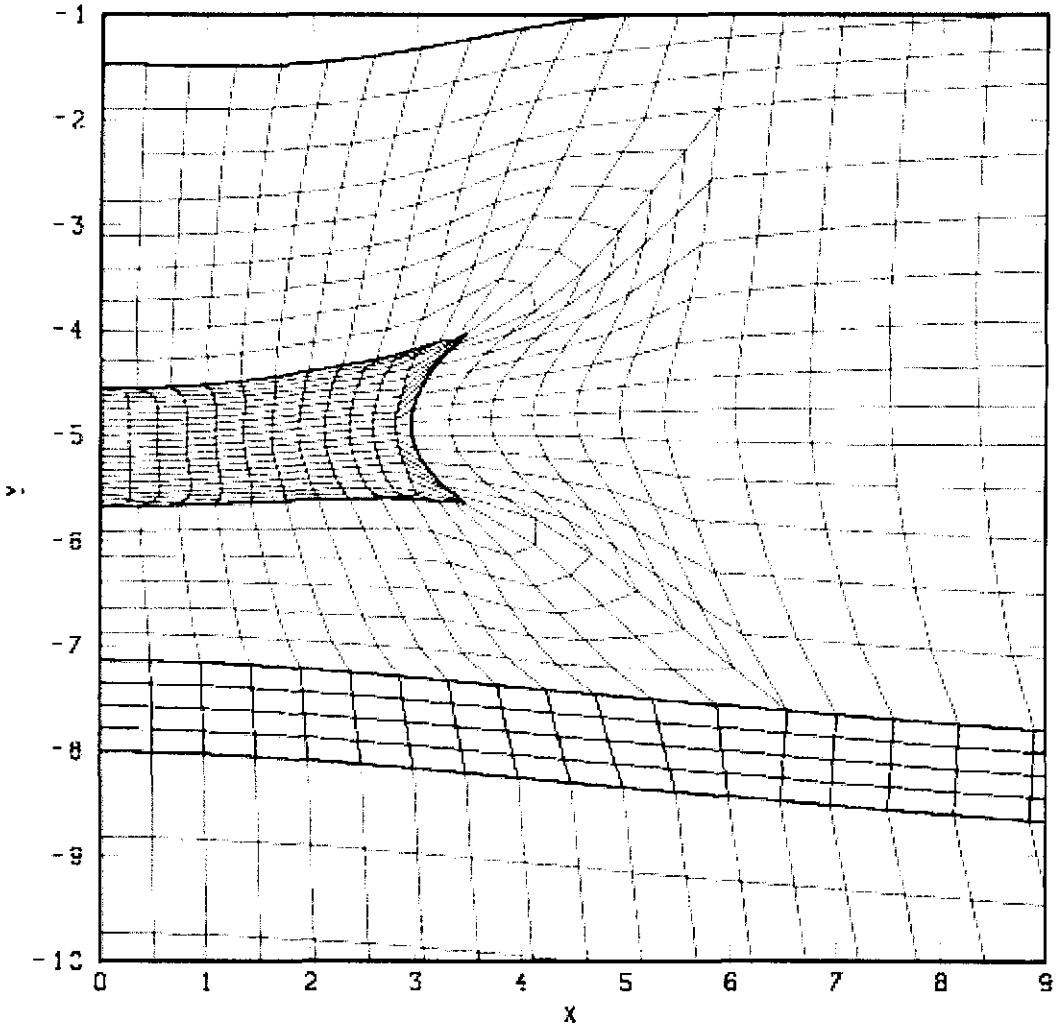

Figure A-45. Deformed Mesh Configuration for the Crushable Foam Analysis Using Parameter Set 1 With Poisson's Ratio Equal to 0.2 at 10,000 Years.

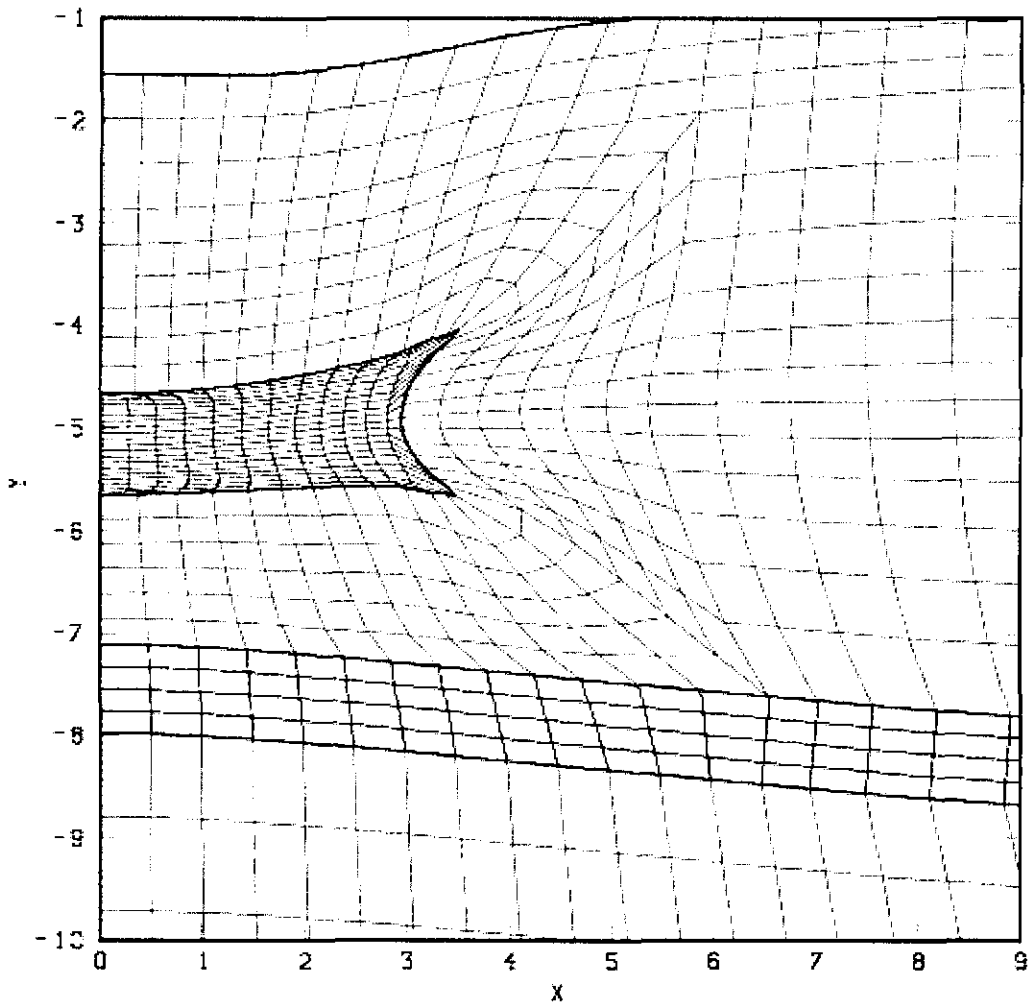

Figure A-46. Deformed Mesh Configuration for the Crushable Foam Analysis Using Parameter Set 3 With Poisson's Ratio Equal to 0.2 at 10,000 Years.

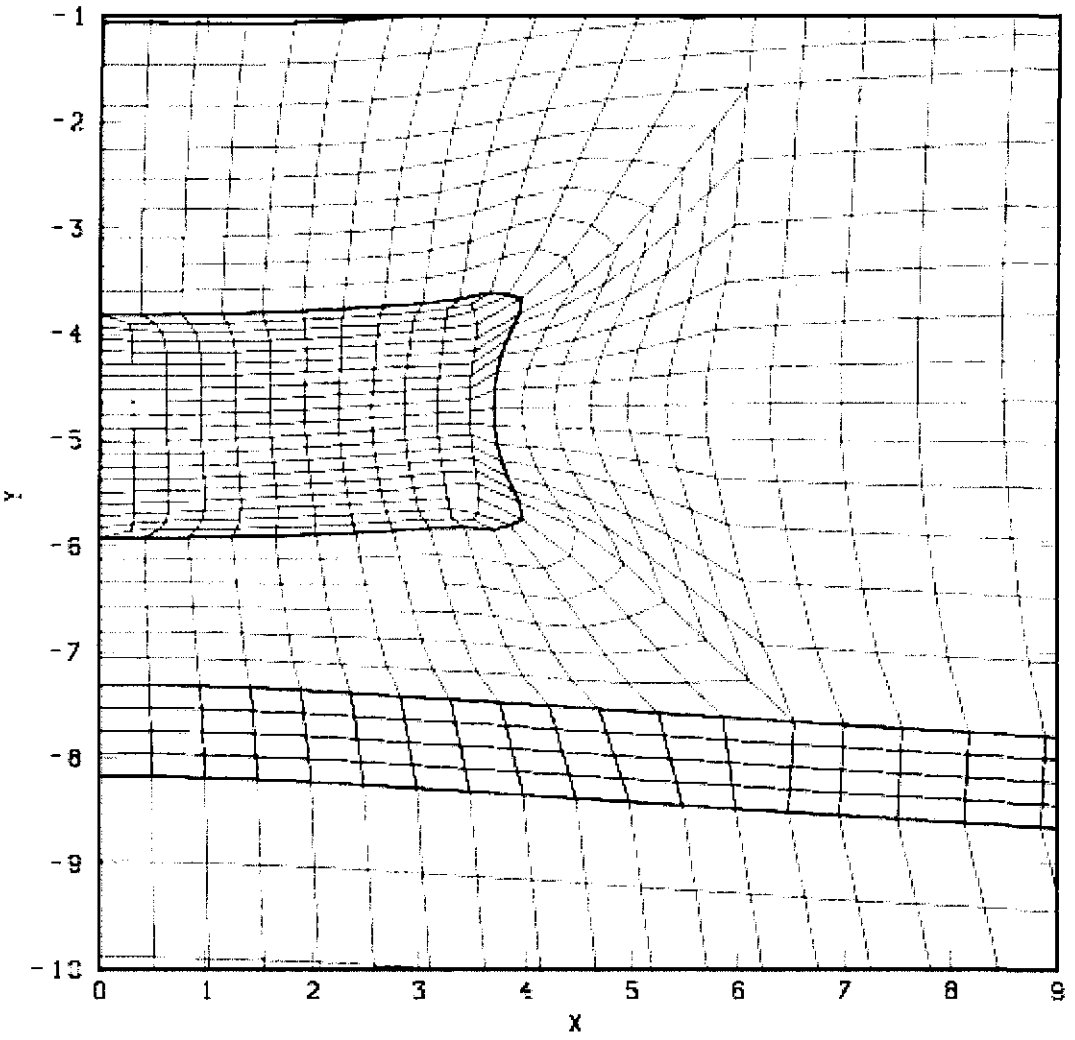

Figure A-47. Deformed Mesh Configuration for the Crushable Foam Analysis Using Parameter Set 1 With Poisson's Ratio Equal to 0.0 Including Gas Generation ($f = 0.4$) at 3,500 Years.

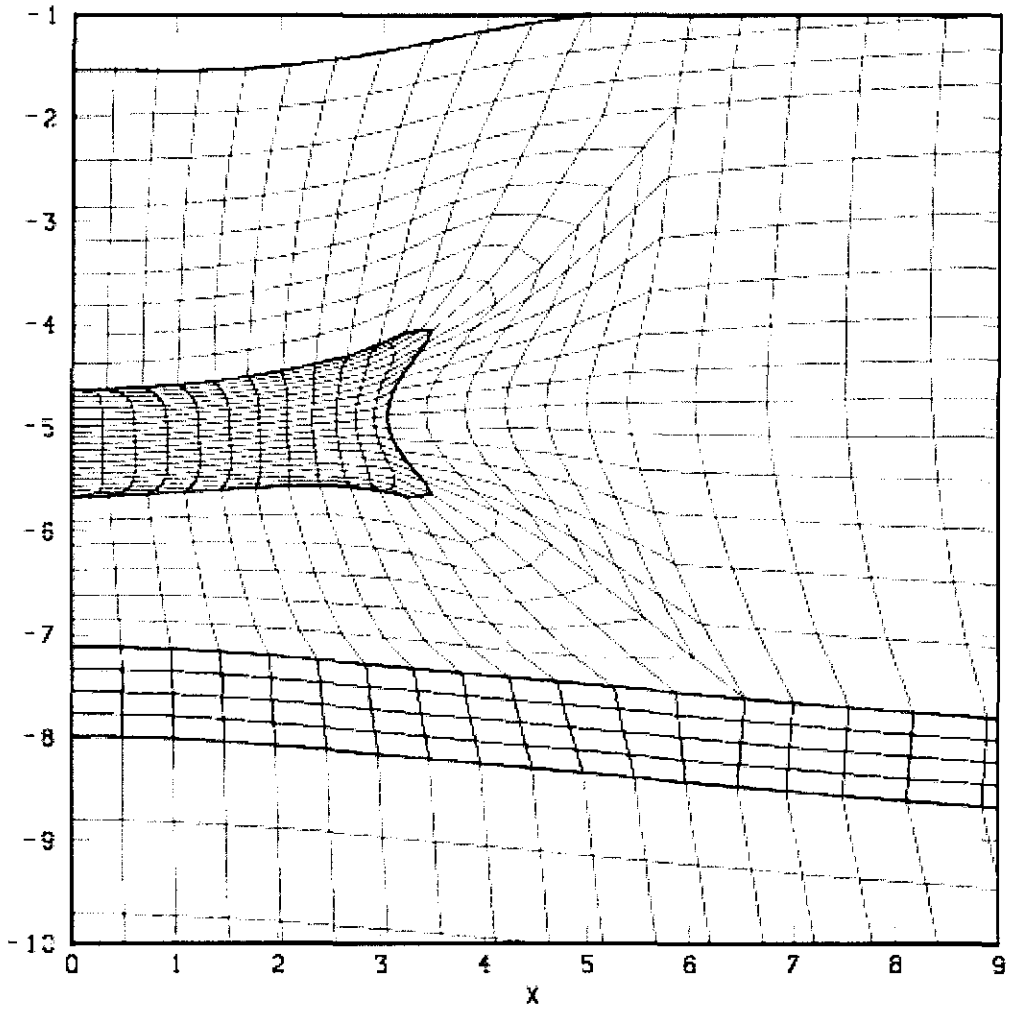

Figure A-48. Deformed Mesh Configuration for the Nonlinear Elastic (ν = 0.0) Analysis at 3,000 Years.

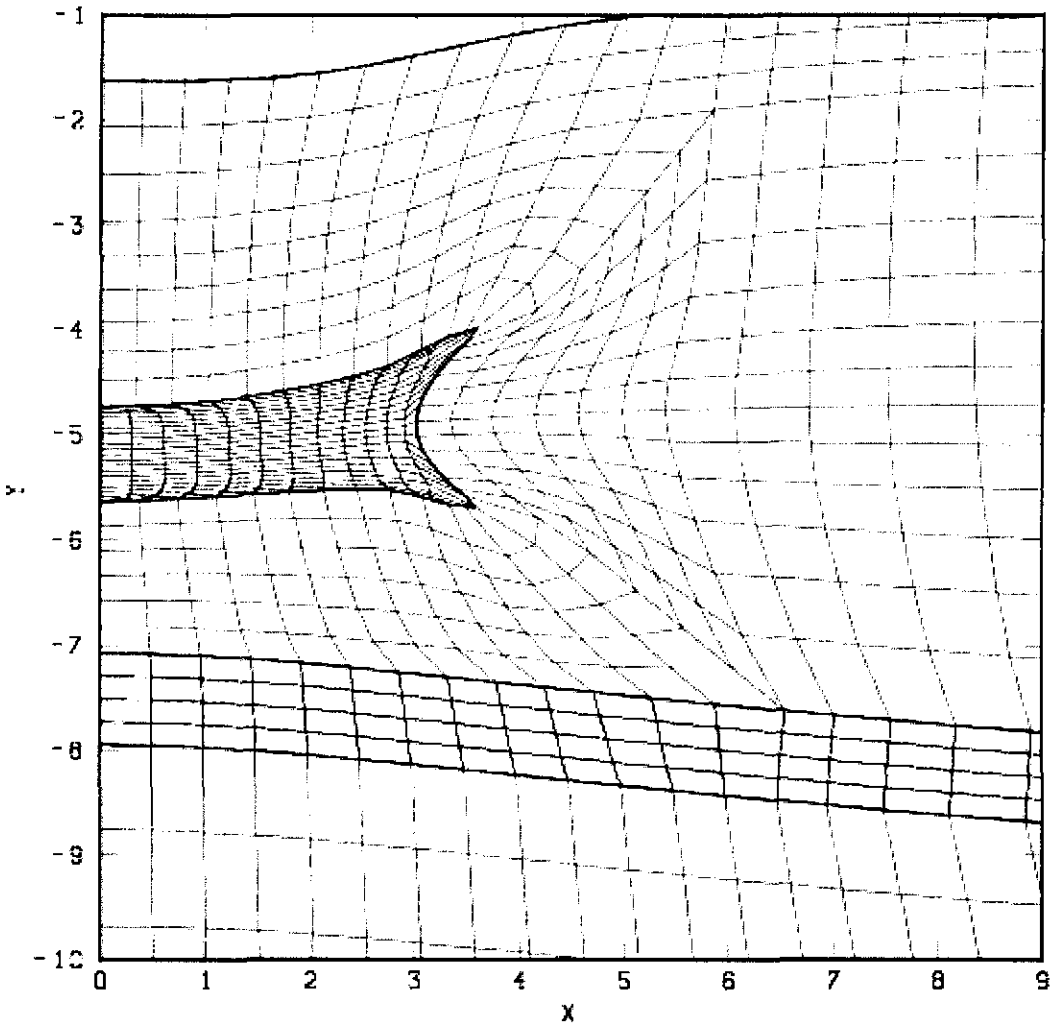

Figure A-49. Deformed Mesh Configuration for the Nonlinear Elastic ($\nu = 0.2$) Analysis at 4,443 Years.

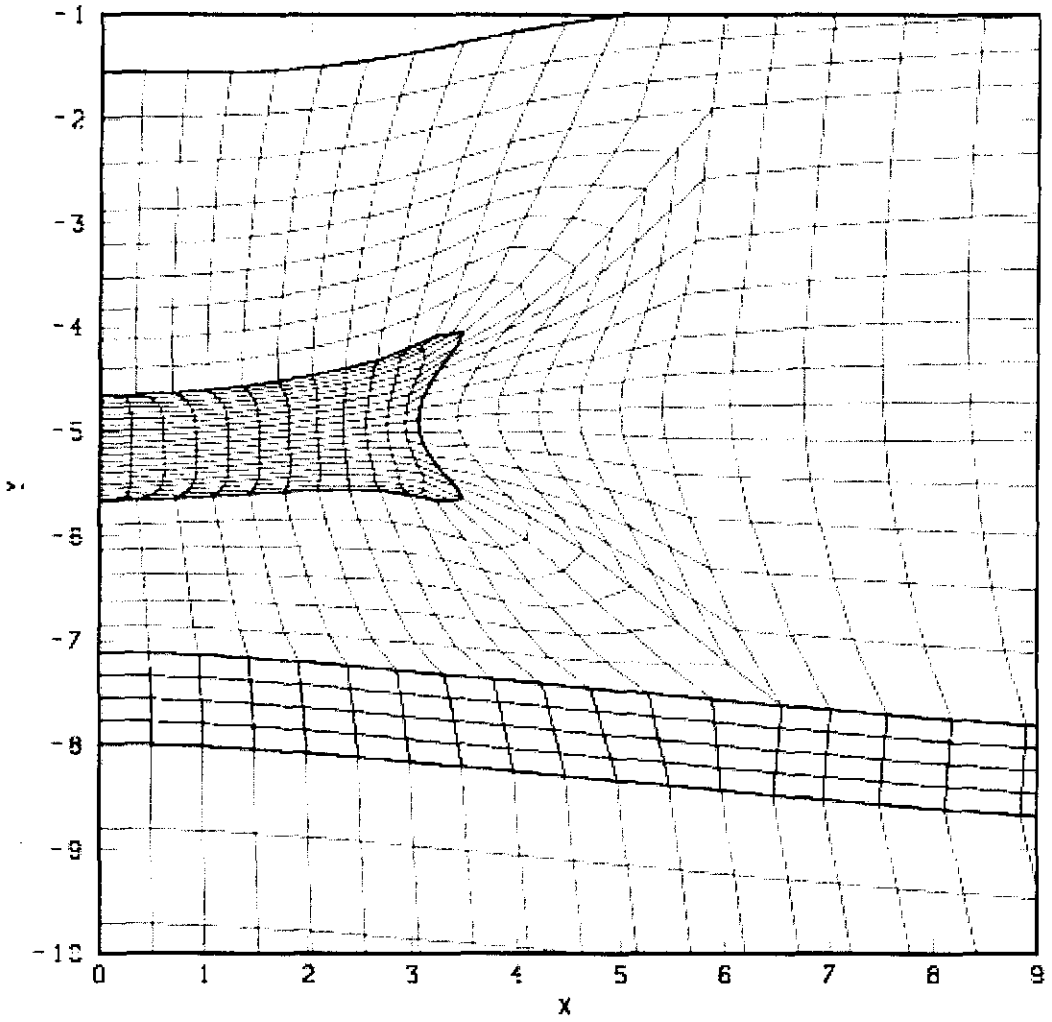

Figure A-50. Deformed Mesh Configuration for the Nonlinear Elastic Analysis With Variable Poisson's Ratio Including No Gas Generation ($f = 0$) at 4,000 Years.

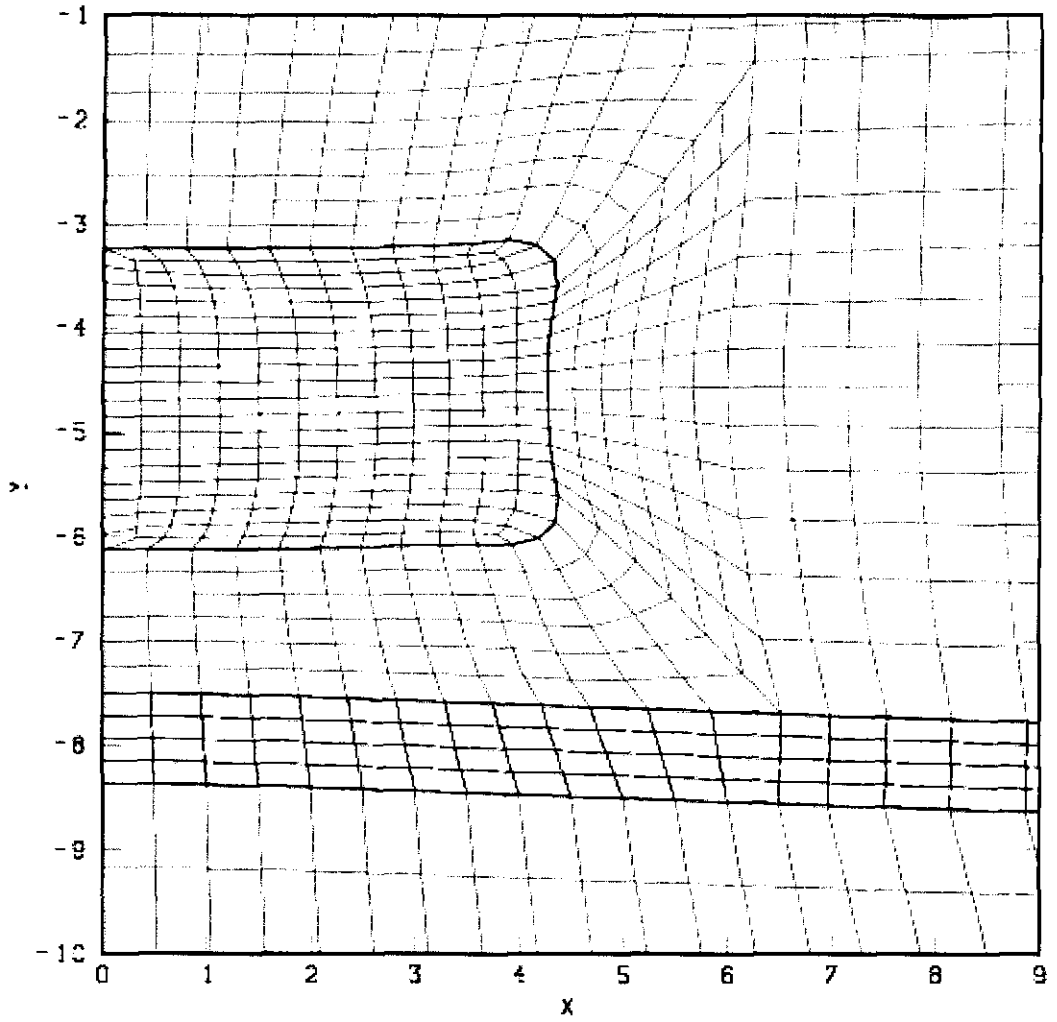

Figure A-51. Deformed Mesh Configuration for the Nonlinear Elastic Analysis With Poisson's Ratio Equal to 0.0 Including Gas Generation ($f = 1$) at 10,000 Years.

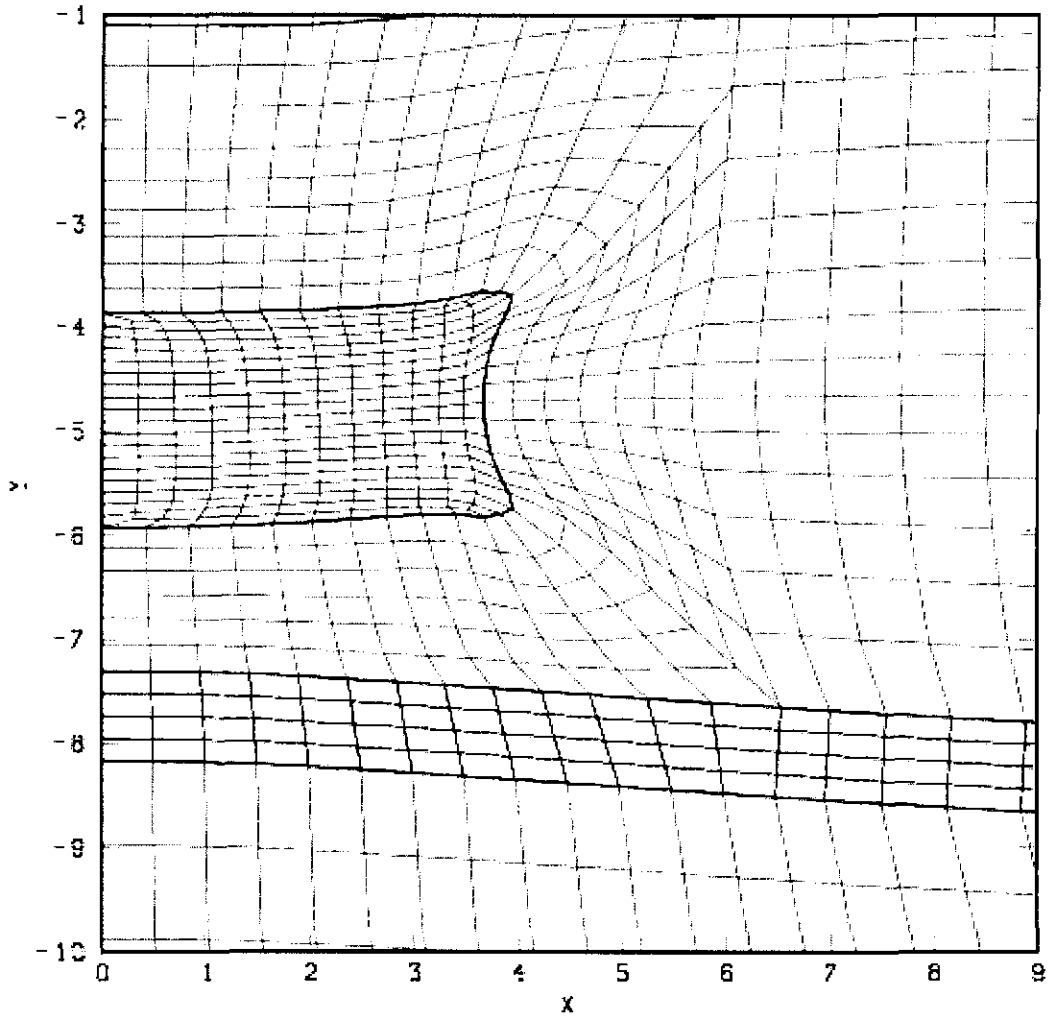

Figure A-52. Deformed Mesh Configuration for the Nonlinear Elastic Analysis With Poisson's Ratio Equal to 0.0 Including Gas Generation ($f = 0.4$) at 10,000 Years.

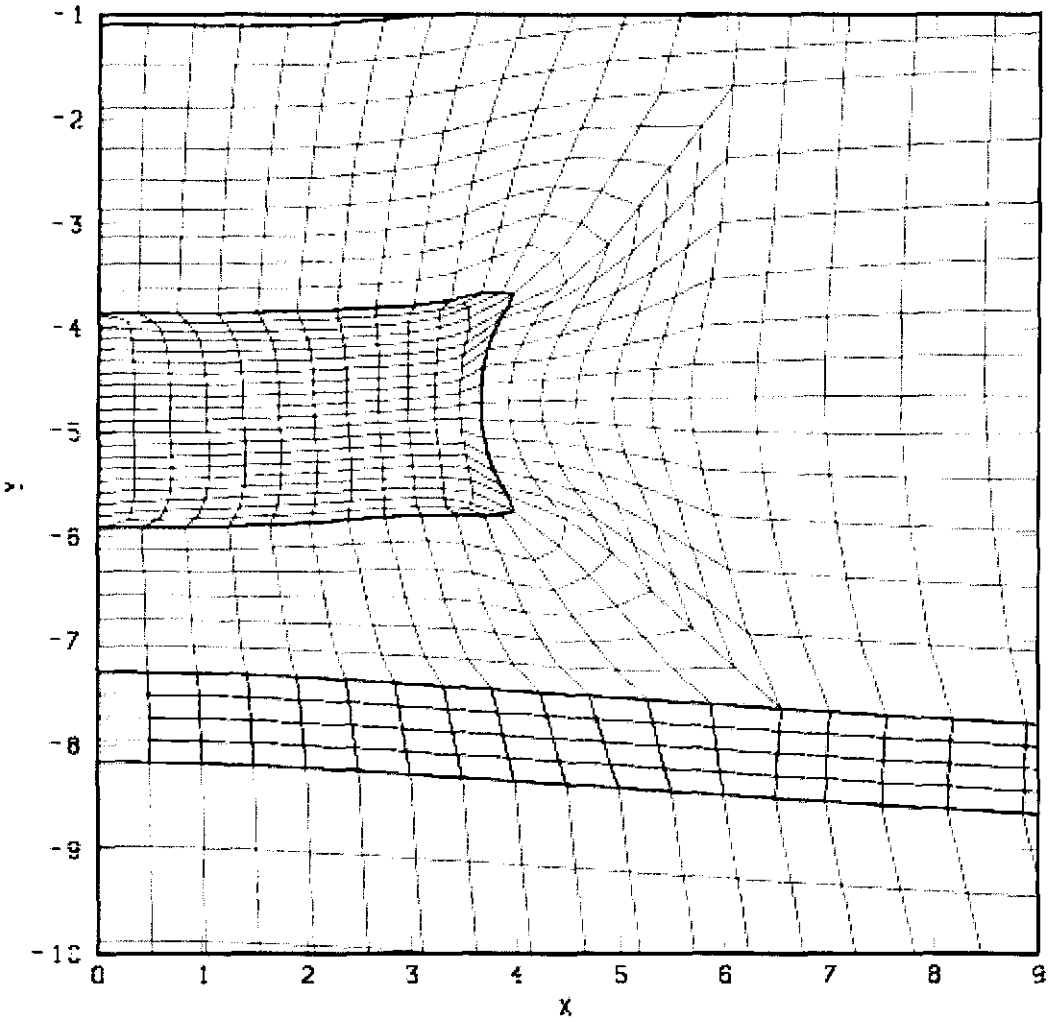

Figure A-53. Deformed Mesh Configuration for the Nonlinear Elastic Analysis With Variable Poisson's Ratio Including Gas Generation ($f = 0.4$) at 10,000 Years.

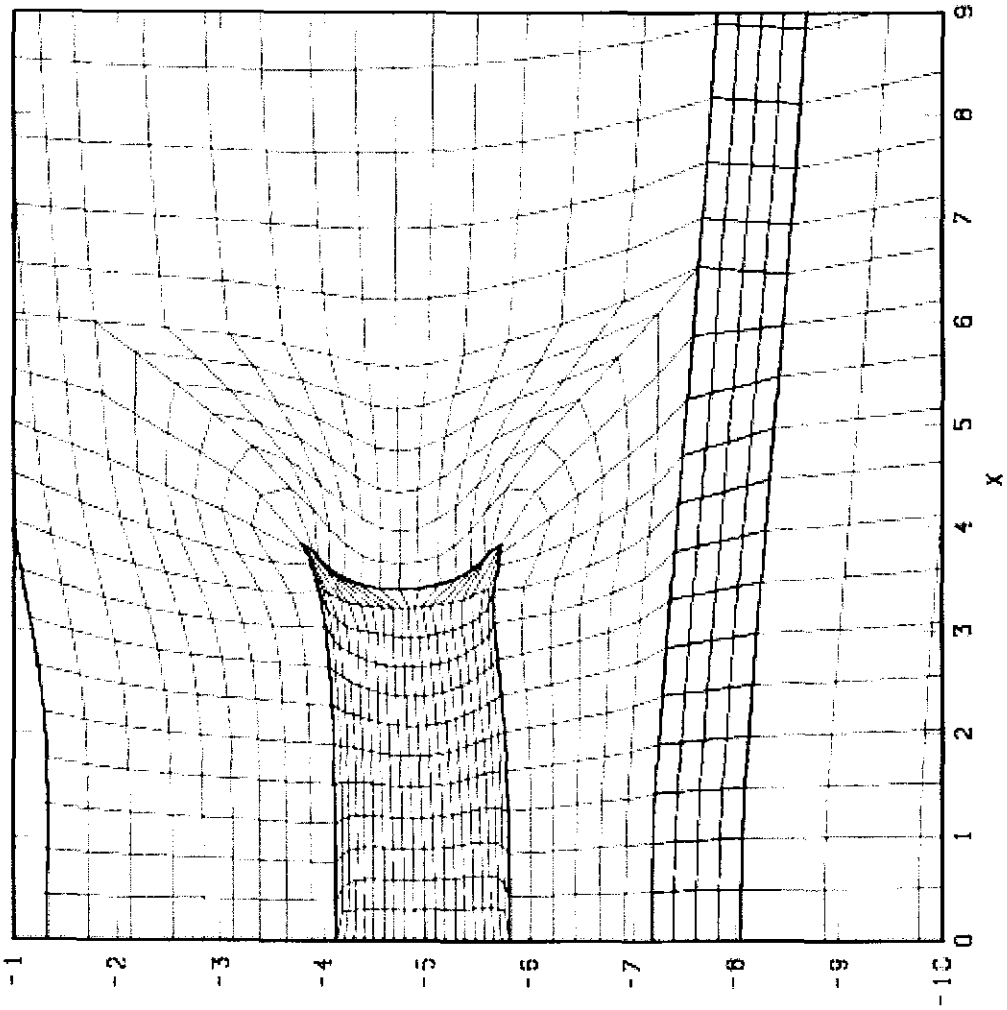

Figure A-54. Deformed Mesh Configuration for the Fluid Analysis at 150 Years.